

INVESTIGATION OF GROUND REACTION FORCE DISTRIBUTION  
BENEATH THE FOOT IN POSTURAL CONTROL

A THESIS SUBMITTED TO  
THE GRADUATE SCHOOL OF NATURAL AND APPLIED SCIENCES  
OF  
MIDDLE EAST TECHNICAL UNIVERSITY

BY

ROSHANAK AKBARIFAR

IN PARTIAL FULFILLMENT OF THE REQUIREMENTS  
FOR  
THE GRADUATE OF MASTER OF SCIENCE  
IN  
BIOMEDICAL ENGINEERING

DECEMBER 2014



Approval of the thesis:

**INVESTIGATION OF GROUND REACTION FORCE DISTRIBUTION  
BENEATH THE FOOT IN POSTURAL CONTROL**

submitted by **ROSHANAK AKBARIFAR** in partial fulfillment of the requirements  
for the degree of **Master of Science in Biomedical Engineering Department,**  
**Middle East Technical University** by,

Prof. Dr. Gülbin Dural Ünver  
Dean, Graduate School of **Natural and Applied Sciences**

Prof.Dr. Vasıf Hasırcı  
Head of Department, **Biomedical Engineering**

Prof.Dr.Uğur Halıcı  
Supervisor, **Electrical and Electronics Engineering Dept., METU**

Assoc.Prof. Dr. Senih Gürses  
Co-supervisor, **Engineering Science Dept., METU**

**Examining Committee Members**

Prof.Dr. Kemal Leblebicioğlu  
Electrical and Electronics Engineering Dept., METU

Prof.Dr.Uğur Halıcı  
Electrical and Electronics Engineering Dept., METU

Assoc.Prof. Dr. Senih Gürses  
Engineering Science Dept., METU

Prof.Dr. Hakan Tarman  
Engineering Science Dept., METU

Prof. Dr. Kemal Özgören  
Mechanical Engineering Dept., METU

**Date:** 03/12/2014

**I hereby declare that all information in this document has been obtained and presented in accordance with academic rules and ethical conduct. I also declare that, as required by these rules and conduct, I have fully cited and referenced all material and results that are not original to this work.**

Name, Last name: Roshanak AKBARIFAR

Signature:

## ABSTRACT

### INVESTIGATION OF GROUND REACTION FORCE DISTRIBUTION BENEATH THE FOOT IN POSTURAL CONTROL

Akbarifar, Roshanak

M.S., Department of Biomedical Engineering

Supervisor: Prof. Dr. Uğur Halıcı

Co-Supervisor: Assoc. Prof. Dr. Senih Gürses

December 2014, 116 Pages

It has been reported that the ground reaction force (GRF) beneath the foot is distributed by the ratio of 1/3 in metatarsals and 2/3 in calcaneous. The main aim of this thesis is to check the ratio of GRF distribution with respect to front and hind regions of the foot and to understand the importance of the distribution ratio/rule in postural control. A mathematical model is designed and simulated using MATLAB® and Simulink® in which the foot is modeled as a deformable body, instead of being rigid, which has widely been used as a modeling attempt in the previous literature. The output signals of model and their behaviors in time were compared with the next stage experimental results for any similarities.

The second stage of the thesis is data collection. Data were collected using a pressure mat, a forceplate and a motion capture system. Data analyses were performed using codes written in MATLAB® and results were interpreted in different sections.

Results showed that subjects were standing more stable during bipedal trials rather than unipedal trials; and more stable during open-eyes trials rather than closed eyes.

The “1/3 & 2/3” rule was observed in all of the trials but there were greater errors in unipedal trials than in bipedal because the stability of subjects was disturbed more frequently.

Calculating the correlation between body center of pressure and different pressure components beneath foot, it was observed that center of pressure was mostly correlated with the pressure component under metatarsals of the right foot.

**Keywords:** Modeling, Simulation, Signal Processing, Posture Analysis, Data Analysis, Ground Reaction Force Distribution

## ÖZ

### POSTUR KONTROLÜNDE AYAK ALTINDAKİ ZEMİN TEPKİ KUVVETİ DAĞILIMININ İNCELENMESİ

Akbarifar, Roshanak

Yüksek Lisans, Biyomedikal Mühendisliği Bölümü

Tez Yöneticisi: Prof. Dr. Uğur Halıcı

Ortak Tez Yöneticisi: Assoc. Prof. Dr. Senih Gürses

Aralık 2014, 116 Sayfa

Ayak altındaki zemin tepki kuvvetinin (GRF) metatars da 1/3 ve topuk da 2/3 şeklinde dağılmış olduğu önceden gösterilmiştir. Bu tezin temel amacı ayağın ön ve arka bölgelerinde GRF dağıtım oranını kontrol etmek ve postural kontrolünde önemini anlamaktır. Önceden literatürde sıkça kullanılmış olan rijit cisim ayak model yerine, burada deforme olabilen bir ayak modeli, MATLAB® ve Simulink® kullanılarak tasarlanmış ve simüle edilmiştir. Bu modelin çıkış sinyalleri ve onların zaman içinde davranışları herhangi bir benzerlik için bir sonraki aşamadaki deney sonuçları ile karşılaştırılmıştır.

Tezin ikinci aşaması veri toplanmasıdır. Veriler bir basınca duyarlı altlık, bir forceplate ve bir hareket yakalama sistemi kullanılarak toplanmıştır. Veri analizleri MATLAB'da yazılmış kodlar kullanılarak yapılmış ve sonuçları farklı bölümlerde yorumlanmıştır.

Sonuçlar deneklerin iki ayaklı denemelerde tek ayaklı denemelere göre daha dengeli ayakta durduğunu göstermiş; açık gözlü denemeler de kapalı gözlü denemelere göre daha dengeli olmuştur.

"1/3 ve 2/3" kuralı tüm çalışmalarda gözlenmiş, ancak deneklerin dengeleri tek ayaklı denemelerde iki ayaklı denemelere göre daha sık bozulduğu için, tek ayaklı denemelerde daha büyük hatalar gözlemlenmiştir.

Vücut basınç merkezi ve ayak altında basınç bileşenleri arasındaki korelasyon hesaplanırken, bu basınç merkezinin çoğunlukla sağ ayağın metatars altındaki basınç bileşeni ile korele olduğu gözlemlenmiştir.

**Anahtar Kelimeler:** Modelleme, Simülasyon, Sinyal İşleme, Postür Analizi, Veri Analizi, Zemin Tepki Gücü Dağılımı

## ACKNOWLEDGMENTS

I would like to express the deepest appreciation to my supervisors, Dr. Uğur HALICI and Dr. Senih GÜRSES, who continually and persuasively gave a spirit of adventure in regard to research, and an excitement in regard to teaching. Without their supervision and constant help this thesis would not have been possible.

I would also like to show gratitude to my committee, Dr. Hakan TARMAN, Dr. Kemal LEBLEBİCİOĞLU and Dr. Kemal ÖZGÖREN, for serving as my committee members even at hardship, and for their brilliant comments and suggestions.

A special thanks to my family. Words cannot express how grateful I am to my husband, parents and siblings for all of the sacrifices that they have made on my behalf. To my parents, who offered their encouragement through phone calls every week. To my loving husband who I could not do any of these without his support from this long distance. To my sister who besides unfailing kindness and support, offered me her proofreading skills as well. To my sister-in-law who helped me with statistics of the analysis. This thesis stands as a testament to your unconditional love and encouragement.

I would also like to thank all of my friends who supported me in writing and I have many people to thank for listening to and tolerate me over the past months. Emre AKÇAY, Okan ALKAN, Raha SHABANI, Fahime Q. BERENJI and Sona K. SHENAS have been unwavering in their personal and professional support during the time I spent at the university.

## TABLE OF CONTENTS

ABSTRACT.....	v
ÖZ .....	vii
ACKNOWLEDGMENTS .....	ix
TABLE OF CONTENTS.....	x
LIST OF TABLES .....	xiii
LIST OF FIGURES.....	xv
LIST OF ABBREVIATIONS .....	xix
LIST OF SYMBOLS.....	xx
CHAPTERS:	
1 INTRODUCTION.....	1
1.1 MOTIVATION OF THE STUDY.....	1
1.2 PRELIMINARY WORK.....	3
1.3 TESTS AND TOOLS.....	6
1.3.1 KOLMOGOROV-SMIRNOV TEST .....	6
1.3.2 STUDENT’S T-TEST .....	7
1.3.3 TREND LINES .....	7
1.4 CONTRIBUTION OF THE STUDY.....	7
1.5 THESIS STATEMENT.....	9
1.6 THESIS OUTLINE.....	9
2 THEORETICAL BACKGROUND.....	11
2.1 GAIT AND POSTURE ANALYSIS .....	11
2.2 QUIET STANCE .....	13
2.3 FOOT MODELS IN LITERATURE .....	17

3	EXPERIMENTAL WORK.....	19
3.1	INTRODUCTION .....	19
3.2	METHODS .....	20
3.3	PRE-VALIDATION.....	22
3.3.1	SIMILARITY BETWEEN COP <sub>x</sub> SIGNALS OBTAINED FROM FORCEPLATE AND PRESSURE MAT .....	22
3.3.2	.....	24
3.3.3	DATA LOSS .....	24
3.4	RESULTS AND DISCUSSION.....	26
3.4.1	GROUND REACTION FORCE DISTRIBUTION IN BIPEDAL.....	26
3.4.1.1	CLOSED-EYES VERSUS OPEN-EYES .....	29
3.4.1.2	RIGHT FOOT VERSUS LEFT FOOT .....	31
3.4.1.3	DOMINANT VERSUS NON-DOMINANT FOOT.....	34
3.4.2	GROUND REACTION FORCE DISTRIBUTION IN UNIPEDAL.....	35
3.4.2.1	CLOSED-EYES VERSUS OPEN-EYES .....	38
3.4.2.2	DOMINANT VERSUS NON-DOMINANT FOOT.....	42
3.4.2.3	GROUND REACTION FORCE DISTRIBUTION ALONG LATERAL- MEDIAL DIRECTION .....	43
3.4.3	CORRELATION BETWEEN COP <sub>x</sub> AND GROUND REACTION FORCE DISTRIBUTION.....	50
3.4.4	COMPARISON BETWEEN COM AND COP.....	52
3.4.5	PLANTAR APONEUROSIS LENGTH .....	54
3.5	CONCLUSION .....	59
4	MODELING .....	61
4.1	INTRODUCTION .....	61
4.2	MODEL .....	61
4.2.1	SIMPLE RIGID FOOT MODEL WITH NO FRICTION FORCES .....	62
4.2.2	SIMPLE RIGID FOOT MODEL WITH FRICTION FORCES.....	68

4.2.3	SWAYING FOOT MODEL WITH NO FRICTION FORCES .....	69
4.2.4	SWAYING FOOT MODEL WITH FRICTION FORCES .....	73
4.2.5	DEFORMABLE FOOT WITH NO FRICTION FORCES.....	78
4.3	CONCLUSION.....	82
5	CONCLUSION .....	85
5.1	SUMMARY.....	85
5.2	DISCUSSIONS.....	86
5.2.1	EXPERIMENTS .....	86
5.2.2	MODELING .....	89
5.3	FUTURE WORK.....	90
	REFERENCES.....	93
	APPENDICES:	
	APPENDIX A: T-TABLE.....	97
	APPENDIX B: MODEL EQUATIONS.....	99
	APPENDIX C: DOUBLE INVERTED PENDULUM .....	105
	APPENDIX D: STABILITY OF THE SYSTEM.....	111

## LIST OF TABLES

### TABLES:

Table 3-1 trial cases .....	21
Table 3-2 Participants demographics.....	22
Table 3-3 Correlation between instability factor and validation time .....	30
Table 3-4 Validation time and instability factor in bipedal trials.....	31
Table 3-5 t-values resulted from t-test for comparing My and Cy between right and left feet .....	34
Table 3-6 Mean and STD for validation time and total instability factor in different cases .....	40
Table 3-7 Validation time and instability factor in unipedal-right trials .....	41
Table 3-8 Validation time and instability factor in unipedal-left trials .....	41
Table 3-9 Right-footed subjects' behavior in unipedal open-eyes trials .....	42
Table 3-10 Left-footed subjects' behavior in unipedal open-eyes trials.....	42
Table 3-11 Right-footed subjects' behavior in unipedal closed-eyes trials .....	43
Table 3-12 Left-footed subjects' behavior in unipedal closed-eyes trials .....	43
Table 3-13 ROI validation time and ROI instability for unipedal-right trials .....	47
Table 3-14 ROI validation time and ROI instability for unipedal-left trials.....	48
Table 3-15 Right-footed subjects' behavior in Unipedal open-eyes case.....	48
Table 3-16 Left-footed subjects' behavior in Unipedal open-eyes case.....	48
Table 3-17 Right-footed subjects' behavior in Unipedal closed-eyes case .....	49
Table 3-18 Left-footed subjects' behavior in Unipedal closed-eyes case .....	49
Table 3-19 Categorization of subjects due to their instability.....	50
Table 3-20 Correlation coefficients in four cases: RCy & COPx, LCy & COPx, RMy & COPx, LMy & COPx.....	51
Table 3-21 Mass fractions and segment definitions, m1-m7 are the 7 MTX markers used from motion capture system.....	53
Table 3-22 Theta (in degrees) in six cases for all of the subjects.....	56

Table 3-23 Average experimental S [cm] .....	57
Table 3-24 Correlation ratios, between S and validation time, and between S and instability factor .....	59
Table 4-1 Nomenclature for Figure 4-2 .....	63
Table 4-2 T-values and mean values of ratios in rigid foot model with no friction forces, poin-by-point analysis.....	64
Table 4-3 T-values and mean values of ratios in rigid foot model with no friction forces, 1 <sup>st</sup> bipedal open-eyes trial.....	65
Table 4-4 T-values and mean values of ratios in rigid foot model with no friction forces, 1 <sup>st</sup> bipedal closed-eyes trial .....	66
Table 4-5 T-values and mean values of ratios in rigid foot model with no friction forces, 2 <sup>nd</sup> bipedal open-eyes trial.....	66
Table 4-6 T-values and mean values of ratios in rigid foot model with no friction forces, 2 <sup>nd</sup> bipedal closed-eyes trial .....	67
Table 4-7 T-values and mean values of ratios in rigid foot model with no friction forces, 3 <sup>rd</sup> bipedal open-eyes trial .....	67
Table 4-8 T-values and mean values of ratios in rigid foot model with no friction forces, 3 <sup>rd</sup> bipedal closed-eyes trial.....	68
Table 4-9 Experimental friction forces in bipedal trials .....	78
Table A-1 T-table for t-test.....	97

## LIST OF FIGURES

### FIGURES:

Figure 1-1 Arches of the foot .....	2
Figure 1-2 Calcaneous and Metatarsals in human foot .....	3
Figure 1-3 A single frame of two specific videos during preliminary work.....	3
Figure 1-4 Dots on foot after image process .....	4
Figure 1-5 Displacement (red) versus Force plot (blue) .....	4
Figure 1-6 $\Delta x$ graph for bottommost point of each line on the foot.....	6
Figure 2-1 A brief review of physiological terminology (FLEX: flexion (of the thigh at the hip joint); EXT: extension (of the leg at the knee joint); AD: adduction; AB: abduction).....	16
Figure 3-1 Average difference (in %) between $COP_{x, f}$ and $COP_{x, p}$ for each subject in every case .....	23
Figure 3-2 Percent error intervals for six experiment cases.....	23
Figure 3-3 $COP_{x, f}$ and $COP_{x, p}$ for one trial of a subject: A) BO case with 1% error, B) BC case with 8% error .....	24
Figure 3-4 $C_y$ and $M_y$ regions of foot shown on a data frame .....	25
Figure 3-5 Percentage error of $C_y+M_y$ from $mg$ .....	26
Figure 3-6 Average $R_{mg}$ & average $Err_{2/3}$ for both bipedal open-eyes and bipedal closed-eyes cases .....	27
Figure 3-7 $C_y/(C_y+M_y)$ ratio compared to the ideal interval .....	28
Figure 3-8 Overall validation time and instability factor in bipedal case (both open-eyes and closed-eyes cases).....	28
Figure 3-9 Validation time percentage and instability factor in BO case .....	29
Figure 3-10 Validation time percentage and instability factor in BC case .....	30
Figure 3-11 Charts of a bipedal case for a specific subject, A) $M_y$ plot, B) $C_y$ plot	32
Figure 3-12 $M_y$ -R in regard to $M_y$ -L with trendline in a specific bipedal trial .....	33

Figure 3-13 Cy-R in regard to Cy-L with trendline in a specific bipedal trial .....	33
Figure 3-14 Average $Cy - RCy - L$ and average $My - RMy - L$ for 14 subjects in bipedal cases, subjects 3, 10, 13 are the left footed ones .....	35
Figure 3-15 Average $R_{mg}$ & average $Err_{2/3}$ in unipedal-R case, subjects 3, 10, 13 are left footed.....	36
Figure 3-16 Average $R_{mg}$ & average $Err_{2/3}$ in unipedal-L case, subjects 3, 10, 13 are left footed.....	36
Figure 3-17 Overall validation time and instability factor for all subjects in unipedal, subjects 3, 10, 13 are left footed .....	37
Figure 3-18 Validation time and instability factor for all subjects in RO, subjects 3, 10, 13 are left footed .....	39
Figure 3-19 Validation time and instability factor for all subjects in unipedal/RC, subjects 3, 10, 13 are left footed .....	39
Figure 3-20 Validation time and instability factor for all subjects in unipedal/LO, subjects 3, 10, 13 are left footed .....	40
Figure 3-21 Validation time and instability factor for all subjects in unipedal/LC, subjects 3, 10, 13 are left footed .....	40
Figure 3-22 ROI and Lat regions of foot shown on a data frame .....	44
Figure 3-23 ROI/Lat ratio compared to the ideal interval.....	45
Figure 3-24 Overall ROI validation time and ROI instability factor in unipedal trials .....	45
Figure 3-25 ROI validation time and ROI instability factor in RO case .....	46
Figure 3-26 ROI validation time and ROI instability factor in RC case.....	46
Figure 3-27 ROI validation time and ROI instability factor in LO case.....	47
Figure 3-28 ROI validation time and ROI instability factor in LC case .....	47
Figure 3-29 Number of instabilities for every subject in each case.....	49
Figure 3-30 Cylinder resembling the upper limb of human body .....	54
Figure 3-31 A schematic view of model showing some parameters and measurements .....	55
Figure 3-32 An explanatory static shape for measurement of S.....	56
Figure 3-33 S in time for a BO trial .....	58

Figure 4-1 Simple schematic description of the model .....	62
Figure 4-2 Free body diagram of rigid foot model with no friction .....	63
Figure 4-3 Free body diagram of rigid foot model with friction .....	69
Figure 4-4 Swaying foot model with no friction forces .....	70
Figure 4-5 Theta obtained from swaying foot model with no friction forces .....	71
Figure 4-6 Swaying foot model with no friction forces and fixed calcaneous .....	71
Figure 4-7 Output signals for swaying foot model with no friction forces and fixed calcaneous .....	72
Figure 4-8 Ratio between $C_y$ and $M_y$ for swaying foot model with no friction forces and fixed calcaneous; red lines show 5% tolerance.....	73
Figure 4-9 Swaying foot model with friction forces.....	74
Figure 4-10 Output signals for swaying foot model with friction forces .....	75
Figure 4-11 Ratio between $C_y$ and $M_y$ for swaying foot model with friction forces; red lines show 5% tolerance .....	76
Figure 4-12 Friction forces and friction coefficient for swaying foot model with friction forces.....	77
Figure 4-13 Experimental friction force .....	78
Figure 4-14 Free body diagram for deformable foot with no friction forces with normal approach .....	79
Figure 4-15 Angular displacements for deformable foot model with no friction forces .....	80
Figure 4-16 Output signals for deformable foot model with no friction forces .....	81
Figure 4-17 $C_y$ and $M_y$ for deformable foot model with no friction forces; red lines show 5% tolerance .....	81
Figure B-1 Rigid foot with no friction forces.....	<b>Error! Bookmark not defined.</b>
Figure B-2 Swaying foot with no friction forces and calcaneous a fixed joint.....	100
Figure B-3 Swaying foot with no friction forces and calcaneous a roller joint .....	101
Figure B-4 Swaying foot with friction forces .....	102
Figure B-5 Deformable foot with no friction forces.....	103
Figure C-1 Deformable foot model with no friction forces, double inverted pendulum approach .....	105

Figure C-2 Single inverted pendulum foot model .....	107
Figure C-3 Output signals for single inverted foot model.....	108
Figure C-4 $C_y/M_y$ ratio with 5% tolerance .....	108
Figure C-5 Output signals for double inverted pendulum.....	109
Figure D-1 PA length for deformable foot model with no friction forces (for longer time than experimental duration) .....	112
Figure D-2 Deformable foot model with friction forces .....	114

## LIST OF ABBREVIATIONS

<i>COP:</i>	Center of Pressure, the point of application of the Ground Reaction Force vector
<i>COM:</i>	Center of Mass, the point in which the whole body mass is concentrated The point about which a body would balance without any tendency to rotate
<i>COG:</i>	Center of Gravity, vertical projection of COM on the ground
<i>GRF:</i>	Ground Reaction Force, sum of all forces acting between a physical object and its supporting surface
<i>DoF:</i>	Degree of Freedom
<i>STD:</i>	Standard Deviation
<i>KS:</i>	Kolmogorov-Smirnov test
<i>ROI:</i>	Region of Interest
<i>Lat:</i>	Lateral region of the foot
<i>PA:</i>	Plantar Aponeurosis
<i>TA:</i>	Tibialis Anterior muscle
<i>GC:</i>	Gastrocnemius muscle

## LIST OF SYMBOLS

$COP_x$ :	Component of COP in x direction
$COP_y$ :	Component of COP in y direction
$COP_{x,f}$ :	Component of COP in x direction measured by force plate
$COP_{x,p}$ :	Component of COP in x direction measured by pressure mat
$A$ :	Ankle joint
$A_x$ :	Component of GRF inserted on ankle joint in x direction
$A_y$ :	Component of GRF inserted on ankle joint in y direction
$C$ :	Calcaneous tuberosity
$C_x$ :	Component of GRF inserted on calcaneous in x direction
$C_y$ :	Component of GRF inserted on calcaneous in y direction
$M$ :	Metatarsals
$M_x$ :	Component of GRF inserted on metatarsals in x direction
$M_y$ :	Component of GRF inserted on metatarsals in y direction
$RC_y$ :	$C_y$ on right foot
$LC_y$ :	$C_y$ on left foot
$RM_y$ :	$M_y$ on right foot
$LM_y$ :	$M_y$ on left foot
$S(t)$ :	Displacement of M (Length of plantar aponeurosis)
$\alpha_1, \alpha_2$ :	Angular displacements of link1 and link2 (relative) respectively
$\theta(t)$ :	Angular displacement of link2
$T1$ &	Control torques on links
$T2$ :	
$F_{sp}$ :	Tensile force on PA
$k$ :	Stiffness of PA
$k_t$ :	Stiffness of torsional spring
$I_1$ :	Moment of inertia of link1 about its Center of Mass (COM)

$I_2$ :	Moment of inertia of link2 about its COM
$m$ :	Body mass
$m_1$ :	Mass of the body except foot
$m_2$ :	Foot mass
$g$ :	Acceleration due to gravity at the Earth's surface and is equivalent to 9.8 N/Kg
$l_1$ :	Length of link1, from ankle joint to calcaneous
$l_2$ :	Length of link2, from ankle joint to body center of mass
$l_3$ :	Length of link3, from ankle joint to matatarsals
$d_1$ :	Distance between the vertical projection of ankle foot and metatarsals
$d_2$ :	Distance between the vertical projection of ankle foot and calcaneous
$h$ :	Distance between the ankle joint and ground surface
$T_c$ :	Control torque
$BC$ :	Bipedal closed-eyes trial
$BO$ :	Bipedal open-eyes trial
$RC$ :	Unipedal right foot closed-eyes trial
$RO$ :	Unipedal right foot open -eyes trial
$LC$ :	Unipedal left foot closed-eyes trial
$LO$ :	Unipedal left foot open -eyes trial
$Err_{cop}$	Average difference between $COP_{x,f}$ and $COP_{x,p}$ , which is defined as: $Err_{cop} = \frac{ COP_{x,f} - COP_{x,p} }{COP_{x,f}} \times 100$
$R_{mg}$	$C_y$ ratio to total pressure beneath the foot: $R_{mg} = \frac{C_y}{C_y + M_y}$
$Err_{\frac{2}{3}}$	Difference between $R_{mg}$ and the reference value 2/3: $Err_{\frac{2}{3}} = \frac{ 2/3 - R_{mg} }{2/3} \times 100$
$TO$ :	validation time in open-eyes case
$TC$ :	validation time in closed-eyes case
$FO$ :	instability factor in open-eyes case
$FC$ :	instability factor in closed-eyes case
$TR$ :	validation time in unipedal-right foot case

<i>TL</i> :	validation time in unipedal-left foot case
<i>FR</i> :	instability factor in unipedal-right foot case
<i>FL</i> :	instability factor in unipedal-left foot case
<i>COM<sub>i</sub></i> :	COM for i <sup>th</sup> body segment
<i>m<sub>i</sub>/M</i> :	Mass fraction for i <sup>th</sup> body segment (M is the total body mass and m <sub>i</sub> is the mass of the i <sup>th</sup> segment of the body)
<i>μ</i>	Friction coefficient

## **CHAPTER 1**

### **INTRODUCTION**

#### **1.1 MOTIVATION OF THE STUDY**

In literature, it has been explained that the human foot (and ankle) is a very unique structure. It contains more than 26 bones, 33 joints and more than a hundred of muscles, tendons, and ligaments. Foot consists of three main parts: forefoot acts as an actuator, hindfoot and midfoot both function as load bearing parts. The uniqueness of this structure can be illustrated by the role of hallux, plantar aponeurosis and plantar sensation in maintaining balance in the human erect posture.

Human foot consists of three arched structures: medial longitudinal, lateral longitudinal and transverse arch [1]. These arches are shown in Figure 1-1. The greatest amount of motion during stance, occurs in the sagittal plane around the talonavicular joint, which can also be described as the deformation of the medial longitudinal arch [2]. Numerous studies show that plantar aponeurosis or plantar fascia is the most important passive arch support in human stance phase [3-9]. Throughout this thesis the medial longitudinal arch has been studied using the deformations of plantar fascia; any change in the height of this arch (due to foot deformations) leads to a change in fascia's length.

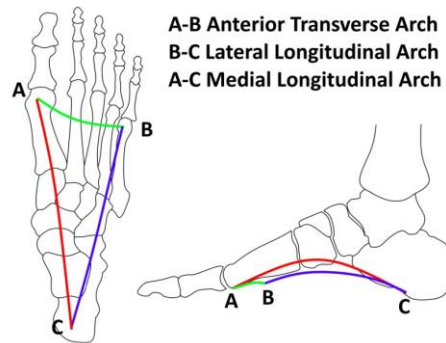


**Figure 1-1 Arches of the foot**

Most of the works in human erect posture literature, up to present, consider the foot as a rigid body with an ankle joint [10-12] and focus on the simple hinge action of the ankle joint, not considering the distributive nature of foot deformations [10]. But in this thesis it is assumed to be active, flexible and sensitive to minute perturbations even if the entire hind and midfoot is stably supported and the ankle joint is unperturbed. This is done by adding the medial longitudinal arch and PA to the foot model to make it a deformable model rather than a rigid one.

It is stated in literature that the ground reaction force has a general pattern of 1/3 in metatarsals and 2/3 in calcaneus [13]. The human foot is shown in

Figure 1-2 with the calcaneus and metatarsals specified on it. This rule has been proven both mathematically and experimentally. Therefore one important matter that needs to be observed in our model is this relation among the pressure distribution components beneath the foot.

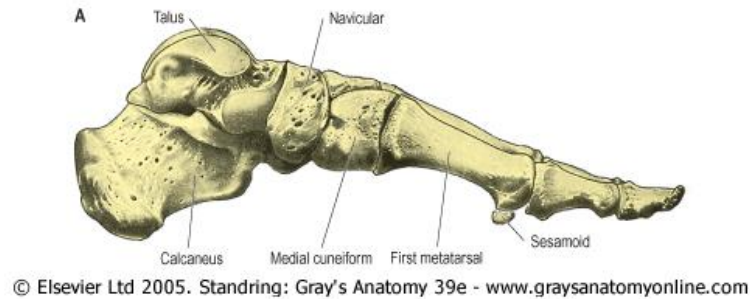


**Figure 1-2 Calcaneous and Metatarsals in human foot [1]**

## 1.2 PRELIMINARY WORK

A preliminary work was done before the main thesis, aiming the importance of shear forces beneath foot in the dynamics to control posture. In that study vertical lines (case 1) or some dots (case 2) were placed on the lateral surface of the subject's foot (using a normal whiteboard marker). The lines were 1.5cm apart from each other and each dot was 5mm apart horizontally and vertically from the adjacent dots. This was done for simplicity in tracking the deformations. The subject had to stand on a perturbed platform (pure sine wave, tilt frequency 0.5 Hz, peak amplitude 6°) and the foot was videotaped. Figure 1-3 shows one frame of such videos.



**Figure 1-3 A single frame of two specific videos during preliminary work**

Then these videos were undergone some video and image processing techniques using personalized codes in MATLAB to obtain deformations of the foot with respect to the given perturbation. After the preprocessing phase, the dots and the lines on the foot were detected as distinct objects as shown in Figure 1-4.

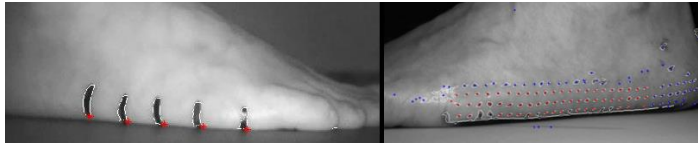


**Figure 1-4 Dots on foot after image process**

Having coordinates of centroids of dots or the start point of the lines, the distance of every point in the first frame from all of the points in the remaining frames were calculated and the minimum was selected as the new position of that point. Since the maximum movement of each point between two frames is less than the distance between two points in one frame, the minimum distance method seems to be rational to use. By this strategy the points were tracked in time and having all of the coordinates in time, deformations of the foot -in response to the force that has been initiated with the tilting surface- were calculated. The subject stood on a force platform and at the same time resultant forces were recorded. The input force and displacements of one point, for one of the dot graph trials, are plotted in Figure 1-5.

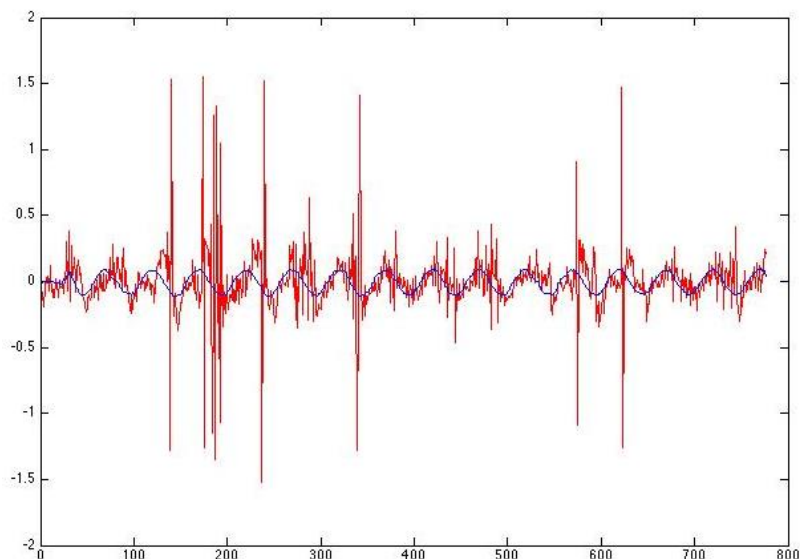


**Figure 1-5 Displacement (red) versus Force plot (blue)**

Figure 1-6 shows a graph indicating the  $\Delta x$  (translation) for the bottommost point in each of the lines in a specific trial. The results show us that 1st line (the nearest to the heel) has the least and 5th line (the nearest to metatarsals) has the most translation. Based on these results, it was decided for the calcaneus in the model to be a fixed point and for metatarsals to be a roller one. So heel is more stable than metatarsals and during the deformations it acts like it is fixed on the ground. This assumption acts an important role in the representation of our model.

During this preliminary study, we observed some deformations on the foot due to perturbations, which can be called soft tissue deformations. Moreover, there are some more deformations, namely shear (or functional) deformations that are response of the foot to the external forces exerted on it. So for calculating them distinctly, there is a need to study the deformations and dynamics of the foot more internally.

Using the observations of the preliminary part of the study, the main idea was initiated. An experimental and a modeling study are done to investigate the role of foot in the control of human erect posture. The mathematical model is presented using MATLAB® and Simulink® to represent deformable human foot using a truss structure and controlled by the ground reaction forces. The experimental part of the study is done in Motion Analysis Laboratory<sup>1</sup> in Middle East Technical University. Collected data from TekScan® pressure mat, Bertec force platform and Xsens® MTx motion trackers is analyzed using different techniques implemented in MATLAB® environment.

---

<sup>1</sup> Located in MODSIMMER building in METU campus

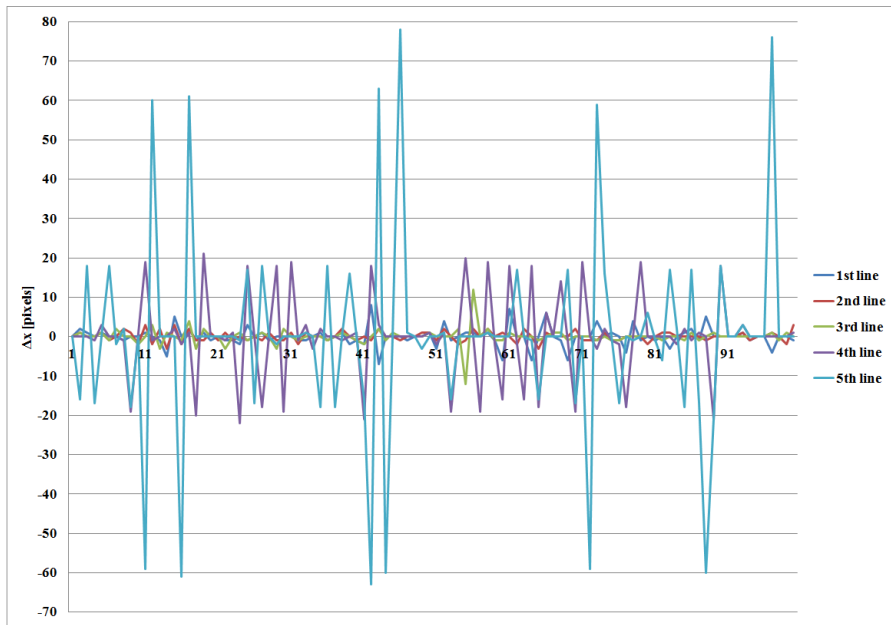


**Figure 1-6  $\Delta x$  graph for bottommost point of each line on the foot**

### 1.3 TESTS AND TOOLS

There have been some tests and tools in the statistical part of this thesis. A brief explanation is stated below for each of them.

#### 1.3.1 KOLMOGOROV-SMIRNOV TEST

Kolmogorov-Smirnov test (KS test) is a nonparametric statistics test which can be used in two different cases:

- to compare a sample with a reference probability distribution (one-sample KS test)
- to compare two samples (two-sample KS test)

This test determines a distance between the distribution function of the sample and the reference distribution (in one-sample test) or between the distribution functions of two samples (in two-sample test). Each of these distributions can be any continuous probability distribution such as normal distribution, which is used for this thesis. This distance can be compared with the values of KS table to decide for the

“goodness of fit” of a sample from the reference distribution (in one-sample test) or between two samples (in two-sample test) [14].

### **1.3.2 STUDENT’S T-TEST**

Student’s t-test is used to check if two sets of data are significantly different from each other. Both data samples have to follow a normal distribution; this can be checked using tests such as KS. It compares the means of two samples even if they have different sizes by calculating a specific value known as t-value and comparing it with the values of t-table. The table should be accessed considering the sizes of two samples and the level of significance required (usually the 0.10, the 0.05, or 0.01 level). If the calculated t-value exceeds the tabulated value, it can be decided that the means of two samples are significantly different at the level of probability.

### **1.3.3 TREND LINES**

Trend line is a line that shows the general behavior or tendency of a set of data points in a graph. So in some cases trend line can help to understand or predict the behavior of a dataset. Such analysis is also called regression analysis.

In this thesis trend lines have been plotted for a number of graphs. In these cases simple linear regression trend lines were used. In linear regression data are modeled using some predefined prediction functions; the unknown parameters of these functions are estimated from data. In this thesis the model is a line.

## **1.4 CONTRIBUTION OF THE STUDY**

This thesis was based on studying the pattern of pressure distribution beneath the foot. In literature it has been shown that the pressure distribution beneath the foot has been disturbed as  $1/3$  in metatarsals and  $2/3$  in calcaneous [5, 15].

For the aim of this thesis some experiments have been done. The details about these experiments and the subjects who participate in them are stated in chapter 3. Also mathematical modeling was done using MATLAB and Simulink. All the measurements and analyzes for the experiments and the simulated model were done

in sagittal plane because the whole study is based on the foot deformations in this plane.

The experiments were performed in quiet stance and data was gathered by three instruments; a pressure mat, a force plate and a motion capture system.

For studying the stability of subjects in quiet stance two types of conditions were included in the experiments. The first one was vision; the trials were done in both open-eyes and closed-eyes situation. Besides vision the stability of subjects was checked both in bipedal and unipedal conditions; both feet have been checked separately for unipedal condition. So there were 6 kinds of trials and each of them has been repeated three times. Specific codes written in MATLAB were used for analyzing data. Data gathered in this stage showed that the rule of GRF<sup>2</sup> distribution stated in literature was true in most of the cases. In the cases that stability of subject has been disturbed greatly -both by lack of vision and using just one foot as unipedal test- this rule was not observed. Experimental data has also been used in modeling part.

Then some planar models were proposed and simulated. The idea of modeling was to study the deformations of the foot by simulating the deformations of medial longitudinal arch in sagittal plane. This idea is implemented in two of the models; the others are mid-stages between them and completely rigid foot model. The observations of this thesis showed that the deformable foot model can explain human foot better than rigid foot model which is being used widely in literature.

In this model the human body posture model is treated as a double inverted pendulum and models the foot deformations as a separate DoF<sup>3</sup> which is the angular displacement of the rigid link between calcaneous and ankle. This angular displacement is dependent to linear displacement of metatarsals which itself is equivalent to linear changes in the length of plantar aponeurosis in the foot sole.

---

<sup>2</sup> Ground Reaction Force, sum of all forces acting between a physical object and its supporting surface

<sup>3</sup> Degree of Freedom

## **1.5 THESIS STATEMENT**

- The most important concept that was being looked for in this thesis is the pressure distribution beneath the foot, which needs to be  $1/3$  in metatarsals and  $2/3$  in calcaneous. This has been done both in model and in experimental data. This could show that the calcaneous bears most of the load in quiet stance [5, 15].
- The second concept in experimental part is the importance of metatarsals in stability of postural dynamics. In case of balance being disturbed, the human body tries to get balanced again using metatarsals.
- A great number of the foot models used in literature are based on the idea that human foot can be viewed as a rigid body and all of its dynamics can be ignored. But in this thesis it is assumed that the behavior of human foot is mostly affected by its dynamics, so it cannot act as a rigid body. The main idea for this part is to model the deformations of the foot by simulating the deformations of medial longitudinal arch in saggital plane and this would be the same as to simulate the linear displacement of plantar aponeurosis. This idea is followed in modeling phase of this thesis to make evidence for comparing rigid foot models with deformable foot models.

## **1.6 THESIS OUTLINE**

Second chapter of this thesis is the literature survey about the concept to give a review on the previous works done on this subject.

In chapter three experimental procedure and the methods used for experimental trials are explained; a brief description about the subjects of the study, measurement and observation devices, data gathering system and data analysis system has been made. Then the experimental results are shown in details and after each set of results a discussion has been made to make them clear. These results have been categorized to make them easier to perceive.

Fourth chapter is explaining the mathematical model and various cases that have been simulated upon it.

The final conclusion of the work and the plans for future works can be found in chapter five. At the end of the document, the references used in this work are stated.

## **CHAPTER2**

### **THEORETICAL BACKGROUND**

#### **2.1 GAIT AND POSTURE ANALYSIS**

The ability to stand is one of the humans' primary abilities; it forms in infancy but changes during whole life. The importance of this particular ability is due to the dependency of other activities on it. Additionally there are some diseases which can alter it and harden the humans' lives. These made the human posture a very important and popular field of study in time. There are numerous studies about posture stability, the factors affecting it and posture control system in literature.

In order to establish posture stability, the human body has to do a repetitive sequence of events constantly; postural control system needs to support body against gravity using body muscles, secure the stability of every element in body in case of movement of one of them, and maintain the balance of COP under the human's foot. The latter is because COP is affecting posture by its amplitude, velocity and acceleration [16].

The time to establish functional stability is a variable controlled in the maintenance of erect posture. Haibach et al., 2006 tested this with different surface types, under the condition of eyes-open and eyes-closed. Their experiments resulted in larger COP displacements for eyes-closed rather than eyes-open trials and shorter time to contact with the stability boundary for more compliant surfaces [16].

In Gerbino et al., 2007 the differences of balance abilities between dancers and soccer players has been compared using COP measurements. It is stated that since there is not any pre-defined and fixed measures or techniques of standing balance in the literature for discriminating between two groups, they have used a pressure mat to obtain COP signals and measurements such as sway index, center acquisition time, sway path length and sway velocity [17].

Standing balance is usually investigated in single-limb (unipedal) and two-limb (bipedal) trials with open-eyes and closed-eyes cases [18]. More recent works using tilting surfaces to disturb stability has been done. For instance Fong et al., 2006 showed that Tai Chi improves standing balance [19] and Schmitt et al., 2005 compared the unipedal standing time intervals for dancers before and after 5 months of training and found almost no difference [20].

For being able to maintain balance while standing still, the most important contributing senses of human body are listed below:

- Proprioception: the internal knowledge of a person about his/her body in space;
- Vestibular system: gives information about the person's head in space;
- Vision: gives information about changes in body (or head) position and helps to reduce the noise while the system tries to adjust for these changes.
- Somatosensory: gives information about the amount and distribution of pressure sensed beneath the foot, the type of the surface the person is standing on and etc.

Naturally a person with troubled proprioception still maintains balance using vestibular system and vision together.

Romberg's test (Romberg's sign) is a protocol used for testing the ability of standing balance. In this test the person is asked to stand still with eyes closed and a loss of balance will be a positive result. It is widely used by therapists to investigate the cause of ataxia -loss of motor coordination; if the test result is positive, the ataxia is

caused by sensory dysfunction otherwise it is caused by some physical problems such as cerebellar dysfunction [21].

In Nataraj et al., 2012 the effectiveness of feedback control systems for maintaining standing balance was compared between two types of feedback which were joint kinematics and COM<sup>4</sup> acceleration, both in a model and experimental data. The experimental data was the 3D position data gathered using a motion capture system. At the end concluded that COM acceleration was a more feasible feedback for control of standing balance. The study was done with the aim of assessing the performance of body control system after spinal cord injury [22].

Ambrozic et al., 2013 is a study about the sensory system of robotic lower-limb ortho-prostheses. They have used pressure insole sensors worn inside sneaker shoes for providing GRF distribution, alongside with inertial and magnetic measurement units attached to body segments which were used as markers for capturing body segments orientations. Experimental data was used to assess human motion kinematics. They have also observed that most of the unbalanced time of the subjects is at the beginning and ending of the trials and therefore it has been suggested that for being stable in their gait, humans take advantage of physical dynamics of the body during steady-state gait[23].

Most of the methods and techniques that are used in balance studies are based on COP which is usually measured using a force plate. In fewer studies there has been used a pressure assessment system such as a pressure mat instead. Force plates use the COG<sup>5</sup> and the GRF shifts in time to calculate COP but pressure assessment systems have many sensory elements and use the pressure distribution across the sensor grid to do the same.

## **2.2 QUIET STANCE**

Although in bipedal quiet stance human body seems to be relatively still, its mechanics is really dynamic and complex. People may think that they are standing

---

<sup>4</sup> Center of Mass, the point in which the whole body mass is concentrated

<sup>5</sup> Center of Gravity, vertical projection of COM on the ground

quiet still but in fact the human body moves constantly in a chaotic way and so does COP [24]. This chaotic pattern of movements is named postural sway.

Maintaining balance in erect posture involves a complex sensorimotor control system which produces erratic outputs [24]. This sway and its correlated noise are indistinguishable and therefore can be modeled as correlated random walks [25].

It has been stated in literature that the COM is located anterior to the second sacral vertebra for a person standing erect with both arms hanging at the sides [26] (Figure 2-1 shows some of anatomical terminology, especially body planes names which are used in this work).

It has been shown that most of the time people alter the contractile activity of the ankle joint dorsiflexors and plantarflexors in order to maintain balance[13]. Only in special circumstances the COM is located directly over the ankle joint axis and there is no need to any muscular contractile activity for ankle joint to maintain balance[27].

If COM is located anterior to ankle joint, an ankle joint plantarflexion<sup>6</sup> moment must be produced (by contractile activity of one or a combination of muscles such as gastrocnemius, soleus, deep posterior compartment or peroneal muscles) in order to keep the person balanced [27]. This way the plantarflexors of ankle joint increase their contractile activity to shift the COP anterior to the COG. This induces a posterior acceleration of COM causing its displacement in posterior direction. When this movement is rapid and vast enough the ankle joint dorsiflexors may be activated to shift the COP posterior to COM. This will cause a series of events that are the reverse form of the previous ones: an anterior acceleration of COM, a progressive deceleration of the posterior movement of the COM, a progressive acceleration of COM anterior movement. These events make COP oscillate in anterior-posterior direction, encounter the forward leaning of the person and maintain the balance of body in sagittal plane during quiet stance [13].

---

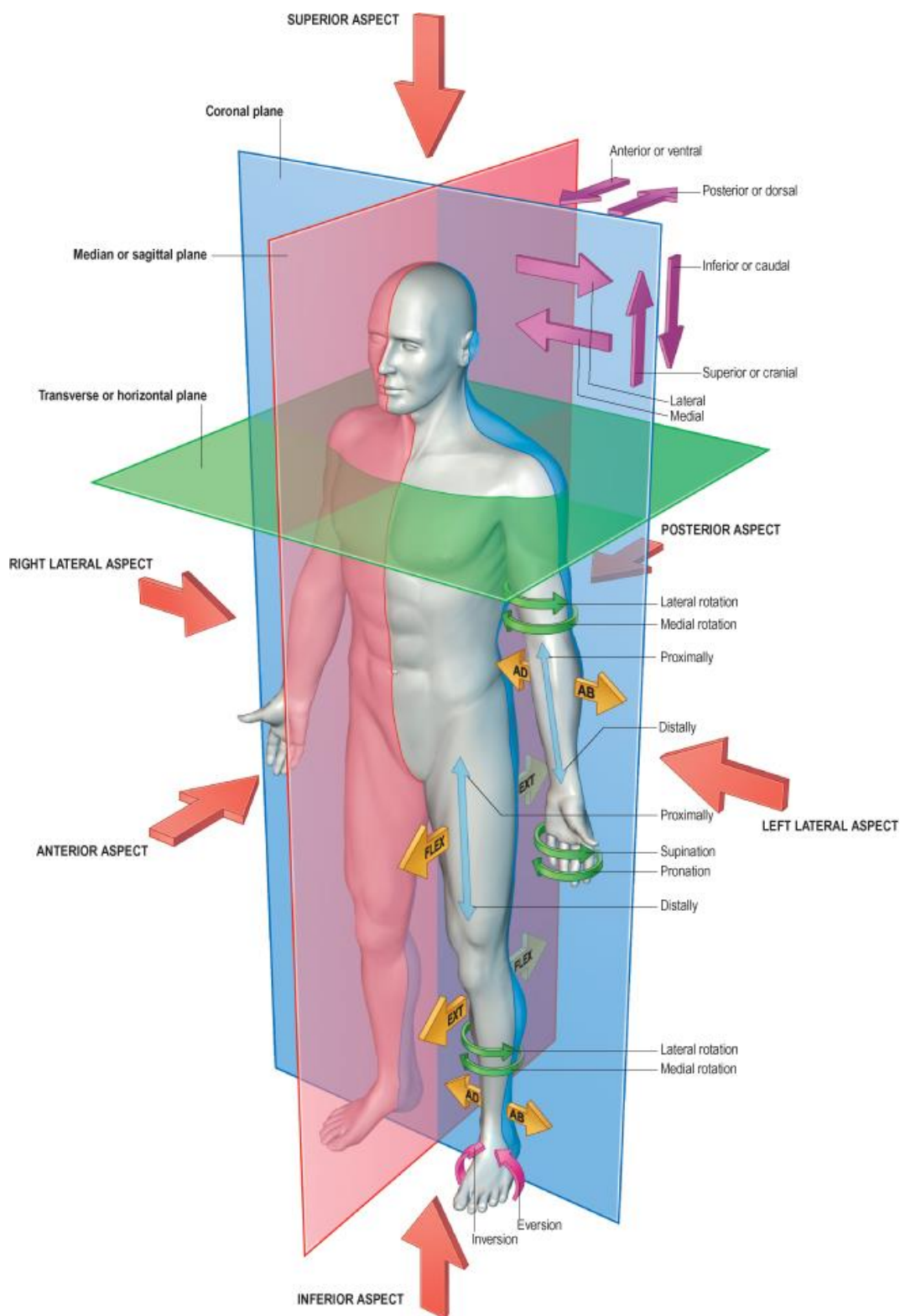
<sup>6</sup> Turning of foot (at ankle joint) or the toes, downward

The COM acceleration has a direct relationship with the distance between COP and COG. As a result the movement of COP should be greater than it for COG to cause their distance be large enough to generate the COM acceleration[13].

Similarly when COM is posterior to ankle joint, there should produce a dorsiflexion<sup>7</sup> moment for ankle joint (by contractile activity of one or a combination of the muscles such as anterior tibial, extensor hallucis longus, extensor digitorum longus and peroneus tertius muscles) to cause the COP to move in anterior to posterior direction of the plantar foot and act to counterbalance the backward leaning of the person[27].

---

<sup>7</sup> Turning of foot (at ankle joint) or the toes, upward



© Elsevier Ltd 2005. Standing: Gray's Anatomy 39e - [www.graysanatomyonline.com](http://www.graysanatomyonline.com)

**Figure 2-1** A brief review of physiological terminology (FLEX: flexion (of the thigh at the hip joint); EXT: extension (of the leg at the knee joint); AD: adduction; AB: abduction)[1]

### 2.3 FOOT MODELS IN LITERATURE

To investigate the characteristics and behavior of human foot during the stance phase of walking, Scott and Winter, 1993, have proposed a model in which the foot is presented as eight rigid segments and eight joints with one DoF<sup>8</sup>. The soft tissue under the foot is divided into seven independent load bearing sections and each of them is modeled as a nonlinear spring and damper [28].

Their simulation results suggested that when the forefoot is loaded, the contributing joints in the medial longitudinal arch get extended. The magnitude of the joint moments of force depended largely on the GRF distribution beneath the foot [28].

This model is useful for the connection that has been made between the arch deformation and GRF distribution. However, as authors stated, it is too complex for many specific questions regarding the foot function.

Simkin and Leichter in their 1990 study investigated the relationship between the energy stored in the medial longitudinal arch and the inclination of the calcaneus in the presence of a vertical load. They presented a two-dimensional model consisting of two rigid links which represent the bony elements of forefoot and hindfoot. A tension spring between two links, which is the energy-storing element of the model and the representation of the foot plantar ligaments as well, is forming the medial longitudinal arch. They concluded that the stored energy depends strongly on the calcaneal inclination. The energy storage capacity is low at both large and small inclinations and rises at an intermediate value and they suggested that the shape of foot structure can affect its load bearing capacity [29].

This model is very simple and easy to understand. Also it investigates the arch using PA which is the strategy of this thesis as well. But it does not take the damping effects into account.

Plantar fascia release is a surgical way of treatment for patients who suffer chronic heel pain. Kim and Voloshin in their 1995 work studied its effects on the load bearing ability of the foot. They concluded that the PA bears 14% of the load on the

---

<sup>8</sup> Degree of Freedom

foot and its release decreases the load by only 10%, thus it should not be a highly recommended solution. For this aim, they have presented a 2-dimensional biomechanical model of the medial aspect of the foot with 1-DoF. In this model PA was represented by characteristics of a muscle by a Kelvin model and the other muscles, tendons and spring effect of foot arch were modeled using a torsional spring and a torsional damper but both calcaneus and metatarsals were fixed joints, so the deformations of medial longitudinal arch were modeled by vertical movements of ankle joint [5].

A similar work is done by Gefen, 2002, presenting a 3D model for investigating the biomechanical effects of releasing the plantar fascia, designed according to geometric data of MRI, includes linear and non-linear elements for different tissue types such as bones, cartilage, ligaments and fat. The resulting GRF signals were compared with the measured GRF signals and they were similar [4].

The fascia has been modeled as a non-linear soft tissue with non-linear material properties taken from Kitaoka, et al., 1994 [30].

They observed that fascia release causes arch deformations during standing to be 2.5 mm greater than normal deformation and tension stresses on plantar ligaments increased and in some cases exceed the normal average stress by 200%. So the release of fascia must be very carefully considered [4].

The last two models are more realistic than the previous ones because they have considered PA as a deformable element, not just a rigid link. But they still have some weaknesses, for instance neither torsional springs nor dampers have physiological equivalents. Additionally there is a need for another DoF to model the deformations of the medial longitudinal arch and changes in the length of PA.

There are lots of other models and studies about foot structure but mostly they have focused on foot as a rigid structure. The minority of studies that have done the modeling as a deformable foot seem to lack some characteristics of PA or arch, such as the damping effects of PA or an additional DoF to show the deformations of the arch, as stated before.

## **CHAPTER3**

### **EXPERIMENTAL WORK**

#### **3.1 INTRODUCTION**

The purpose of this project as stated previously (in thesis statement) is to study the pattern of force and pressure distribution beneath the foot to perceive the concept of quiet stance and various behaviors of people. For this aim 14 healthy subjects with no lower limb disorder or injury have been examined and their motion data has been collected via pressure mat, force plate and 3D motion capture system. Then this data was analyzed using personalized specific MATLAB codes.

In “Methods” section the information about subjects, devices and data gathering methods and procedures are explained.

The “Pre-validation” section 3.3 with two subsections illustrates the pre-validation approaches on the collected data. The first approach is to check whether the outputs of two of the devices -pressure mat and force plate- agree with each other. The second approach is to observe and handle the data loss and errors in the dataset.

The next sections basically are the discussion part of the thesis and all the results obtained throughout this study are illustrated. The hypothesis has been being looked for in every step of these sections and is explained thoroughly in the subsections. Since the experiments have been done in two major conditions which are unipedal and bipedal conditions, the discussion has been done regarding to that categorization

too. Then inside each category different sub-conditions and parameters have been observed and analyzed.

### **3.2 METHODS**

14 healthy, active in their daily lives and without any visual handicaps participants consisting of 7 male and 7 female volunteered to participate in this study. Participants were students in Middle East Technical University and therefore were in a similar age range. Participants reported having no existing lower limb injuries or balance disorders and had not undergone any major lower limb surgery. A questionnaire was given which assessed subjects' height, weight, age, dominant foot and history of injuries.

A MatScan<sup>®</sup> 3150 pressure mat (TekScan, Inc.), a FP4060-07-1000 forceplate (Bertec, Co.) and a MVN Biomech 3D motion capture system (Xsens Inc.) each connected to a separate personal computer were used to collect the data of the subjects' posture. Computers were synchronized using an external pulse. The calibration procedure was done according to manufacturer's user's manual. All the measurements were taken at a sampling rate of 100 per second.

MatScan measures the vertical force applied to its sensory elements (sensels) and thereby calculates the COP signal based on the pressure applied in time. MatScan has a density of 1.4 sensels per cm<sup>2</sup> and contains a total of 2288 sensels in 435.9×368.8 mm<sup>2</sup>. The maximum pressure range is 862kPa.

The forceplate measures three force components along x, y and z axes and three moment components about x, y and z axes. These comprehensive outputs can be used to compute the COP signal. The FP4060-07-1000 forceplate has a maximum load capacity of 5000 N and hence it does not have any limits in our work range.

MVN Biomech is a 3D human kinematic measurement system which uses MEMS inertial sensors, sensor fusion algorithms and biomechanical models. This equipment is a full body system with 17 MTx inertial motion trackers but for this project's specific aim only the lower body sensors (7 trackers) were used.

All the experiments were done in quiet stance situation. The subjects had to stand still and try to get balanced while the posture data was collected. Because the aim of the study was to assess normal quiet stance, self selected foot placement was more appropriate so the participants were not limited or instructed about the place of their feet on the force plate or the style of their posture.

The data for each participant was collected in one session. All the tests were done barefoot. There were six scenarios for trials which are explained below in Table 3-1:

**Table 3-1 trial cases**

	<i>Bipedal</i>	<i>Unipedal-Right foot</i>	<i>Unipedal-Left foot</i>
<b>Eyes-closed</b>	BC	RC	LC
<b>Eyes-open</b>	BO	RO	LO

Each scenario was repeated three times, so all the subjects passed 18 trials. The sequence of trials was arranged randomly so the subjects could not look ahead the next case. Duration for unipedal cases was 30 seconds and for bipedal cases was 3 minutes. A 1-minute rest was allowed between trials and longer rests were possible on the need of the subject.

In Unipedal trials while the subjects were trying to get balanced on their test leg, the other leg was held with knee flexed and foot facing backwards so the angle of the knee was ninety degrees and the tibia parallel to the floor. Subjects were instructed to direct their focus straight ahead and could use their arms for balance freely. If the subject failed to maintain balance for a specific trial and touched the floor with the other foot, the data for that trial was discarded and the test repeated. A total of 3 retests were necessary because of such errors; one for a female subject and two for two different male subjects.

All the calculations and analyses were done using a code written in MATLAB® (Version 2012b, MathWorks, Inc.). Since for each case there were three

trials, an average of these trial measurements was used to provide a robust estimate for each individual.

Age, height and weight of the participants are tested using KS test and since they followed a normal distribution, they are expressed by the means and standard deviations in Table 3-2. Analysis of the data was performed using SPSS software package (Version 21, SPSS Inc.).

**Table 3-2 Participants demographics**

<i>Variable</i>	<i>All</i>	<i>Female</i>	<i>Male</i>
<b>Age(years)</b>	29.6±3.18	29.5±3.02	29.7±3.67
<b>Height(cm)</b>	169±9.53	162±4.45	179±4.55
<b>Weight(kg)</b>	65.46±13.57	55.81±8.194	78.33±6.088

All the equipments and methods were used to measure the data and compute the parameters in the sagittal plane because the model that has been simulated (and described in chapter 4) is based on the foot deformations in this plane.

### **3.3 PRE-VALIDATION**

#### **3.3.1 SIMILARITY BETWEEN COP<sub>x</sub> SIGNALS OBTAINED FROM FORCEPLATE AND PRESSURE MAT**

Firstly there was a need to investigate whether the data obtained from pressure mat had the same meaning as the data obtained from forceplate. For this purpose COP<sub>x</sub><sup>9</sup> signals from these two datasets were compared. As it is shown in equation 3-1 the difference of these two signals (COP<sub>x,f</sub> is the COP<sub>x</sub> signal obtained from force plate and COP<sub>x,p</sub> is the COP<sub>x</sub> signal obtained from pressure mat) was calculated point-to-point, relative to the COP<sub>x,f</sub> at that point then the averages for each of 6 types of cases were determined. The result of this comparison is shown in Figure 3-1.

---

<sup>9</sup> COP: Center of Pressure, the point of application of the Ground Reaction Force vector  
COP<sub>x</sub> is the component of COP in x direction

$$Err_{cop} = \frac{|COP_{x,f} - COP_{x,p}|}{COP_{x,f}} \times 100$$

3-1

In equation 3-1,  $COP_{x,f}$  has been taken as reference because almost all of the researches in literature are done based on force data.

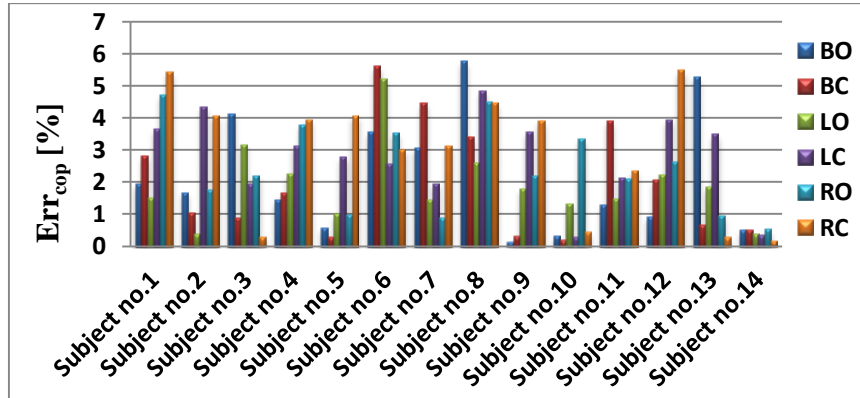


Figure 3-1 Average difference (in %) between  $COP_{x,f}$  and  $COP_{x,p}$  for each subject in every case

Figure 3-2 shows the percent error intervals for six experiment cases. For all data calculated here, Kolmogorov-Smirnov test was executed and since the data had normal distribution it could be represented by mean and STD<sup>10</sup>. This figure has been plotted using these statistical measurements, minimum/maximum values and the confidence intervals.

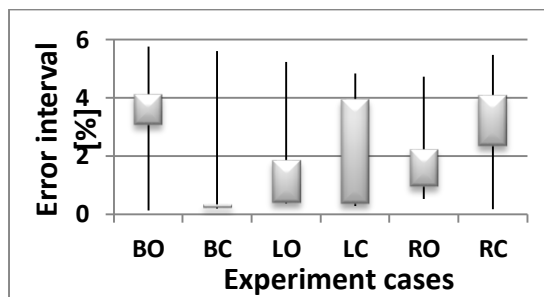
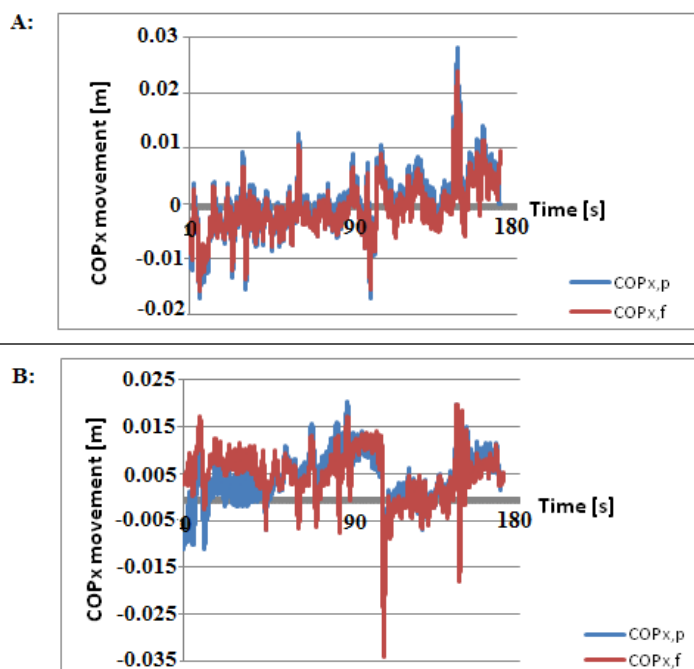


Figure 3-2 Percent error intervals for six experiment cases

<sup>10</sup> Standard Deviation

Figure 3-2 shows that most of these data points (92.86%) contain errors less than 5%. These two figures together show that the  $COP_{x,f}$  and  $COP_{x,p}$  signals are similar enough to ensure that the forceplate and pressure mat data carry the same meaning. As an example  $COP_{x,f}$  and  $COP_{x,p}$  are shown together in one plot in Figure 3-3.



**Figure 3-3**  $COP_{x,f}$  and  $COP_{x,p}$  for one trial of a subject: A) BO case with 1% error, B) BC case with 8% error

### 3.3.2 DATA LOSS

One important problem to study was the distribution of ground reaction force. Using the data from pressure mat the distribution of pressure in two regions is calculated,  $M_y$  (pressure distribution in metatarsals) and  $C_y$  (pressure distribution in calcaneous).

Figure 3-4 shows one frame of pressure data in a unipedal trial. In every frame the region of sesamoid is selected as  $M_y$ . The lower boundary of this region is shown by the black line in the figure; toes are not included in this region. Similarly the hint region of foot is selected for  $C_y$ .

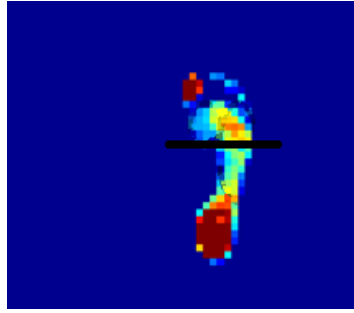


**Figure 3-4  $C_y$  and  $M_y$  regions of foot shown on a data frame**

As an assurance, the error of  $C_y + M_y$  from total  $mg$  is calculated as shown in equation 3-2 for each data point:

$$Err_{mg} = \frac{|mg - (C_y + M_y)|}{mg} \times 100 \quad 3-2$$

Then the average  $Err_{mg}$  is calculated for three cases: bipedal, unipedal (right foot), unipedal (left foot). In bipedal case the subjects were expected to stand in a quiet steady state but in unipedal case they were not stable most of the time. The unipedal trials have been checked several times to discard the ones in which the subjects have touched the ground by the other foot but they are not checked if the subjects have touched the walls by their hands or other similar scenarios. In such cases there may be great data losses.

Another path for data loss can be hardware malfunctions, environmental noise and random behavior of subjects. Regardless of the reason, it reduces the quality of results.

The results are shown in Figure 3-5 and can be summarized as below:

- After this step one trial was discarded due to high  $Err_{mg}$ . It was a BO case with error equal to 10.98 .
- KS test showed that errors for each subject have a normal distribution. The total set of the errors has a mean of 7.004% and STD of 2.148%.
- As expected before, errors in unipedal cases are mainly greater than bipedal cases.

- A total of 11 out of 14 subjects have all of their  $Err_{mg}$  factors less than 10%.
- All of bipedal errors are less than 8%.
- Although we expected unipedal errors to be greater than bipedal errors for all the subjects but there are 3 subjects whose ‘Unipedal-left’ error is less than bipedal error and 4 subjects whose ‘Unipedal-right’ error is less than bipedal error.

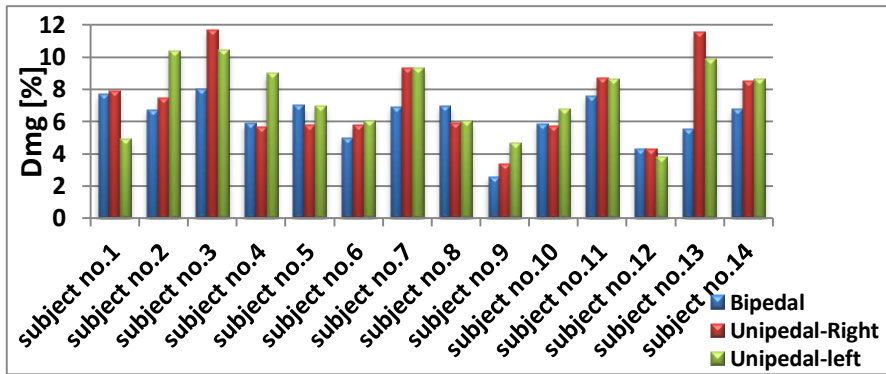


Figure 3-5 Percentage error of  $C_y+M_y$  from  $mg$

### 3.4 RESULTS AND DISCUSSION

#### 3.4.1 GROUND REACTION FORCE DISTRIBUTION IN BIPEDAL

As it is stated before in 1<sup>st</sup> chapter, the literature shows that the ground reaction force has a general pattern of 1/3 in metatarsals and 2/3 in calcaneous.

Figure 3-6 to Figure 3-9 show the average  $R_{mg}$  (portion of ground reaction force in calcaneous-to be 2/3, explained in equation 3-3) and the average relative error of this ratio towards 2/3 (3-4).

$$R_{mg} = \frac{C_y}{C_y + M_y} \quad 3-3$$

$$Err_{\frac{2}{3}} = \frac{|\frac{2}{3} - R_{mg}|}{\frac{2}{3}} \times 100 \quad 3-4$$

As it can be seen in the figures, the ratio is not fixed on  $2/3$  in time but it is not a bad result because the errors are quite meaningful. In bipedal case (Figure 3-6, BO and BC cases together) the errors are too small, even the maximum error is less than 7% which is a fine value to show that in this study the “ $1/3$  &  $2/3$ ” rule has been observed.

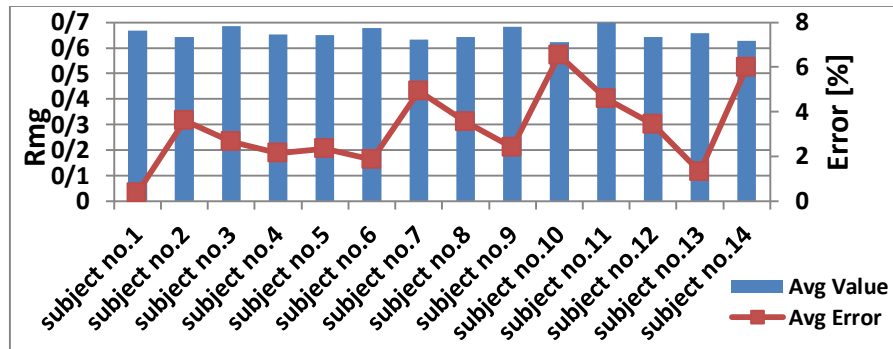


Figure 3-6 Average  $R_{mg}$  & average  $Err_{2/3}$  for both bipedal open-eyes and bipedal closed-eyes cases

Figure 3-7 shows the ratio of  $\frac{C_y}{C_y+M_y}$  in a specific trial for one of the subjects. The two red lines indicate the range for the ideal value of  $2/3$  with 5% tolerance, i.e. the interval from 0.63 to 0.7. Parts of the plot which are located between these two lines show the period of time during which the “ $1/3$  &  $2/3$ ” rule is valid (with 5% tolerance). This time period is called “*validation time*”.

When the plot passes one of these red lines it means that the  $\frac{C_y}{C_y+M_y}$  ratio is changing from within the valid interval towards the values that violate the “ $1/3$  &  $2/3$ ” rule. Hence the subject has undergone instability and has changed his/her COP to get restabilized, resulting in changes in the values of  $C_y$  and  $M_y$  relatively.. The number of times that the plot passes these two lines is called the “*Instability factor*”. Since the duration of unipedal and bipedal trials are not the same, this factor has been normalized by time to make it possible to be compared among different cases.

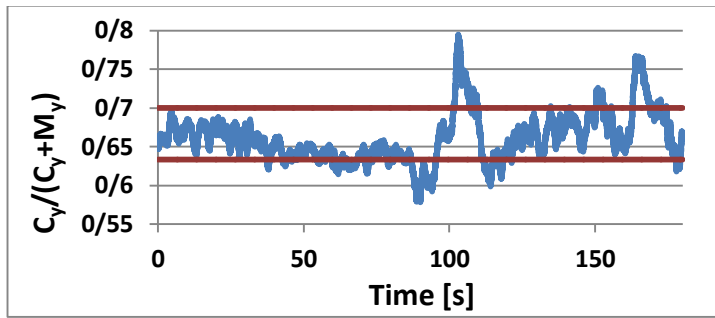


Figure 3-7  $C_y/(C_y+M_y)$  ratio compared to the ideal interval

Figure 3-8 shows that each subject at least in 73.7% of his/her total bipedal (both open-eyes and closed-eyes cases) experimental time is experiencing the “1/3 & 2/3” rule. The average validation time for all of the subjects is 92.168% and the STD is equal to 8.555% with 9 subjects having their validation times greater than 90%, which is a reasonable fraction of time to be complying the rule.

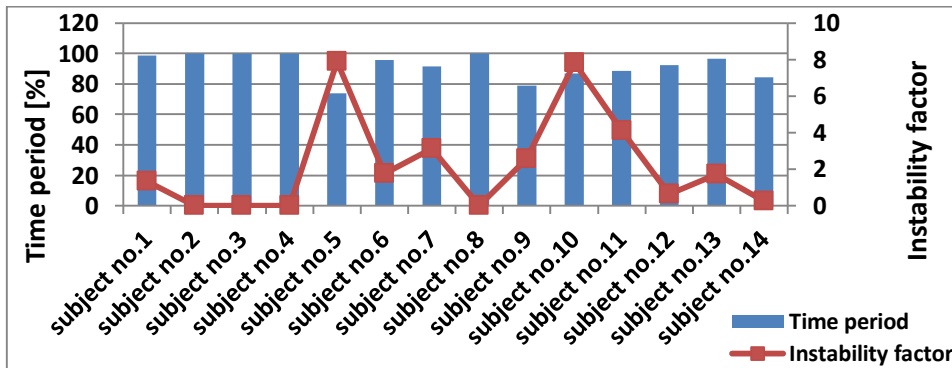


Figure 3-8 Overall validation time and instability factor in bipedal case (both open-eyes and closed-eyes cases)

The figure shows the relationship between instability factor and validation time. Subjects who comply the rule in almost 100% of the time have instability factor near to zero. When validation time decreases, the factor increases, as for subject no.5 which has the least time period and the largest instability factor. As it is shown in

Table 3-3 the correlation between instability factor and validation time is almost -1 for all of the subjects.

### 3.4.1.1 CLOSED-EYES VERSUS OPEN-EYES

In Figure 3-9 and Figure 3-10 same parameters are shown as Figure 3-8 but distinctly for BO and BC cases. As a comparison between these two cases the mean values for validation times can be stated which are 94.387% for BO and 89.422% for BC. T-test between these two cases showed that they do not differ significantly (t-value equal to 1.13). Although the difference is not large enough but the slightly longer validation time for BO shows that in open-eyes cases subjects were more stable and the “1/3 & 2/3 rule” was less violated. 9 subjects have their BC validation time period shorter than their BO validation time.

Similarly t-test showed no significant difference for the instability factor between BO and BC (t-value equal to 0.78). The average instability factor is 2.23 for BO and 0.89 for BC and there are only 3 subjects who have a greater instability factor in BO rather than BC. So despite no significant difference due to t-test results, it seems like most of the subjects have greater values for instability factors in BC and greater instability factor means more times to experience instability thus shorter validation periods.

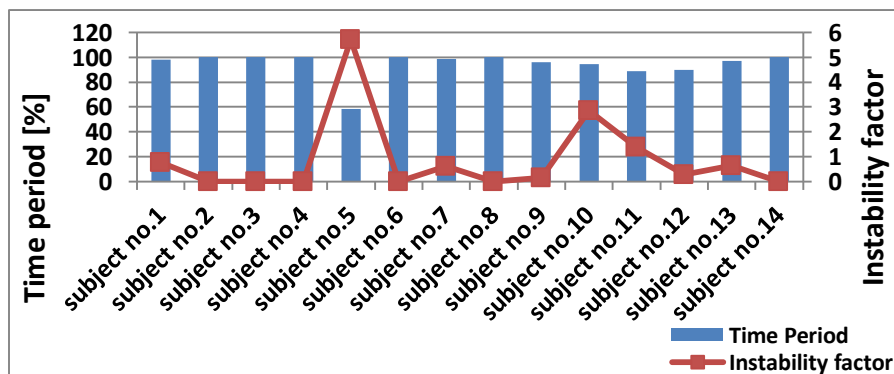


Figure 3-9 Validation time percentage and instability factor in BO case

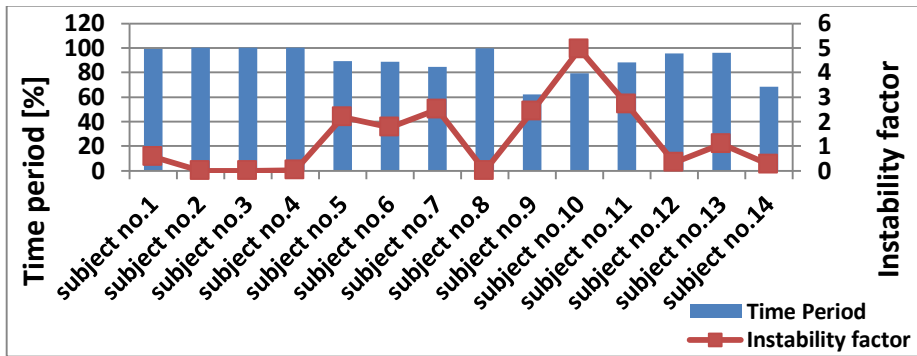


Figure 3-10 Validation time percentage and instability factor in BC case

Table 3-3 confirms the observations of the last three figures. In this table the correlation between instability factor and the validation time is listed in three categories: bipedal open-eyes, bipedal closed-eyes and all of bipedal trials. Most of the correlation rates are negative values between -0.9 and -1 and the average correlation in total is -0.91.

Table 3-3 Correlation between instability factor and validation time

	<i>Bipedal (BO &amp; BC)</i>	<i>BO</i>	<i>BC</i>
<i>subject no.1</i>	-0.96	-1.00	-1.00
<i>subject no.2</i>	-1.00	-0.98	-0.99
<i>subject no.3</i>	-0.99	-1.00	-0.98
<i>subject no.4</i>	-1.00	-0.98	-1.00
<i>subject no.5</i>	-0.92	-1.00	-1.00
<i>subject no.6</i>	-1.00	-1.00	0.43
<i>subject no.7</i>	-0.78	-1.00	-0.92
<i>subject no.8</i>	-1.00	-1.00	-0.90
<i>subject no.9</i>	-0.97	-0.64	-0.92
<i>subject no.10</i>	-0.80	-0.79	-0.78
<i>subject no.11</i>	-0.69	-0.82	-0.87
<i>subject no.12</i>	-0.66	-0.98	0.52
<i>subject no.13</i>	-0.99	-1.00	-1.00
<i>subject no.14</i>	-1.00	-0.98	-1.00

In Table 3-4 the top right cell is the condition that is in favor of our assumptions. It means validation time is larger and instability factor is smaller in open-eyes trials than closed-eyes ones. In bipedal trials 10 out of 14 subjects (71.4%) follow this

pattern. These are the majority of subjects' population that comply a common behavior. All of the left-footed subjects are in this group.

**Table 3-4 Validation time and instability factor in bipedal trials; TO: validation time in open-eyes case, TC: validation time in closed-eyes case, FO: instability factor in open-eyes case, FC: instability factor in closed-eyes case**

	$T_o < T_c$	$T_o > T_c$
$F_o < F_c$	1	10
$F_o > F_c$	2	1

#### **3.4.1.2 RIGHT FOOT VERSUS LEFT FOOT**

In a first glance it looks like the dominant foot in every person may bear more load than the other foot while standing still. But the measurements showed exact opposite of this thought. Figure 3-11 shows  $M_y$  and  $C_y$  signals for both feet in the same bipedal trial.

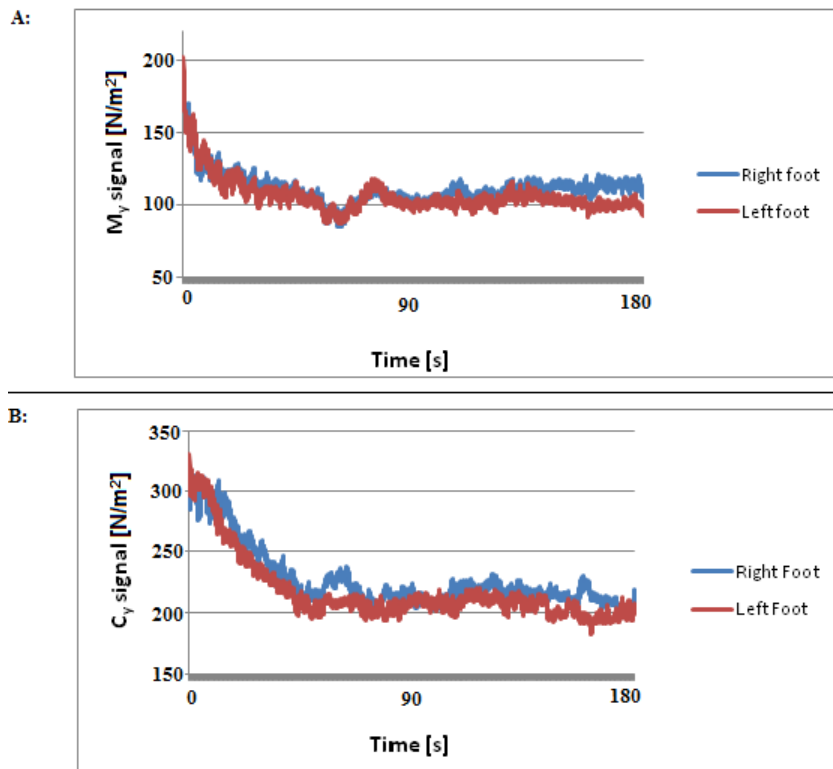


Figure 3-11 Charts of a bipedal case for a specific subject, A)  $M_y$  plot, B)  $C_y$  plot

The first quarter of the plots are not established a steady state yet, so there seem to be a high noise in those parts. The signals in each of A and B parts of this figure are so similar to each other.

The ratio of average  $M_y$  for right foot over left foot and the ratio of average  $C_y$  for right foot over left foot were calculated. The first ratio is 1.052 and the second one is 1.045; both of them so near to 1. Additionally the scatter charts of R  $M_y$  ( $M_y$  for right foot) in regard to L  $M_y$  ( $M_y$  for left foot) and R  $C_y$  ( $C_y$  for right foot) in regard to L  $C_y$  ( $C_y$  for left foot) are plotted in Figure 3-12 and Figure 3-13 respectively. The trendlines have been plotted for each of them and the equations of those lines were shown on the figures. Both trendlines have slopes about 1, which shows that not only the mean values ratios are near to 1, but also the data point to data point ratios for all points are near to 1. This shows that both feet are functioning so similar in the sense of ground reaction force bearing.

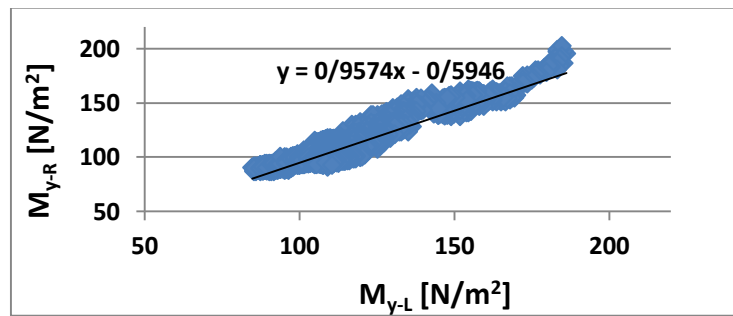


Figure 3-12 My-R in regard to My-L with trendline in a specific bipedal trial

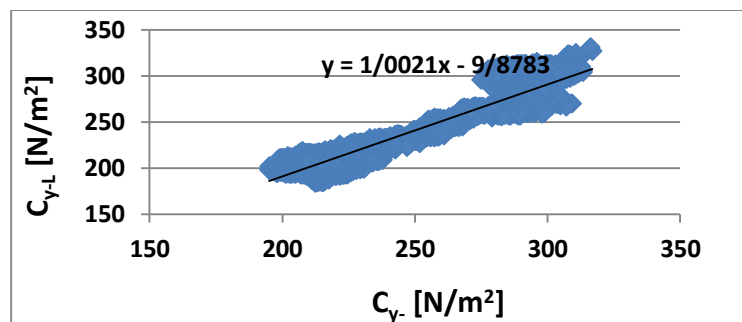


Figure 3-13 Cy-R in regard to Cy-L with trendline in a specific bipedal trial

A t-test between  $RM_y$  and  $LM_y$  resulted in t-values which were larger than the tabulated value in t-table, so it showed that  $RM_y$  and  $LM_y$  were significantly different. Same results were concluded when a t-test was done for  $RC_y$  and  $LC_y$ . The resulted t-values are shown in Table 3-5.

**Table 3-5 t-values resulted from t-test for comparing  $M_y$  and  $C_y$  between right and left feet**

	<i>t-values between <math>RM_y</math> &amp; <math>LM_y</math></i>	<i>t-values between <math>RC_y</math> &amp; <math>LC_y</math></i>
<i>subject No.1</i>	57.89	83.15
<i>Subject No.2</i>	82.11	46.33
<i>Subject No.3</i>	231.53	349.81
<i>Subject No.4</i>	271.82	251.18
<i>Subject No.5</i>	227.67	335.33
<i>Subject No.6</i>	127.66	137.38
<i>Subject No.7</i>	61.55	105.14
<i>Subject No.8</i>	193.60	420.47
<i>Subject No.9</i>	82.69	128.20
<i>Subject No.10</i>	91.27	117.92
<i>Subject No.11</i>	51.00	115.30
<i>Subject No.12</i>	839.11	838.92
<i>Subject No.13</i>	24.34	69.00
<i>Subject No.14</i>	54.04	136.11

### **3.4.1.3 DOMINANT VERSUS NON-DOMINANT FOOT**

For more details the ratio of  $\frac{M_{y-R}}{M_{y-L}}$  was calculated for all bipedal trials. According to KS test these values were following a normal distribution and their mean and STD were 1.054 and 0.146 respectively.

Since more eccentric results were expected for left footed subjects, they were studied separately here. 3 out of 14 subjects were left footed. Their  $\frac{M_{y-R}}{M_{y-L}}$  ratios had smaller values than right footed subjects. Although in previous section it was seen that left and right feet act so similar to each other but still there is a slight difference between them, which makes  $M_{y-R}$  greater than  $M_{y-L}$  for right footed and vice versa for left footed people.

Similarly the ratio of  $\frac{C_{y-R}}{C_{y-L}}$  was calculated. Again the values were following a normal distribution and their mean and STD were 1.046 and 0.167 respectively. And the same observations were made about this ratio for left footed subjects. It was concluded that the  $C_y$  and  $M_y$  for dominant foot are always a bit greater than they are

in the other foot though their ratio is almost 1. Figure 3-14 shows the  $\frac{C_{y-R}}{C_{y-L}}$  and  $\frac{M_{y-R}}{M_{y-L}}$  ratios for all of the subjects.

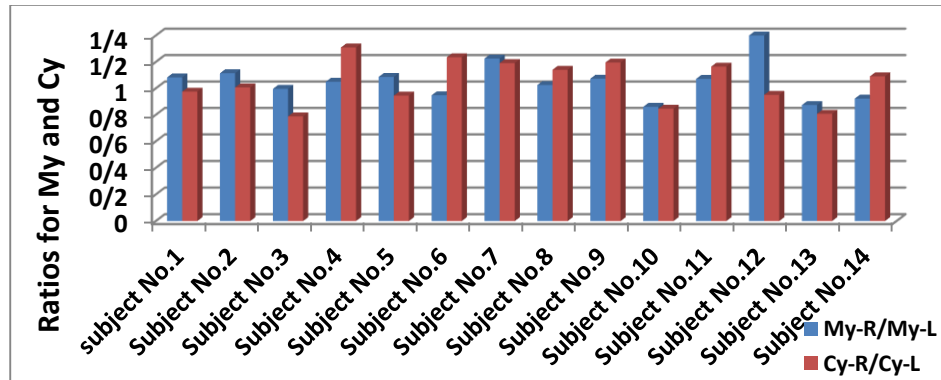


Figure 3-14 Average  $\frac{C_{y-R}}{C_{y-L}}$  and average  $\frac{M_{y-R}}{M_{y-L}}$  for 14 subjects in bipedal cases, subjects 3, 10, 13 are the left footed ones

### 3.4.2 GROUND REACTION FORCE DISTRIBUTION IN UNIPEDAL

Following two figures are showing the values for parameters explained in equations 3-3 and 3-4 in unipedal cases. Obviously the errors are greater than the ones indicated in Figure 3-6 for bipedal. In unipedal-R case (Figure 3-15) there are errors up to 25% and in unipedal-L case (Figure 3-16) although errors for half of the subjects are less than 5%, the other half's errors are more than 10%. But for bipedal case (Figure 3-6) the errors were less than 7% for all of the subjects. These are really large errors but they are not unexpected. All of them are happening due to frequent instabilities in unipedal stance. Because the subjects were trying to stand still on one foot, they were placing the majority of their ground reaction force in every part of the foot to find the best place to be stable. While doing this they could not keep the theoretical ratio between  $C_y$  and  $M_y$  and this is the reason of high errors. Since in bipedal cases such instabilities occur rarely, errors are less than unipedal cases.

A t-test was done comparing  $C_y$  and  $M_y$  values between unipedal-right and unipedal-left cases. All of the calculated t-values were smaller than the tabulated t-values and

this showed that there was no significant difference between  $RM_y$  and  $LM_y$  in unipedal cases, or between  $RC_y$  and  $LC_y$ .

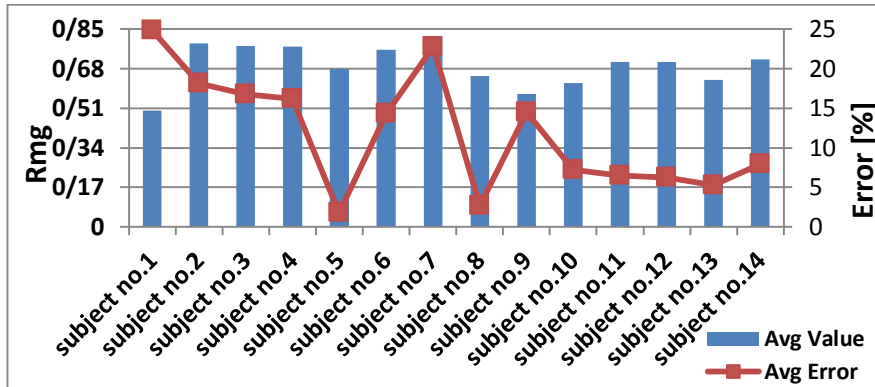


Figure 3-15 Average  $R_{mg}$  & average  $Err_{2/3}$  in unipedal-R case, subjects 3, 10, 13 are left footed

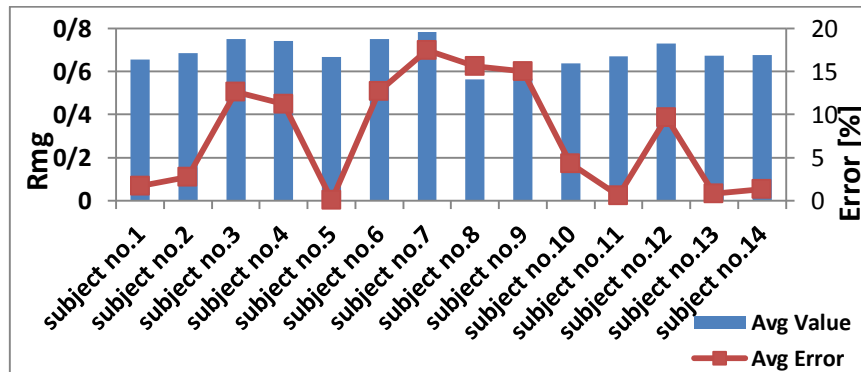


Figure 3-16 Average  $R_{mg}$  & average  $Err_{2/3}$  in unipedal-L case, subjects 3, 10, 13 are left footed

Figure 3-17 shows the overall validation time percentage and instability factor in unipedal cases. Due to this figure, it is very clear that unipedal results do not comply with the rule for a convincing period of time. The validation time has an average of 78.253% and STD of 24.832% and the total instability factor equals to 105.27.

This rule has a very important role in this thesis because it shows the stability of normal standing method. When this rule is violated, it means that the foot has lost its stability and needs to use different regions of its surface, focus the ground reaction force on those regions and try to stabilize. This leads to a decrease in  $C_y$  and increase in other pressure elements. The specific element that has been looked for is  $M_y$ , because the main idea is when losing stability, transferring the larger part of foot pressure to  $M_y$  is one of the strategies to gain stability back. So the subjects try to use some rapid transfers on metatarsals to keep themselves standing still and stable.

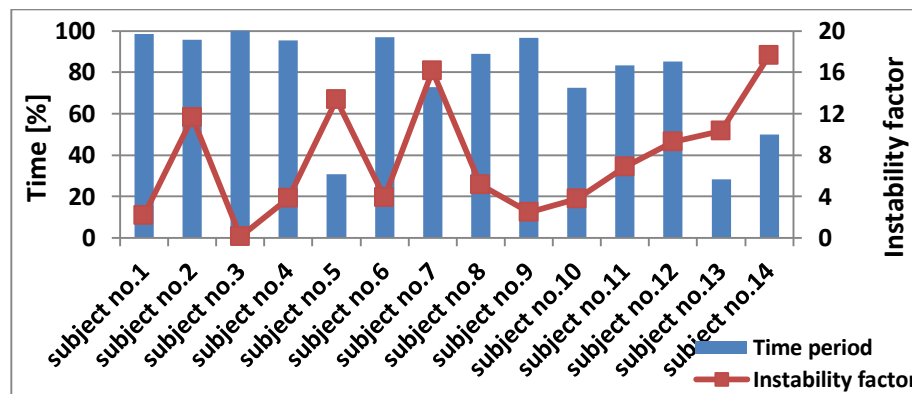


Figure 3-17 Overall validation time and instability factor for all subjects in unipedal, subjects 3, 10, 13 are left footed

Figure 3-17 is a very interesting plot because it shows a wide range of behaviors some of which are described below:

- In theory validation time has an inverse relation with instability factor. By increasing each one the other one decreases.

In this experiment there are exceptions for this rule such as subject no.7. It can be due to the stance strategies of these subjects. For instance subject no.7 has a large instability factor so we expect him/her to have a very short validation time but it is not this way. Every time this subject undergoes instability, he/she can outdo it easily and goes back to validation region instantly. The other subjects behavior can be explained this way too.

- Subject no.3 has instability factor equal to 0, so this subject has experienced no instability and the validation time of 100% confirms this too.
- Subject no.12 and no.13 both have instability factors near to 300 but subject 12 has a high validation time near 80% and subject 13 has a validation time near 30%. Again this can be due to differences in their stance strategies. When subject 12 experiences an instability he/she could tolerate it very quickly and went back to his/her stable state and established the “1/3 & 2/3” rule instantly. But subject 13 by arising each of these instabilities could not tolerate it easily and stayed out of validation range in most of the time.
- The largest instability factor is shown for subject no.14 which is equal to 539 and the validation time is 49.793%. Even having the largest factor, this subject’s validation period is not the smallest one. It can be explained by the weaknesses in stance strategies too.
- The instability factor of subject no.11 is larger than subject no.10 but their validation time does not follow this sequence. Validation time of subject no.11 is expected to be shorter than validation time of subject no.10 but it is longer.

#### **3.4.2.1 CLOSED-EYES VERSUS OPEN-EYES**

In unipedal trials when it was a case of closed-eyes, the subjects seemed to undergo more troubles to keep their stability. This observation suggests that open-eyes cases are more stable than closed-eyes cases. For this aim the ground reaction force distribution is investigated. Both  $C_y$  and  $M_y$  are traced in time for each trial and the overall validation time is calculated.

Figure 3-18 and Figure 3-19 show the validation period and instability factor for RO and RC cases while Figure 3-20 and Figure 3-21 show same parameters for LO and LC cases, respectively.

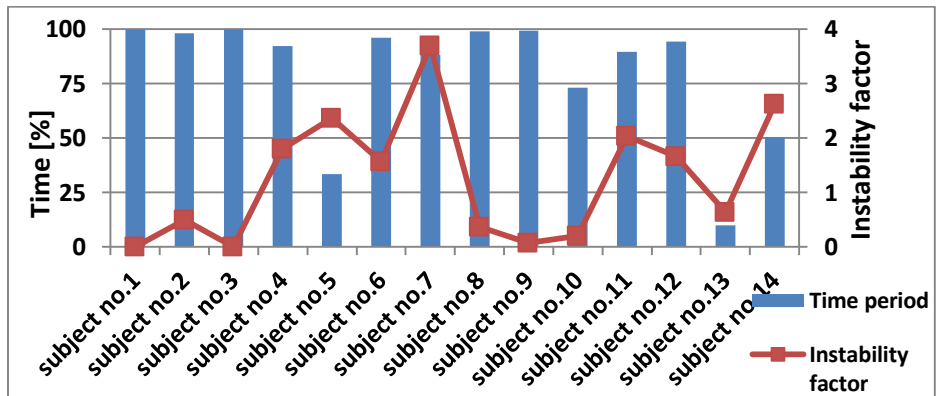


Figure 3-18 Validation time and instability factor for all subjects in RO, subjects 3, 10, 13 are left footed

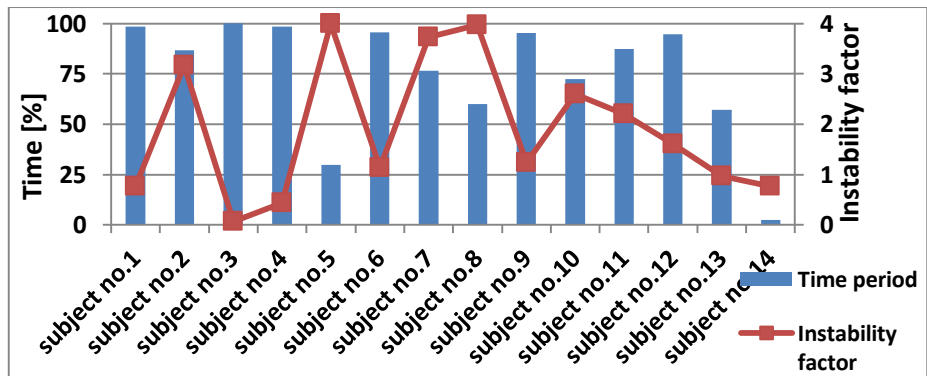


Figure 3-19 Validation time and instability factor for all subjects in unipedal/RC, subjects 3, 10, 13 are left footed

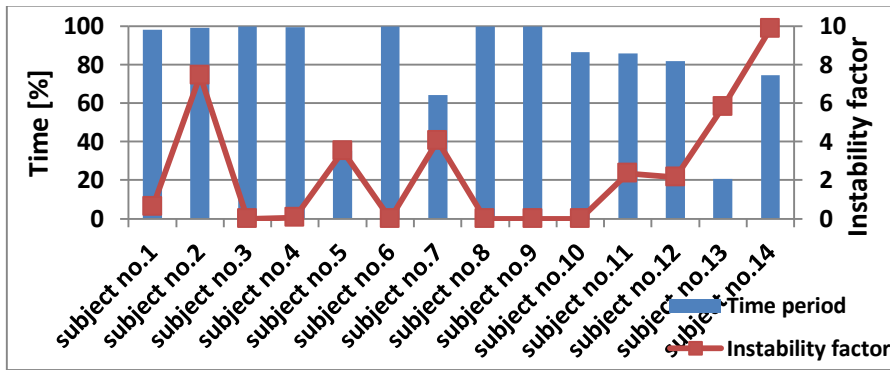


Figure 3-20 Validation time and instability factor for all subjects in unipedal/LO, subjects 3, 10, 13 are left footed

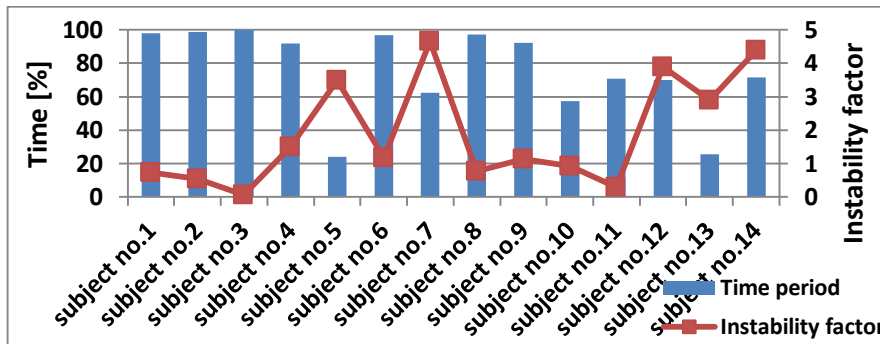


Figure 3-21 Validation time and instability factor for all subjects in unipedal/LC, subjects 3, 10, 13 are left footed

Since KS test proved these values to be following the normal distribution, the average and STD values are shown in Table 3-6 for each case.

Table 3-6 Mean and STD for validation time and total instability factor in different cases

	Validation time Average [%]	Validation time STD [%]	Total instability factor
<b>RO</b>	80.318	28.009	526
<b>RC</b>	75.327	29.193	799
<b>LO</b>	81.876	25.571	935
<b>LC</b>	75.491	26.032	796

Studying these four figures together gives us more information to understand the closed and open-eyes conditions some of which are summarized below:

- Comparing the validation time in unipedal-right foot trials, there are 11 subjects with larger and 3 with smaller values in open-eyes than closed-eyes. The same comparison in left foot trials shows 13 larger and 1 smaller in open-eyes than closed-eyes.
  - In both unipedal-right and left cases, comparing the instability factors shows that 10 subjects have smaller factors and 4 subjects have larger factors in open-eyes than closed-eyes.
  - Not all the subjects have the same path of variation, meaning if one subject has a smaller validation time in RO rather than RC, the respective instability factor in RO is not necessarily smaller or larger than it is in RC.
  - More details about these observations can be described as in Table 3-7 and Table 3-8.

**Table 3-7 Validation time and instability factor in unipedal-right trials;  $T_o$ : validation time in open-eyes case,  $T_c$ : validation time in closed-eyes case,  $F_o$ : instability factor in open-eyes case,  $F_c$ : instability factor in closed-eyes case**

	$T_o < T_c$	$T_o > T_c$
$F_o < F_c$	1	11
$F_o > F_c$	2	0

**Table 3-8 Validation time and instability factor in unipedal-left trials**

	$T_o < T_c$	$T_o > T_c$
$F_o < F_c$	0	10
$F_o > F_c$	0	4

Top right cell of these tables are the condition that is in favor of our assumptions. They show the subjects who have larger validation time and smaller instability factors in open-eyes trials rather than closed-eyes ones. It shows that for unipedal-right foot trials 11 out of 14 subjects (78.6%) and for unipedal-left foot trials 10 out of 14 subjects (71.4%) follow this pattern, 7 of which are common. These are the majority of subjects' population that comply a common behavior. All of the left-footed subjects have their validation time and instability factor in the range of last column.

### 3.4.2.2 DOMINANT VERSUS NON-DOMINANT FOOT

One other idea is dominant foot being stronger than non-dominant one, so standing unipedal on dominant foot would be more stable than standing on non-dominant foot. Hence validation time would be larger while instability factor is smaller for dominant feet. Having a second look on Figure 3-19 to Figure 3-22 and extracting the behavior of left-footed and right-footed subjects on their dominant and non-dominant foot trials, Table 3-9 to Table 3-12 were generated.

**Table 3-9 Right-footed subjects' behavior in unipedal open-eyes trials,  $T_R$ : validation time in unipedal-right foot case,  $T_L$ : validation time in unipedal-left foot case,  $F_R$ : instability factor in unipedal-right foot case,  $F_L$ : instability factor in unipedal-left foot case**

	$T_R < T_L$	$T_R > T_L$
$F_R < F_L$	2	4
$F_R > F_L$	5	0

**Table 3-10 Left-footed subjects' behavior in unipedal open-eyes trials**

	$T_R < T_L$	$T_R > T_L$
$F_R < F_L$	2	0
$F_R > F_L$	1	0

**Table 3-11 Right-footed subjects' behavior in unipedal closed-eyes trials**

	$T_R < T_L$	$T_R > T_L$
$F_R < F_L$	2	3
$F_R > F_L$	2	4

**Table 3-12 Left-footed subjects' behavior in unipedal closed-eyes trials**

	$T_R < T_L$	$T_R > T_L$
$F_R < F_L$	0	2
$F_R > F_L$	0	1

For right-footed subjects the top right cell and for left-footed subjects the bottom left cell are the ideal conditions. According to these tables, in open-eyes case there were 4 right-footed subjects who had longer validation time and smaller instability factor for unipedal-right trials rather than unipedal-left. The number of left-footed subjects is too few to make a statement about their behavior. For right footed subjects again it is not possible to make a strong statement because number of subjects in every condition is less than half of them and the numbers of subjects in the other conditions are not small. In closed-eyes case, the number of subjects in the ideal condition is 3 which is even smaller than before.

Unlike bipedal case, no evidence was found here to prove the strength of dominant foot regarding to non-dominant one.

### **3.4.2.3 GROUND REACTION FORCE DISTRIBUTION ALONG LATERAL-MEDIAL DIRECTION**

In all sections of the thesis till here, ground reaction force distribution was studied along anterior-posterior direction; in this section as a new approach, it was studied along lateral-medial direction.

The frames of pressure data has been masked by a frame containing two ovals. One of these ovals is used to mask a specific region of the foot in sesamoid (which is

called ROI<sup>11</sup> now on) while the other is used to mask the lateral part of the foot (Lat) excluding calcaneus and its adjacent parts. The area of ROI is nearly 1/3 of Lat. Figure 3-22 shows a masked frame of data as an example.

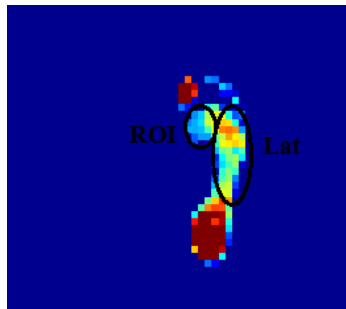


**Figure 3-22 ROI and Lat regions of foot shown on a data frame**

For every frame of data, the mean pressures for each oval have been calculated and compared with each other. Then the time period in which  $ROI \geq Lat$  has been calculated. This is the time during which the ROI part of the foot bears more pressure than the Lat part, meaning that the subjects are using their ROI more than Lat for restabilizing when their stability has been disturbed. This is done using the previously used strategy which is showed again in

Figure 3-23. The two red lines show the values of “1-0.05” and “1+0.05”. When the  $\frac{ROI}{Lat}$  plot is between these two lines it is considered to have the relation of  $ROI = Lat$  and when the plot is on the top of the “1+0.05” line it is considered to have the relation of  $ROI > Lat$ . The time during which these two conditions are valid, is called “ROI validation time” now on. The number of times that  $\frac{ROI}{Lat}$  plot passes these two lines -normalized by the time duration of the trial- is called “ROI instability factor”. This factor shows the number of times that the subject has changed the focus of pressure between ROI and Lat. The mean value of these time

---

<sup>11</sup> Region of Interest

periods is 70.4654% and the STD equal to 30.743% with a total factor equal to 145.17. These parameters are shown in Figure 3-24.

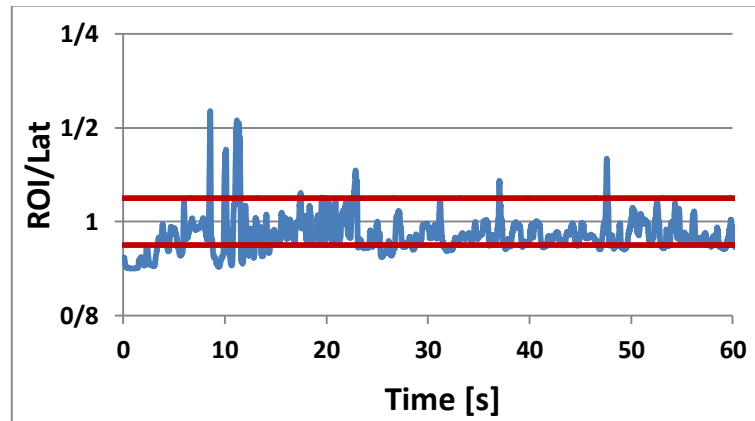


Figure 3-23 ROI/Lat ratio compared to the ideal interval

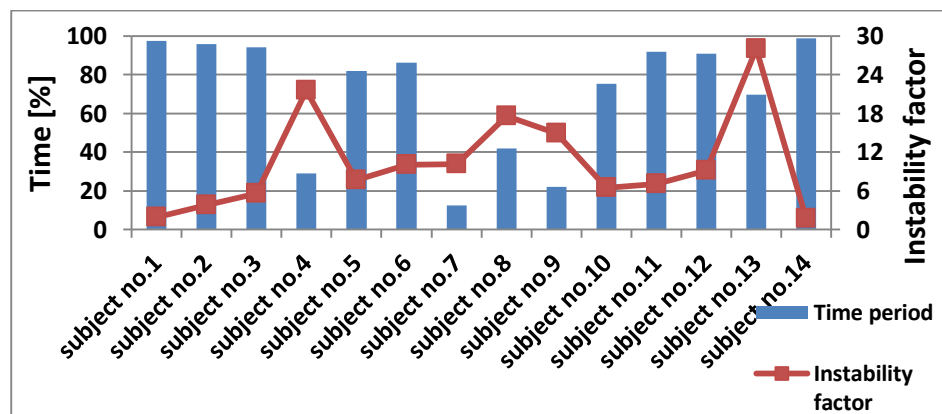


Figure 3-24 Overall ROI validation time and ROI instability factor in unipedal trials

Observations in this part, which led to Figure 3-24 indicate that in case of stability being disturbed, making metatarsal to bear most of the pressure beneath foot, helps more than any other strategy –such as meeting the lateral part of the foot- to regain the stability. Even though *Lat* has a larger area than *ROI*, subjects prefer to use *ROI* more than *Lat*. In Figure 3-25 to Figure 3-28 same parameters are shown as Figure 3-24 but for the specific cases RO, RC, LO and LC respectively.

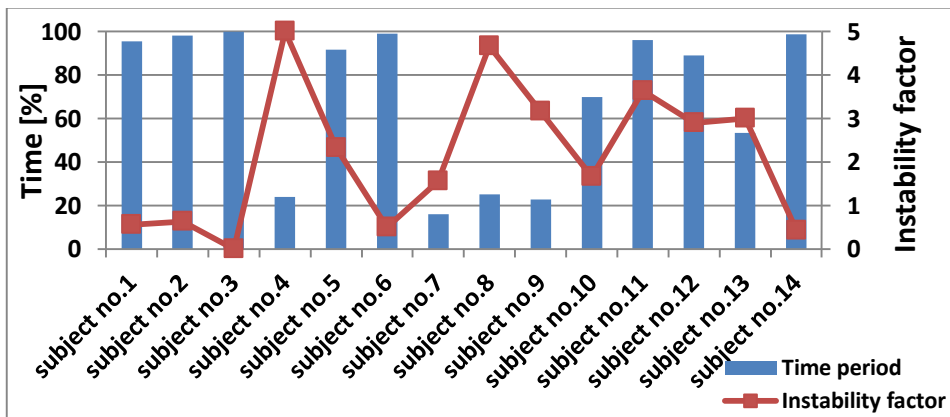


Figure 3-25 ROI validation time and ROI instability factor in RO case

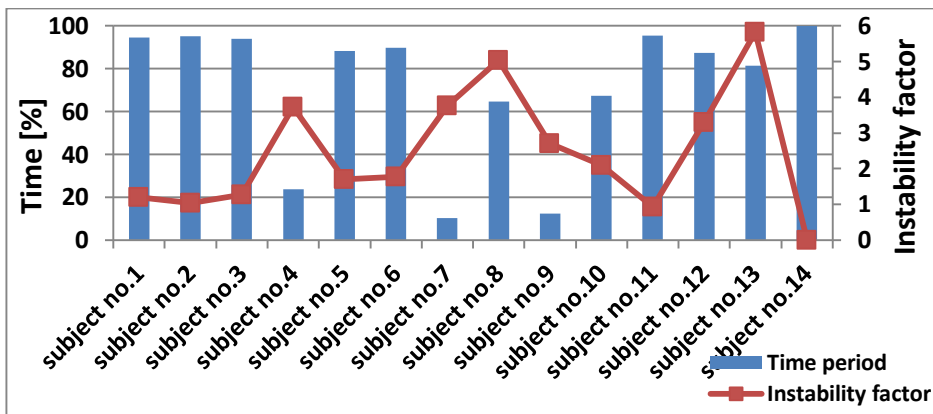


Figure 3-26 ROI validation time and ROI instability factor in RC case

As it is shown in Figure 3-25 and Figure 3-26 though behaviors of subjects in open-eyes and closed-eyes cases are so similar, they have significant differences. For example when the instability factor of a subject is more than 100 in RO, it may show some small changes in RC but still remains higher than 50. This is also valid for the validation time. Same explanations can be used for Figure 3-27 and Figure 3-28. Since subject's stance strategy has not changed between the cases it is clear that there would be similarities between these plots, but the differences are due to the different levels of difficulties among cases.

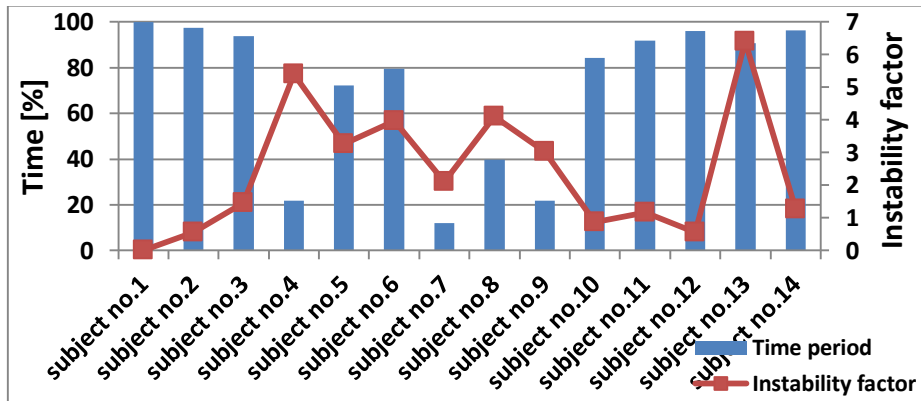


Figure 3-27 ROI validation time and ROI instability factor in LO case

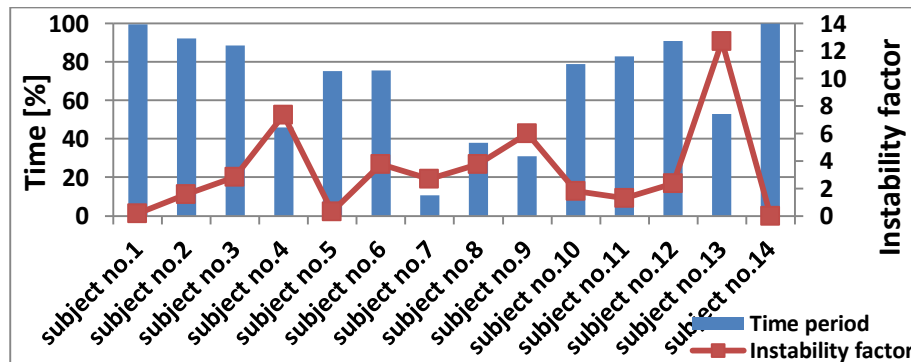


Figure 3-28 ROI validation time and ROI instability factor in LC case

Comparing open-eyes with closed-eyes cases, Table 3-13 and Table 3-14 have been derived from these four figures. Only the top right cell is the condition that has been desired. In each of unipedal-left and unipedal-right cases there are 8 subjects which have longer ROI validation time and smaller ROI instability factor in open-eyes case rather than closed-eyes, 7 of which are common between these two cases.

Table 3-13 ROI validation time and ROI instability for unipedal-right trials;  $RT_o$ : ROI validation time in open-eyes case,  $RT_c$ : ROI validation time in closed-eyes case,  $RF_o$ : ROI instability factor in open-eyes case,  $RF_c$ : ROI instability factor in closed-eyes case

	$RT_o < RT_c$	$RT_o > RT_c$
$RF_o < RF_c$	2	8
$RF_o > RF_c$	1	3

**Table 3-14 ROI validation time and ROI instability for unipedal-left trials**

	$RT_o < RT_c$	$RT_o > RT_c$
$RF_o < RF_c$	2	8
$RF_o > RF_c$	2	2

Table 3-15 shows a comparison between right-footed and left-footed subjects in different classes of trials. For right-footed subjects the first row and for left-footed subjects the last row is the ideal condition. According to this table, in open-eyes case there were 6 right-footed subjects and in closed-eyes cases there were 2 right-footed subjects who are in the ideal condition. The number of left-footed subjects in ideal condition is 1, for both open-eyes and closed-eyes cases. Like Table 3-9 these numbers are too few to make a statement about subjects' behavior. It can be stated that unlike bipedal case, no evidence was found here to prove the strength of dominant foot regarding to non-dominant one.

**Table 3-15 Right-footed subjects' behavior in Unipedal open-eyes case;  $T_R$ : validation time in unipedal-right foot case,  $T_L$ : validation time in unipedal-left foot case,  $F_R$ : instability factor in unipedal-right foot case,  $F_L$ : instability factor in unipedal-left foot case**

	$T_R < T_L$	$T_R > T_L$
$F_R < F_L$	0	6
$F_R > F_L$	3	2

**Table 3-16 Left-footed subjects' behavior in Unipedal open-eyes case**

	$T_R < T_L$	$T_R > T_L$
$F_R < F_L$	1	0
$F_R > F_L$	1	1

**Table 3-17 Right-footed subjects' behavior in Unipedal closed-eyes case**

	$T_R < T_L$	$T_R > T_L$
$F_R < F_L$	3	2
$F_R > F_L$	4	2

**Table 3-18 Left-footed subjects' behavior in Unipedal closed-eyes case**

	$T_R < T_L$	$T_R > T_L$
$F_R < F_L$	1	0
$F_R > F_L$	1	1

Since we assumed that changing the pressure focus between *ROI* and *Lat* means more instability, one can explain these results by thinking that right-footed people are more stable while standing on their right foot, so they would experience fewer disturbances and need fewer metatarsal meets. But there is no strong evidence for this. Figure 3-29 shows the number of instabilities for each subject in each case.

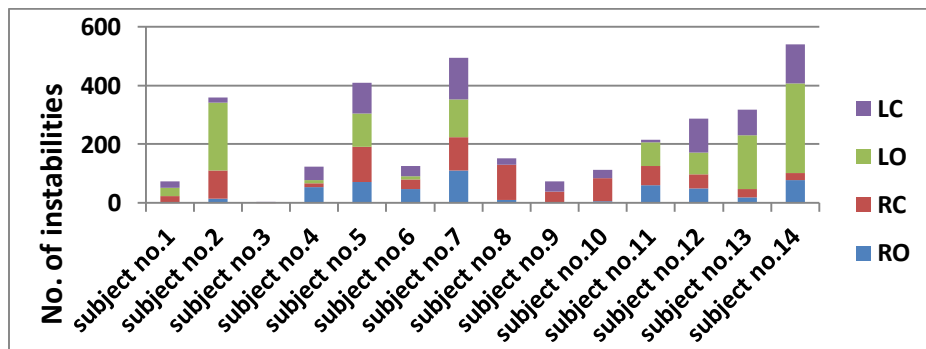


**Figure 3-29 Number of instabilities for every subject in each case**

According to this figure subjects are categorized in 3 groups shown in Table 3-19.

**Table 3-19 Categorization of subjects due to their instability**

<b>Category</b>	<b>Feature</b>	<b>Subjects</b>
Highly stable	instability factor less than 100	1, 3, 9
Medium stable	instability factor between 100 and 200	4, 6 ,8, 10
Poorly stable	instability factor more than 200	2, 5, 7, 11, 12, 13, 14

Highly stable subjects are the ones who gave us results so near to the theoretical explanations. Medium stable subjects' behaviors differ widely in various situations. They could be so ideal in one situation while acting awfully in other one. Poorly stable subjects showed unappealing behaviors in almost all the cases and situations. Subjects 3, 10 and 12 are the left footed ones so every category has one of them. Note that this table is based on unipedal results only hence it is not unexpected to have most of the population poorly stable.

### **3.4.3 CORRELATION BETWEEN COPX AND GROUND REACTION FORCE DISTRIBUTION**

Since the beginning of this study it was assumed that the stance of human body basically depends on the pressure on both calcaneouses and it was investigated whether the stability of this stance depends on metatarsal meets or not. The latter was observed in different situations. As a way to prove it statistically, the correlation coefficients of COPx with pressure components were calculated. These are shown in Table 3-20.

**Table 3-20 Correlation coefficients in four cases: RCy & COPx, LCy & COPx, RMy & COPx, LMy & COPx**

	<i>RCy&amp;COPx</i>					<i>LCy&amp;COPx</i>					<i>RMy&amp;COPx</i>					<i>LMy&amp;COPx</i>				
	<i>BO</i>	<i>BC</i>	<i>RO</i>	<i>RC</i>	<i>avg</i>	<i>BO</i>	<i>BC</i>	<i>LO</i>	<i>LC</i>	<i>avg</i>	<i>BO</i>	<i>BC</i>	<i>RO</i>	<i>RC</i>	<i>avg</i>	<i>BO</i>	<i>BC</i>	<i>LO</i>	<i>LC</i>	<i>avg</i>
<i>Subject no.1</i>	0.20	0.30	0.25	0.59	0.33	0.22	0.35	0.14	0.68	0.35	0.73	0.72	0.95	0.82	0.81	0.71	0.75	0.89	0.75	0.78
<i>Subject no.2</i>	0.33	0.85	0.65	0.70	0.63	0.22	0.38	0.50	0.58	0.42	0.84	0.87	0.72	0.74	0.79	0.58	0.53	0.67	0.88	0.67
<i>Subject no.3</i>	0.37	0.71	0.85	0.63	0.64	0.84	0.81	0.92	0.86	0.86	0.93	0.89	0.88	0.77	0.87	0.83	0.77	0.92	0.84	0.84
<i>Subject no.4</i>	0.14	0.26	0.69	0.31	0.35	0.32	0.30	0.61	0.43	0.41	0.84	0.65	0.65	0.60	0.68	0.56	0.31	0.65	0.71	0.56
<i>Subject no.5</i>	0.33	0.36	0.18	0.23	0.28	0.34	0.50	0.18	0.24	0.31	0.73	0.89	0.81	0.79	0.80	0.74	0.78	0.81	0.77	0.78
<i>Subject no.6</i>	0.74	0.91	0.37	0.69	0.68	0.52	0.58	0.68	0.46	0.56	0.91	0.79	0.68	0.71	0.77	0.83	0.60	0.73	0.47	0.66
<i>Subject no.7</i>	0.17	0.15	0.41	0.40	0.29	0.30	0.37	0.60	0.67	0.48	0.88	0.89	0.88	0.91	0.89	0.87	0.86	0.95	0.98	0.92
<i>Subject no.8</i>	0.07	0.07	0.13	0.16	0.11	0.08	0.12	0.12	0.25	0.14	0.62	0.76	0.92	0.86	0.79	0.77	0.77	0.65	0.98	0.79
<i>Subject no.9</i>	0.33	0.63	0.74	0.49	0.55	0.42	0.48	0.68	0.64	0.55	0.96	0.92	0.91	0.99	0.95	0.97	0.92	0.91	0.95	0.94
<i>Subject no.10</i>	0.12	0.19	0.36	0.29	0.24	0.19	0.26	0.50	0.65	0.40	0.74	0.88	0.84	0.71	0.79	0.69	0.83	0.77	0.53	0.70
<i>Subject no.11</i>	0.64	0.56	0.45	0.47	0.53	0.68	0.42	0.58	0.62	0.57	0.68	0.93	0.86	0.86	0.83	0.73	0.92	0.71	0.78	0.79
<i>Subject no.12</i>	0.44	0.51	0.83	0.94	0.68	0.59	0.70	0.45	0.90	0.66	0.81	0.60	0.79	0.67	0.72	0.81	0.57	0.53	0.71	0.65
<i>Subject no.13</i>	0.07	0.09	0.19	0.13	0.12	0.08	0.01	0.01	0.23	0.08	0.68	0.57	0.70	0.91	0.72	0.76	0.77	0.77	0.81	0.78
<i>Subject no.14</i>	0.00	0.01	0.01	0.01	0.01	0.03	0.04	0.04	0.05	0.04	0.82	0.91	0.90	0.83	0.87	0.91	0.91	0.82	0.85	0.88
<i>Average</i>	0.28	0.40	0.44	0.43	0.39	0.34	0.38	0.43	0.52	0.42	0.80	0.80	0.82	0.80	0.81	0.77	0.74	0.77	0.78	0.76

Using this table, it can be seen that in general subjects have larger correlation values between their COPx and  $M_y$  signals than their COPx and  $C_y$  signals. This shows that any change in  $M_y$  component has a direct effect on COPx signal and hence overall stance of the body. Of course the values of these correlation coefficients are not too close to 1 but since this is a relative comparison between two cases, the absolute values do not change the conclusion.

For  $C_y$  correlations there are 4 subjects who have larger and 9 subjects who have smaller right  $C_y$  correlation than left one with COPx and one subject has equal correlation value. In  $M_y$  correlations there are 10 subjects with larger and 3 with smaller right  $M_y$  than left  $M_y$  correlation with COPx and again one subject has equal correlation value. So it seems like in this population  $RM_y$  and  $LC_y$  pressure components have greater effects on COPx signal. In all of the four cases which are shown in Table 3-20 the average correlation value for bipedal is less than it is for unipedal. Using student's t-test for the correlation values of bipedal and unipedal case groups, t-value was calculated equal to 0.17, which shows that there is not a meaningful difference between these two correlation groups. So it is not rational to conclude that these two cases have very different impacts on COPx signal.

The larger  $M_y$  correlation for unipedal cases can be another proof for our hypothesis. In unipedal experiments during which the subjects have undergone more instabilities, it was  $M_y$  which had the great effect on re-stabilization of the subjects and hence their COPx. But in bipedal cases -where there are less instabilities- the  $M_y$  is less correlated with COPx.

#### **3.4.4 COMPARISON BETWEEN COM AND COP**

COM is calculated using data obtained from motion capture system and equation 3-5 [13]. In this equation  $M$  is the total body mass and  $m_i$  is the mass of the  $i^{\text{th}}$  segment of the body, so  $\frac{m_i}{M}$  is the mass fraction for  $i^{\text{th}}$  body segment. Similarly  $COM_i$  is the COM for  $i^{\text{th}}$  body segment. Hence the equation shows that the overall COM signal is the summation of all segments' COM signals with the weight of respective segments' mass fraction.

$$COM = \sum_{i=1}^n \frac{m_i}{M} COM_i \quad 3-5$$

In this study there were 7 MTX sensors used for lower limb but no sensors for upper limb, so the COM calculation was done using the lower limb sensors in addition to some assumptions for upper limb. Table 3-21 –driven from literature- illustrates the body segments used in this part and the corresponding MTX markers and coefficients [13, 31, 32].

**Table 3-21 Mass fractions and segment definitions, m1-m7 are the 7 MTX markers used from motion capture system**

<i>Segments</i>		<i>mass fraction</i>	<i>Respective markers</i>	
<i>Thighs</i>	<i>R</i>	0.1	Right Lower Leg (m3) & Right Upper Leg (m5)	0.433*m3+0.567*m5
	<i>L</i>	0.1	Left Lower Leg (m4) & Left Upper Leg (m6)	0.433*m4+0.567*m6
<i>Legs &amp; feet</i>	<i>R</i>	0.06	Right Foot (m1) & Right Lower Leg (m3)	0.606*m1+0.394*m3
	<i>L</i>	0.06	Left Foot (m2) & Left Lower Leg (m4)	0.606*m2+0.394*m4
<i>Pelvis</i>		0.142	Pelvis (m7)	m7
<i>Upper limbs</i>		0.538	-	-
<i>Total</i>		1		

Considering the mass fractions given in Table 3-21 it can be stated that the mass of upper limb dominates the body center of mass but while walking the energy changes in lower limbs will become dominant [31]. Since only quiet stance is studied here and the latter is a division of gait analysis, it is not studied and the former is handled by a strategy explained below.

The upper part of the body was assumed to be a vertical cylinder with its base centered on the pelvis marker (m7) as is illustrated in Figure 3-30. Using anthropometric measurements[13] it is known that the height of the upper limb

cylinder is 0.47 of body height and the diameter of its base is 0.259 of body height. Hence the x coordinate for the COM of this cylinder which is the center of it, is the same as the x coordinate for m7 marker.

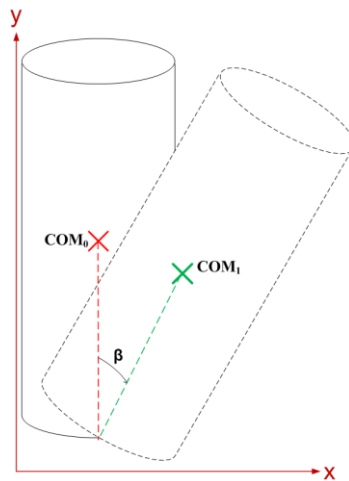


**Figure 3-30 Cylinder resembling the upper limb of human body**

Both displacement and rotation angles are small enough to make the assumption:  $COM_{1,x} \approx COM_{0,x}$ . By this assumption x component of  $COM_{upper-limb}$  can be used equal to  $COM_{pelvis}$  in equation 3-5. Using this method COM signals were calculated in all 6 cases for whole subjects.

### **3.4.5 PLANTAR APONEUROSIS LENGTH**

Figure 3-31 shows some of the parameters of the model presented before. Recalling chapter 3,  $\theta$  was the angle of human's body relative to the vertical line in quiet stance. Equation 3-6 shows this angle.

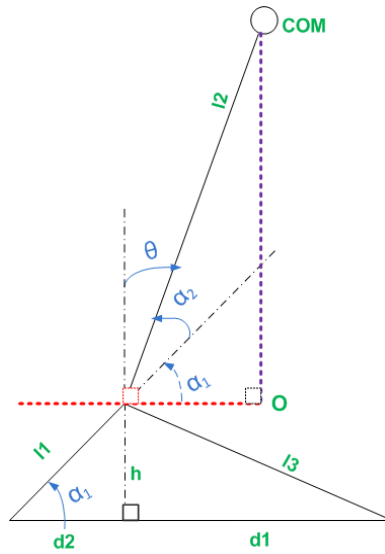


Figure 3-31 A schematic view of model showing some parameters and measurements

$$\theta = \frac{\pi}{2} - (\alpha_1 + \alpha_2) = \frac{\pi}{2} - \sin^{-1} \frac{COM_z - h}{l_2} = \frac{\pi}{2} - \sin^{-1} \frac{COM_z - d_2 \tan \alpha_1}{l_2} \quad 3-6$$

Regarding biological facts, the value of angular displacement  $\alpha_1$  can be assumed to be approximately  $45^\circ$ , this assumption leads to:

$$\theta = \frac{\pi}{2} - \sin^{-1} \frac{COM_z - d_2}{l_2}$$

Knowing  $COM_z$  from motion capture system,  $\theta$  can be computed in time. Table 3-22 shows the average value of  $\theta$  for each subject in six cases. For most of the subjects average  $\theta$  seems to be less than  $10^\circ$ , which is in coordination with theoretical studies [13]. Few subjects have  $\theta$  just a bit larger than  $10^\circ$  but the difference is too little that would not make diversity in conclusion of the study.

Table 3-22 Theta (in degrees) in six cases for all of the subjects

	<i>BO</i>	<i>BC</i>	<i>LO</i>	<i>LC</i>	<i>RO</i>	<i>RC</i>	<i>avg.</i>
<i>Subject no.1</i>	8.12	9.14	11.16	10.68	7.75	10.13	9.50
<i>Subject no.2</i>	10.10	11.38	11.27	12.89	11.65	10.89	11.37
<i>Subject no.3</i>	8.52	8.17	9.23	9.55	7.52	7.90	8.48
<i>Subject no.4</i>	8.46	8.21	11.43	11.50	11.10	13.56	10.71
<i>Subject no.5</i>	3.76	7.64	7.97	8.33	11.42	9.94	8.17
<i>Subject no.6</i>	9.91	14.06	10.23	16.17	12.30	17.05	13.29
<i>Subject no.7</i>	10.25	11.43	10.89	12.84	14.69	10.08	11.70
<i>Subject no.8</i>	7.90	7.52	8.03	9.49	12.04	8.04	8.84
<i>Subject no.9</i>	5.96	6.59	6.26	8.64	6.70	10.61	7.46
<i>Subject no.10</i>	7.30	9.61	9.39	10.68	10.24	8.05	9.21
<i>Subject no.11</i>	6.03	9.77	9.17	12.36	10.45	8.84	9.44
<i>Subject no.12</i>	7.74	7.64	6.92	7.57	7.16	8.93	7.66
<i>Subject no.13</i>	11.53	8.23	8.59	9.09	9.53	12.89	9.98
<i>Subject no.14</i>	4.87	6.25	6.30	10.41	6.95	12.99	7.96

Using the value of  $\theta$  in time, length of plantar aponeurosis can be calculated. This can be assumed equal to the length of foot sole from calcaneus to metatarsals and as shown in Figure 3-32 its rest length is equal to  $d_1 + d_2$ . In quiet stance, regarding to the hypothesis of this study, there would be deformations in the foot and therefore this length is not constant all the time.

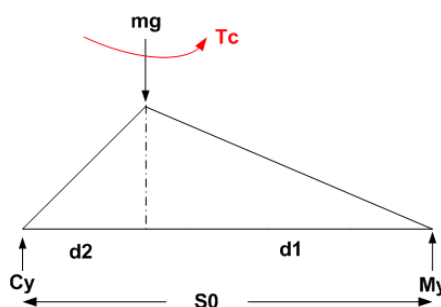


Figure 3-32 An explanatory static shape for measurement of S

Considering this figure and equations 3-7 and 3-8:

$$M_y S = mgd_2 + T_c \quad 3-7$$

$$T_c = mgl_2 \sin \theta \quad 3-8$$

Value of S can be calculated by  $S = \frac{mg(d_2+l_2 \sin \theta)}{M_y}$  and as a result Table 3-23 can be concluded. In this table, S\* is the average experimental S for all of the experimental trials and S<sub>0</sub> is the value which has been measured directly on subjects' feet. The last column of the table is the average variation in experimental S (S\*) from measured S (S<sub>0</sub>).

The variation between S\* and S<sub>0</sub> was calculated data point by data point using the formula:

$$variation = \frac{S^* - S_0}{S_0}$$

Then the mean of these values was calculated as the average variation.

**Table 3-23 Average experimental S [cm]**

	<b>BO</b>	<b>BC</b>	<b>LO</b>	<b>LC</b>	<b>RO</b>	<b>RC</b>	<b>S*</b>	<b>S<sub>0</sub></b>	<b>avg. var.</b>
<i>Subject no.1</i>	23.4	25.4	26.3	25.2	24.9	25.5	25.1	25.7	0.568
<i>Subject no.2</i>	21.9	21.0	21.1	21.9	21.4	21.6	21.5	21.5	0.020
<i>Subject no.3</i>	21.1	21.6	21.8	21.7	21.5	21.2	21.5	21.8	0.325
<i>Subject no.4</i>	20.4	20.6	20.5	20.3	20.3	20.4	20.4	20.5	0.068
<i>Subject no.5</i>	31.1	28.2	30.4	30.6	30.8	31.5	30.4	30.0	0.422
<i>Subject no.6</i>	25.1	26.2	24.7	24.7	24.5	25.2	25.1	25.0	0.085
<i>Subject no.7</i>	29.6	29.4	29.0	29.0	29.8	29.5	29.4	29.1	0.272
<i>Subject no.8</i>	23.5	24.2	24.1	23.2	24.0	23.8	23.8	23.6	0.222
<i>Subject no.9</i>	23.1	23.0	22.9	22.2	22.9	23.5	22.9	22.3	0.635
<i>Subject no.10</i>	24.1	24.6	24.4	24.5	25.1	25.0	24.6	24.8	0.184
<i>Subject no.11</i>	21.7	21.5	22.1	21.2	22.1	21.5	21.7	21.8	0.111
<i>Subject no.12</i>	25.6	25.7	25.3	25.2	25.9	26.1	25.6	25.5	0.120
<i>Subject no.13</i>	20.8	21.1	21.0	20.8	20.4	22.1	21.0	20.7	0.340
<i>Subject no.14</i>	26.6	26.2	26.6	25.2	25.9	26.9	26.3	26.4	0.149

The average variation of experimental S from measured S for all of the subjects is less than 4% which is a desirable error rate for such a matter. Hence the largest average variation in Table 3-23 is 0.635 centimeters and average variation among all subjects is 0.251centimeters. This shows that the foot sole length may be changing with dynamics of foot in respect to the theory of the study and the presented model. The variations are small enough to eliminate the possibility of intentional movements of feet by subjects in most of the cases, but also large enough to not being ignored or assumed to be noises of the recording system. Nevertheless there might be some movements or noises involved in these variation slightly. Figure 3-33 shows the changes of S in time for one of the cases.

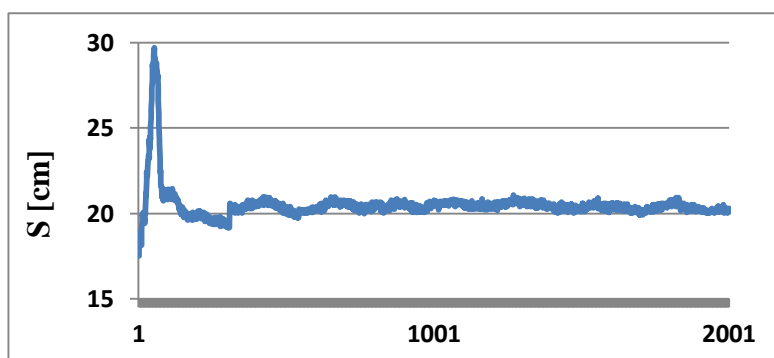


**Figure 3-33 S in time for a BO trial**

Throughout this study unipedal conditions always expected to have larger deformations than bipedal due to lower stability but here 7 subjects -50% of the population- have the largest variations of S in their bipedal tests, 4 subjects have the largest variations in unipedal right tests and 3 in their unipedal left tests. Only 4 subjects out of 14 have their largest variations in open-eyes tests.

The first row of Table 3-24 shows the correlation ratios between S and validation time in six different cases and the second row shows the correlation ratio between S and instability factor. This table shows that S has an inverse correlation with validation time and a direct correlation with instability factor. This again shows that

the validation time and instability factor affect the deformations of foot in two inverse directions and generally validation time is more correlated with these deformations. Amongst six cases, “bipedal closed-eyes” is least correlated with these two parameters.

**Table 3-24 Correlation ratios, between S and validation time, and between S and instability factor**

	<i>BO</i>	<i>BC</i>	<i>LO</i>	<i>LC</i>	<i>RO</i>	<i>RC</i>
<i>S &amp; validation time</i>	-0.58	-0.31	-0.61	-0.60	-0.56	-0.63
<i>S &amp; instability factor</i>	0.56	0.28	0.27	0.55	0.46	0.44

### 3.5 CONCLUSION

This chapter showed the procedure of study aiming the ultimate purpose of this thesis which is to study and observe the pattern of force and pressure distribution on the sole of foot in quiet stance. Aiming this purpose 14 healthy subjects with no lower limb disorder or injury have been passed through some experiments and their motion data has been collected using three devices: pressure mat, force plate and 3D motion capture system and their output was analyzed and combined together using specific MATLAB codes.

The results proved our hypothesis true in most of the cases. As it is detailed in subsections, in some cases there was not enough evidence for proving the hypothesis which can be due to low population of study.



## **CHAPTER4**

### **MODELING**

#### **4.1 INTRODUCTION**

The thesis was pursued by designing and simulating mathematical models using MATLAB® and Simulink®. Previously in chapter 0 it was illustrated that in order to understand the functional deformations of the foot there is a need to model the foot as a deformable body rather than modeling as a rigid body. Aiming this, a set of mathematical models is presented here. This set consists of 4 steps of modeling, each of which has a detail added to the previous model to make it more close to the ideal deformable foot model.

#### **4.2 MODEL**

The idea of modeling was to study the deformations of the foot by simulating the deformations of medial longitudinal arch in saggital plane (thus the model is a planar model).

The study of this idea is started using a simple rigid foot model that has been explained in literature [33-35]. Then it continues toward the model shown in Figure 4-1. In this figure A stands for ankle joint, C for calcaneous tuberosity and M for metatarsals.

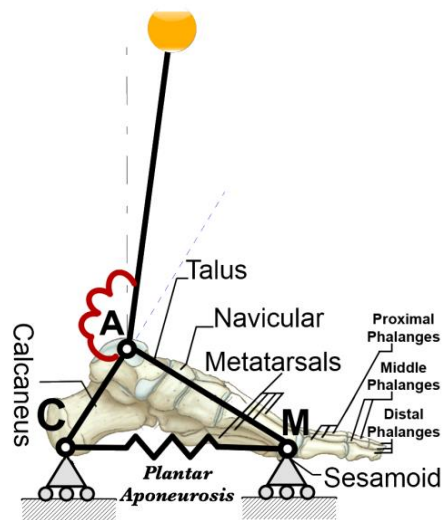


**Figure 4-1 Simple schematic description of the model**

In next subsections each step of the modeling is illustrated and its results are shown. All of the equations used in these steps are shown in APPENDIX B.

#### **4.2.1 SIMPLE RIGID FOOT MODEL WITH NO FRICTION FORCES**

This is the simplest foot model that has been used widely in postural research literature [33, 34, 36]. In this first step the friction forces are ignored for simplicity, so are the dynamics of the foot. The free body diagram of this model is shown in Figure 4-2 and some of parameters on this figure are explained in Table 4-1.

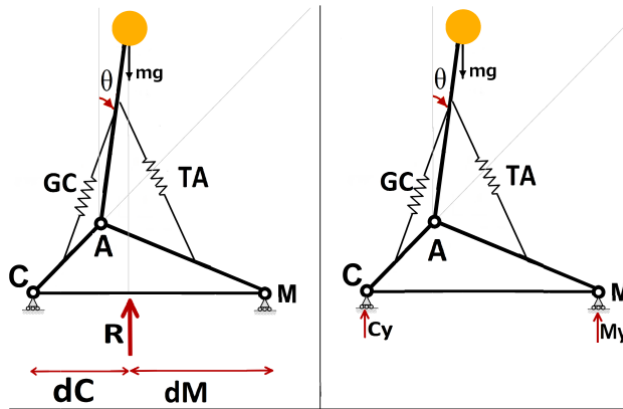


Figure 4-2 Free body diagram of rigid foot model with no friction

Table 4-1 Nomenclature for Figure 4-2

Parameter	Explanation
$\theta(t)$	Angular displacement of link2
$C_y, M_y$	Ground reaction forces
$dC$	Distance between heel and the application point of the resultant of the Ground Reaction Force (R or GRF) in antero-posterior direction
$dM$	Distance between application point of GRF and metatarsals
TA	Tibialis Anterior muscle
GC	Gastrocnemius muscle

As it is shown in APPENDIX B, 1.11, from Figure 4-2 it can be stated that  $\frac{C_y}{M_y} = \frac{dM}{dC}$ .

The left half of this equation can be calculated using pressure mat data and the right half from force plate data. In the figure, R is the net ground reaction force and its point of application is presented by force plate, so dC and dM are calculated after removing the offset from COPx (x-component of center of pressure) measured by force plate. This offset has been forced to data by some aspects such as the standing position of each subject on the force plate and by removing it, the origins of data for all subjects have been uniformed.

First, these two ratios ( $\frac{C_y}{M_y}$  and  $\frac{dM}{dC}$ ) were calculated for all data points in bipedal trials. Since bipedal trials duration is 3 minutes and data is collected at 100Hz, two data sets each consisted of 18000 data points are generated. Then for each subject, the related pair of these sets was compared using t-test. Most of the resulted t-values are less than tabulated t-value which is 1.96 for 95% accuracy. Just two of subjects have t-values more than 1.96 which indicates that the two sets of data for them are significantly different from each other. For other subjects the two sets of data do not differ significantly. Since there have been six bipedal trials for all of the subjects, t-test has been performed six times for each of the subjects. In Table 4-2 the mean values of these ratios for each subject are shown. So each of them is an average for 6 datasets each of which consists of 18000 data points ( $\overline{C_y/M_y}$  and  $\overline{dM/dC}$ ).

**Table 4-2 T-values and mean values of ratios in rigid foot model with no friction forces, point-by-point analysis**

	$\overline{C_y/M_y}$	$\overline{dM/dC}$	<i>t-values</i>
<i>Subject no.1</i>	1.900 ± 0.280	1.898 ± 0.350	1.47
<i>Subject no.2</i>	1.840 ± 0.200	1.843 ± 0.400	1.91
<i>Subject no.3</i>	1.987 ± 0.201	1.966 ± 0.154	26.96
<i>Subject no.4</i>	1.784 ± 0.311	1.788 ± 0.591	1.95
<i>Subject no.5</i>	2.002 ± 0.465	1.998 ± 0.495	1.94
<i>Subject no.6</i>	1.938 ± 0.584	1.933 ± 0.756	1.72
<i>Subject no.7</i>	1.878 ± 0.405	1.881 ± 0.294	1.96
<i>Subject no.8</i>	2.025 ± 0.160	2.027 ± 0.342	1.74
<i>Subject no.9</i>	2.132 ± 0.310	2.129 ± 0.340	1.93
<i>Subject no.10</i>	1.967 ± 0.370	1.970 ± 0.340	1.95
<i>Subject no.11</i>	2.204 ± 0.350	2.201 ± 0.330	1.91
<i>Subject no.12</i>	1.899 ± 0.640	1.905 ± 0.780	1.95
<i>Subject no.13</i>	1.982 ± 0.610	1.986 ± 0.610	1.52
<i>Subject no.14</i>	1.900 ± 0.44	1.870 ± 0.400	16.52

This has been a static analysis so far and since for all subjects there has been  $\frac{C_y}{M_y} > 1$ , meaning that calcaneus always bears more load than metatarsals, it shows that the segmentation of the foot has been done properly (explained in chapter 3 using Figure 3-4) and in consistency with the theory that we have been looking for.

Following there are six tables (Table 4-3 to Table 4-8) same parameters as Table 4-2 are presented for six bipedal trials separately.

**Table 4-3 T-values and mean values of ratios in rigid foot model with no friction forces, 1<sup>st</sup> bipedal open-eyes trial**

	$\overline{C_y/M_y}$	$\overline{dM/dC}$	<i>t-values</i>
<i>Subject no.1</i>	1.874 ± 0.058	1.877 ± 0.264	0.464
<i>Subject no.2</i>	1.701 ± 0.098	1.698 ± 0.342	0.317
<i>Subject no.3</i>	1.990 ± 0.412	1.961 ± 0.168	2.902
<i>Subject no.4</i>	1.771 ± 1.008	1.774 ± 0.333	0.126
<i>Subject no.5</i>	1.926 ± 0.092	1.928 ± 0.367	0.259
<i>Subject no.6</i>	1.958 ± 0.340	1.956 ± 0.146	0.087
<i>Subject no.7</i>	1.732 ± 0.149	1.731 ± 0.096	0.253
<i>Subject no.8</i>	2.020 ± 0.132	2.022 ± 0.182	0.417
<i>Subject no.9</i>	2.155 ± 0.189	2.146 ± 0.258	1.331
<i>Subject no.10</i>	1.946 ± 0.504	1.938 ± 0.289	0.608
<i>Subject no.11</i>	2.003 ± 0.207	2.003 ± 0.141	0.091
<i>Subject no.12</i>	1.969 ± 0.157	1.966 ± 0.178	0.529
<i>Subject no.13</i>	1.947 ± 0.402	1.941 ± 0.303	0.582
<i>Subject no.14</i>	1.942 ± 0.216	1.942 ± 0.256	0.029

**Table 4-4 T-values and mean values of ratios in rigid foot model with no friction forces, 1<sup>st</sup> bipedal closed-eyes trial**

	$\overline{C_y/M_y}$	$\overline{dM/dC}$	<i>t-values</i>
<i>Subject no.1</i>	1.963 ± 0.137	1.964 ± 0.293	0.117
<i>Subject no.2</i>	1.870 ± 0.187	1.855 ± 0.137	2.822
<i>Subject no.3</i>	1.963 ± 0.072	1.963 ± 0.077	0.192
<i>Subject no.4</i>	1.963 ± 0.063	1.965 ± 0.211	0.527
<i>Subject no.5</i>	1.969 ± 0.427	1.967 ± 0.224	0.185
<i>Subject no.6</i>	1.674 ± 0.182	2.004 ± 0.146	17.411
<i>Subject no.7</i>	1.898 ± 0.168	2.010 ± 0.084	26.545
<i>Subject no.8</i>	1.908 ± 0.522	2.038 ± 0.154	10.653
<i>Subject no.9</i>	2.232 ± 0.132	2.228 ± 0.169	0.990
<i>Subject no.10</i>	1.965 ± 0.187	1.965 ± 0.170	0.008
<i>Subject no.11</i>	2.227 ± 0.291	2.218 ± 0.128	1.323
<i>Subject no.12</i>	1.813 ± 0.274	1.992 ± 0.136	26.139
<i>Subject no.13</i>	2.041 ± 0.187	2.038 ± 0.162	0.654
<i>Subject no.14</i>	1.821 ± 0.304	1.786 ± 0.185	4.501

**Table 4-5 T-values and mean values of ratios in rigid foot model with no friction forces, 2<sup>nd</sup> bipedal open-eyes trial**

	$\overline{C_y/M_y}$	$\overline{dM/dC}$	<i>t-values</i>
<i>Subject no.1</i>	1.920 ± 0.087	1.918 ± 0.278	0.273
<i>Subject no.2</i>	1.834 ± 0.123	1.836 ± 0.090	0.721
<i>Subject no.3</i>	2.077 ± 0.155	2.077 ± 0.148	0.042
<i>Subject no.4</i>	1.733 ± 0.028	1.731 ± 0.388	0.246
<i>Subject no.5</i>	2.046 ± 0.438	2.046 ± 0.247	0.007
<i>Subject no.6</i>	1.923 ± 0.389	1.921 ± 0.146	0.052
<i>Subject no.7</i>	1.872 ± 0.259	1.870 ± 0.110	0.330
<i>Subject no.8</i>	1.942 ± 0.392	1.996 ± 0.199	5.477
<i>Subject no.9</i>	1.944 ± 0.122	1.944 ± 0.172	0.063
<i>Subject no.10</i>	2.052 ± 0.207	2.051 ± 0.261	0.090
<i>Subject no.11</i>	2.112 ± 0.347	2.124 ± 0.152	1.378
<i>Subject no.12</i>	1.839 ± 0.258	1.866 ± 0.160	4.029
<i>Subject no.13</i>	2.023 ± 0.186	2.023 ± 0.218	0.018
<i>Subject no.14</i>	1.784 ± 0.414	1.983 ± 0.197	19.432

**Table 4-6 T-values and mean values of ratios in rigid foot model with no friction forces, 2<sup>nd</sup> bipedal closed-eyes trial**

	$\overline{C_y/M_y}$	$\overline{dM/dC}$	<i>t-values</i>
<i>Subject no.1</i>	1.923 ± 0.101	1.892 ± 0.273	4.808
<i>Subject no.2</i>	1.890 ± 0.152	1.880 ± 0.098	2.559
<i>Subject no.3</i>	1.812 ± 0.108	1.982 ± 0.072	58.204
<i>Subject no.4</i>	1.749 ± 0.050	1.746 ± 0.410	0.285
<i>Subject no.5</i>	2.027 ± 0.190	2.028 ± 0.142	0.331
<i>Subject no.6</i>	1.731 ± 0.063	1.930 ± 0.146	15.404
<i>Subject no.7</i>	1.909 ± 0.155	1.713 ± 0.068	51.813
<i>Subject no.8</i>	2.033 ± 0.344	1.920 ± 0.118	13.894
<i>Subject no.9</i>	2.175 ± 0.120	2.218 ± 0.148	9.979
<i>Subject no.10</i>	1.963 ± 0.116	1.965 ± 0.208	0.481
<i>Subject no.11</i>	2.091 ± 0.187	2.254 ± 0.111	33.533
<i>Subject no.12</i>	1.949 ± 0.206	1.950 ± 0.111	0.190
<i>Subject no.13</i>	1.989 ± 0.125	1.987 ± 0.180	0.517
<i>Subject no.14</i>	1.879 ± 0.127	1.779 ± 0.144	23.141

**Table 4-7 T-values and mean values of ratios in rigid foot model with no friction forces, 3<sup>rd</sup> bipedal open-eyes trial**

	$\overline{C_y/M_y}$	$\overline{dM/dC}$	<i>t-values</i>
<i>Subject no.1</i>	1.917 ± 0.075	1.899 ± 0.286	2.856
<i>Subject no.2</i>	1.859 ± 0.193	1.858 ± 0.147	0.297
<i>Subject no.3</i>	1.964 ± 0.123	1.933 ± 0.106	8.634
<i>Subject no.4</i>	1.833 ± 0.041	1.832 ± 0.402	0.137
<i>Subject no.5</i>	2.026 ± 0.245	2.023 ± 0.110	0.475
<i>Subject no.6</i>	1.902 ± 0.237	1.903 ± 0.146	0.042
<i>Subject no.7</i>	2.035 ± 0.130	2.032 ± 0.074	0.773
<i>Subject no.8</i>	1.958 ± 0.231	1.956 ± 0.125	0.287
<i>Subject no.9</i>	2.194 ± 0.130	2.196 ± 0.180	0.540
<i>Subject no.10</i>	1.961 ± 0.136	1.959 ± 0.206	0.335
<i>Subject no.11</i>	2.165 ± 0.199	2.164 ± 0.115	0.215
<i>Subject no.12</i>	2.062 ± 0.164	2.062 ± 0.126	0.115
<i>Subject no.13</i>	1.911 ± 0.151	1.911 ± 0.191	0.130
<i>Subject no.14</i>	1.964 ± 0.241	1.763 ± 0.128	32.956

**Table 4-8 T-values and mean values of ratios in rigid foot model with no friction forces, 3<sup>rd</sup> bipedal closed-eyes trial**

	$\overline{C_y/M_y}$	$\overline{dM/dC}$	<i>t-values</i>
<i>Subject no.1</i>	1.799 ± 0.102	1.797 ± 0.316	0.210
<i>Subject no.2</i>	1.897 ± 0.041	1.899 ± 0.380	0.302
<i>Subject no.3</i>	1.846 ± 0.103	1.853 ± 0.093	2.216
<i>Subject no.4</i>	1.572 ± 0.047	1.538 ± 0.402	3.742
<i>Subject no.5</i>	1.968 ± 0.487	1.966 ± 0.232	0.165
<i>Subject no.6</i>	2.196 ± 0.618	2.194 ± 0.146	0.048
<i>Subject no.7</i>	1.872 ± 0.266	1.790 ± 0.174	11.644
<i>Subject no.8</i>	2.190 ± 0.256	2.140 ± 0.073	8.424
<i>Subject no.9</i>	2.247 ± 0.082	2.150 ± 0.263	15.812
<i>Subject no.10</i>	1.995 ± 0.212	1.786 ± 0.242	29.100
<i>Subject no.11</i>	2.441 ± 0.380	2.441 ± 0.131	0.017
<i>Subject no.12</i>	2.027 ± 0.201	2.019 ± 0.170	1.490
<i>Subject no.13</i>	1.921 ± 0.169	1.914 ± 0.277	0.910
<i>Subject no.14</i>	1.882 ± 0.553	1.980 ± 0.189	7.482

Studying these tables may not give a definitive pattern about subjects' behavior but still they show how each of them have been acting during the experiments. But it can be stated that in open-eyes trials most of the subjects (in 1<sup>st</sup> BO trial 13 subjects, in 2<sup>nd</sup> and 3<sup>rd</sup> BO trials 11 subjects each) show no significant difference between two sets of data with 95% accuracy but the same cannot be stated for closed-eyes cases (in 1<sup>st</sup> BC trial 8 subjects, in 2<sup>nd</sup> BC trial 5 subjects and in 3<sup>rd</sup> BC trial 7 subjects have no significant difference (with 95% accuracy) between the two sets of data). This model approves our experimental data (in the sense of comparison done in this section) but still it does not contain any foot dynamics.

#### **4.2.2 SIMPLE RIGID FOOT MODEL WITH FRICTION FORCES**

This model is the same as previous one except that the friction forces ( $f_M$  and  $f_C$ ) have been added to the M and C points.

The free body diagram of this model is shown in Figure 4-3. In this figure and the following figures in this chapter for other free body diagrams, T is not an external

torque; it is representing the net internal torque exerted by the muscles such as tibialis anterior and Gastrocnemius muscle.

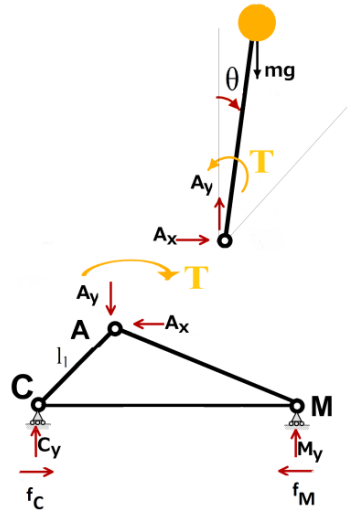


Figure 4-3 Free body diagram of rigid foot model with friction

There is no dynamic force in this model so there is no joint reaction force in horizontal direction, so  $f_C = f_M$ . And since the link between C and M is rigid, it cannot bear these two forces in opposite directions. So it seems like this model is not reasonable at all and it cannot be simulated.

#### 4.2.3 SWAYING FOOT MODEL WITH NO FRICTION FORCES

As it can be seen in Figure 4-4 this model is similar to first model except that some dynamics are added to the top so the model can have postural sway.

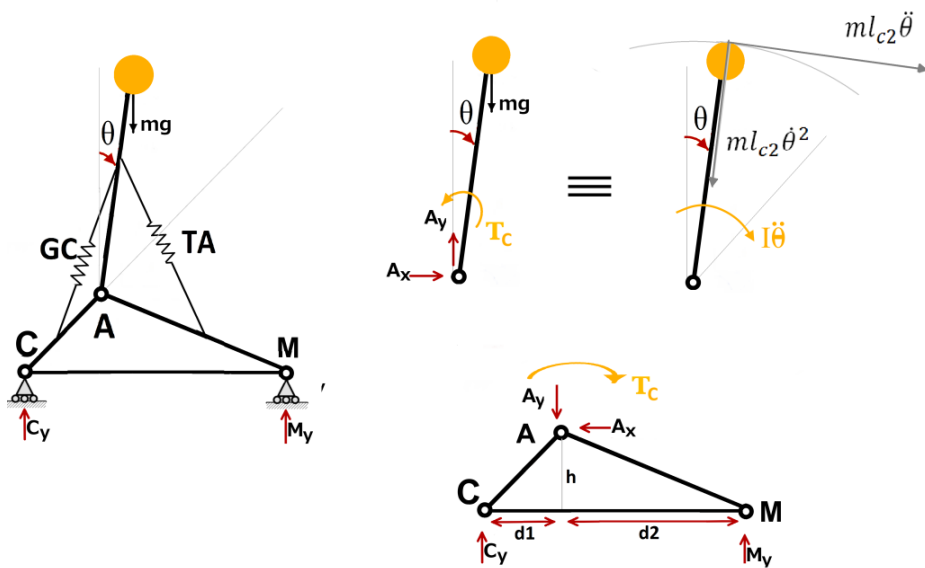


Figure 4-4 Swaying foot model with no friction forces

Having all relations and equations for this model (APPENDIX B, 1.1) it can be concluded:

$$\begin{aligned} \dot{\theta}^2 \sin \theta = \ddot{\theta} \cos \theta \Rightarrow \theta(t) &= \sin^{-1}(\theta_0 + t\sqrt{1 - \theta_0^2}) \\ &\approx \sin^{-1}(\theta_0 + t) \end{aligned} \quad 4-1$$

But when this  $\theta$  is calculated and compared to the experimental  $\theta$  from motion capture system, it can be seen that these sets of data are not the same. Additionally it can be seen from the equation above that this  $\theta$  is diverging and cannot be oscillating in any limited intervals.

Figure 4-5 shows the  $\theta$  obtained by this equation for an initial condition ( $\theta_0$ ). It can be seen easily  $\theta$  is out of rational boundaries. Since  $(\theta_0 + t)$  is ascending always in time, it is obvious that from one point on, its values can be out of defined intervals for arcsine function domain and hence it can be concluded that it is impossible to have this model as a human foot model.

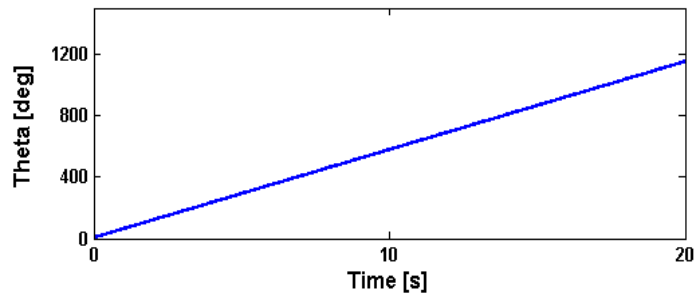


Figure 4-5 Theta obtained from swaying foot model with no friction forces

Trying to have a better study on this model, the C joint has been changed to a fixed joint rather than a roller one (Figure 4-6). In this case the equations will change to the ones shown in APPENDIX B, 2.8 to 2.13.

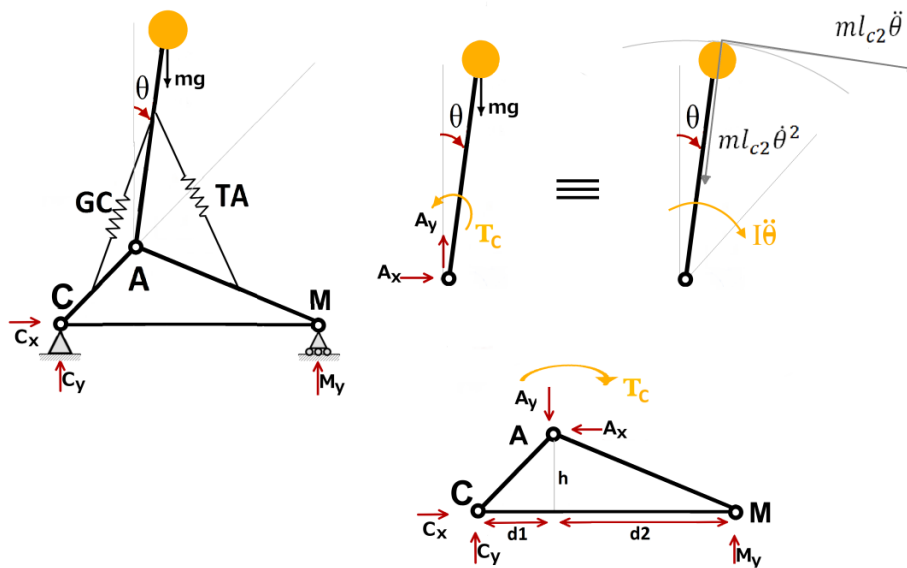
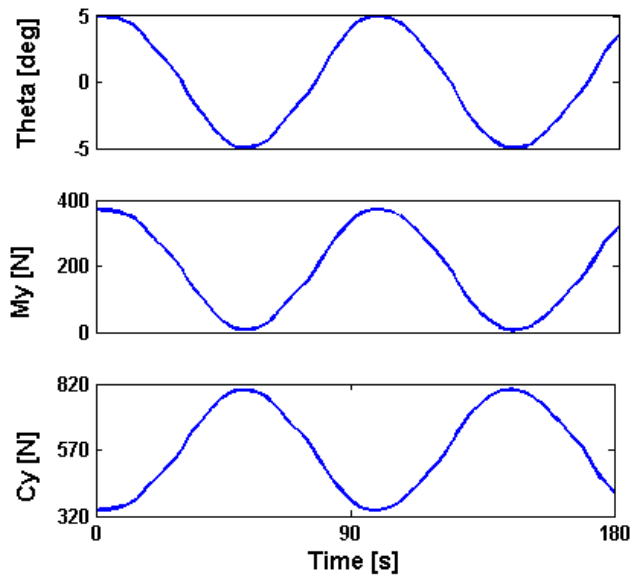


Figure 4-6 Swaying foot model with no friction forces and fixed calcaneus

The new model has been simulated in Simulink and the output signals are shown in Figure 4-7. Since there was an inconsistency problem for solving this model (the number of unknowns were less than the number of equations) a control strategy was added to system:  $T_c = k\theta$  where  $k \approx mgl_{c2}$ .



**Figure 4-7 Output signals for swaying foot model with no friction forces and fixed calcaneus**

As it can be seen in the figure, the mean value of  $C_y$  and  $M_y$  do not have the relation  $C_y = 2M_y$ , the ratio between them is approximately 2.85. The ratio  $\frac{C_y}{M_y}$  is calculated for all of data points; the mean of these ratios is 3.19. Although the mean ratio is not the same as the experimental value but still it shows that mean  $C_y$  value is greater than mean  $M_y$  value; meaning that this foot model is basically depending on the calcaneus rather than metatarsals as the real human foot does. Figure 4-8 shows the plot for this ratio in time, the red lines indicate the 5% tolerance ( $2 \pm 2 * 0.05$ ). This is similar to calculation of validation time in chapter 3. The parts of plot that are placed between red lines show the duration of time that  $\frac{C_y}{M_y}$  ratio is complying the “1/3 & 2/3” rule with 5% tolerance.

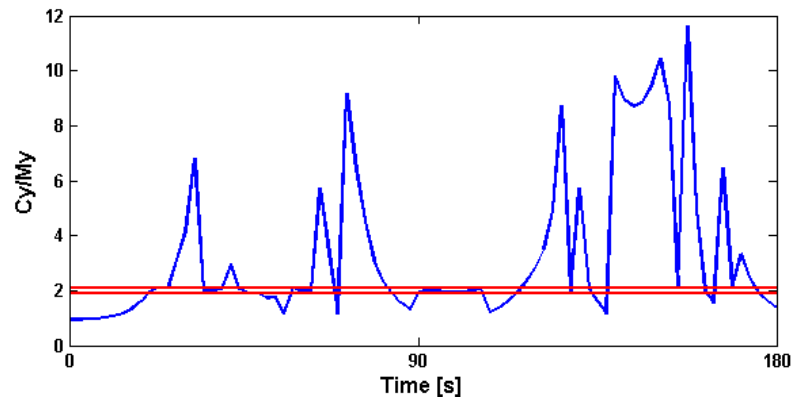


**Figure 4-8 Ratio between  $C_y$  and  $M_y$  for swaying foot model with no friction forces and fixed calcaneus; red lines show 5% tolerance**

Here only in 30.48% of time the model is acting inside the valid intervals of “1/3 & 2/3” rule with 5% tolerance. So it can be stated that this model is showing the behavior of human foot very weakly.

#### **4.2.4 SWAYING FOOT MODEL WITH FRICTION FORCES**

For this subsection, the previous model is repeated but the friction forces are not ignored this time (Figure 4-9).

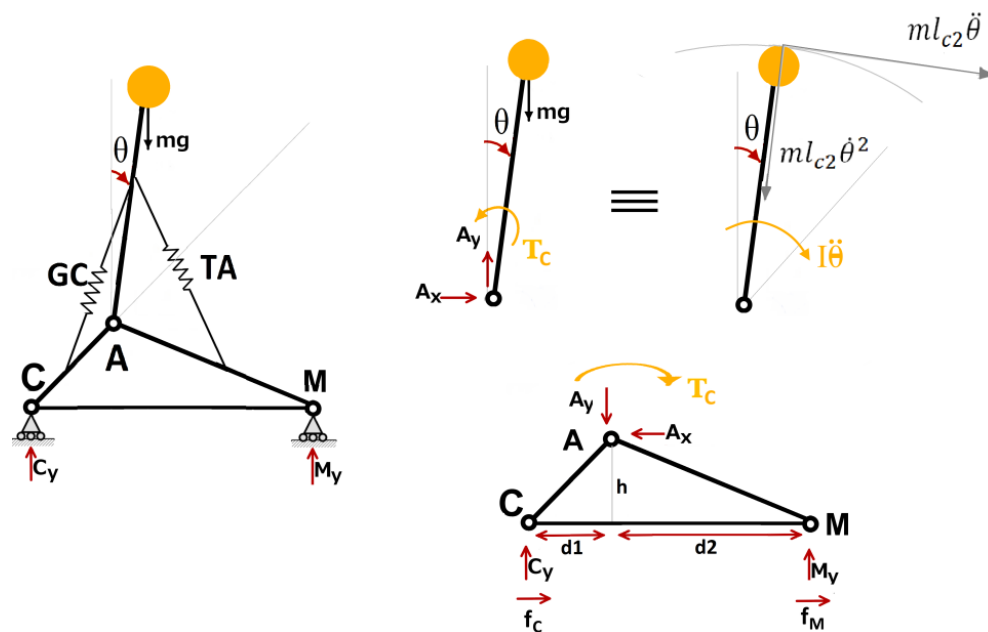
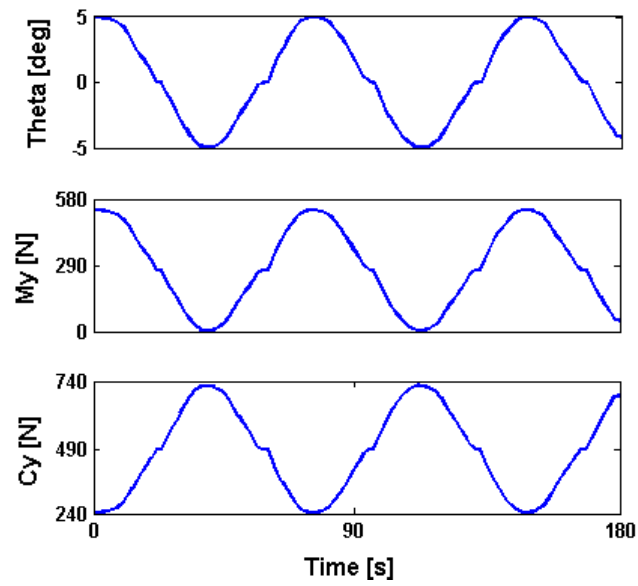


Figure 4-9 Swaying foot model with friction forces

Using the equations of this model shown in APPENDIX B, 3, GRF distribution is calculated. This model has been simulated using Simulink and its output signals are shown in Figure 4-10. Just like the previous model, here also number of unknowns was less than the number of equations. In order to solve this problem a control strategy has been added to system:  $T_c = k\theta$  where  $k \approx mgl_{c2}$ .



**Figure 4-10 Output signals for swaying foot model with friction forces**

As it can be estimated from figure, mean value of  $M_y$  is equal to 292.7 and the mean value of  $C_y$  is equal to 492.1; the ratio between them is 1.68. After calculating this ratio for each data point and the mean value of this set of ratios, it is observed that the mean of them is 1.99 and in 67.27% of time the ratio is in the valid interval of “1/3 & 2/3” rule with 5% tolerance. This calculation is done like in the previous model and experimental data. Figure 4-11 shows the ratio between  $C_y$  and  $M_y$  in time and the red lines in this figure indicate the 5% tolerance. So it seems like the GRF distribution in this model is in the same pattern as the experimental data, though mean validation time for experimental data is more than 90%.

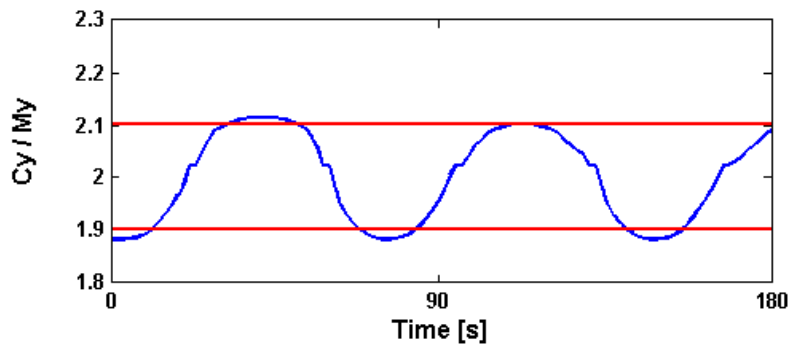


**Figure 4-11 Ratio between Cy and My for swaying foot model with friction forces; red lines show 5% tolerance**

The other concept that can be studied in this model is the friction coefficient ( $\mu$ ) of human skin. It has been shown to be greater than 0.2 and typically around 0.5 in case of dry skin and more than 1 in case of wet skin [37]. The friction coefficient has been calculated for this model. Since the skin beneath the feet of a human being show almost the same physical properties in all of its points, it is rational to assume the friction coefficients in calcaneous and metatarsals to be equal ( $\mu_C = \mu_M$ ). Figure 4-12 shows the friction forces and friction coefficient calculated in this model. As it can be seen in this figure, the coefficient is not inside valid intervals ( $3.5E-5 \pm 3.3E-5$ ).

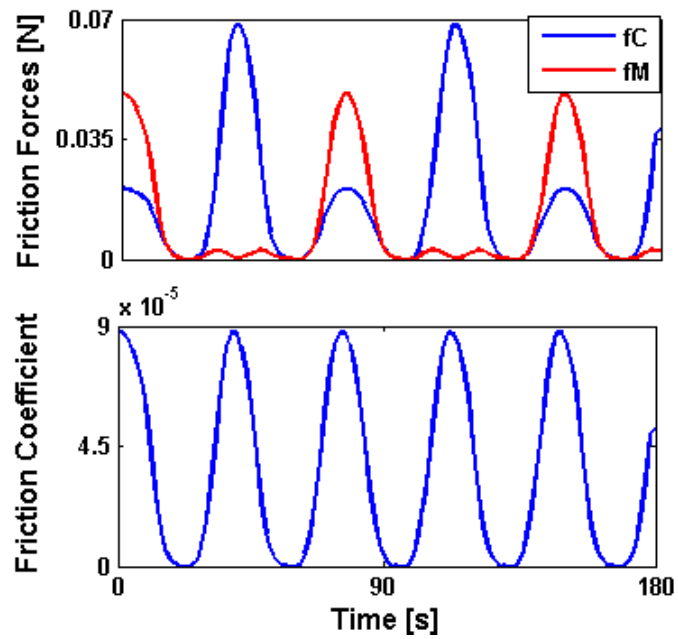
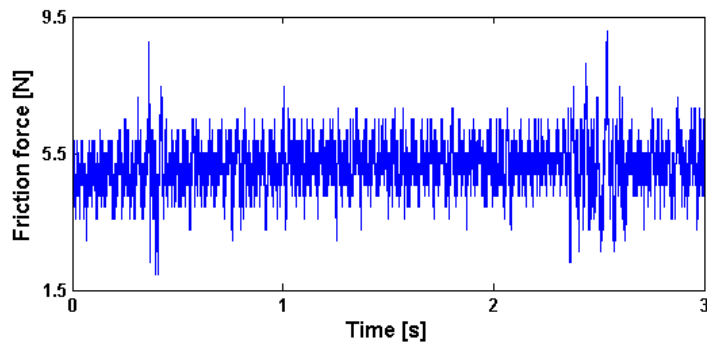


Figure 4-12 Friction forces and friction coefficient for swaying foot model with friction forces

Table 4-9 shows the mean and STD values for the resultant friction force measured in bipedal trials of experiments and Figure 4-13 shows this force in one of the trials. Comparing these values with the friction forces obtained from model, it can be seen that the model is not representing the friction forces like the measured values from experiments.

**Table 4-9 Experimental friction forces in bipedal trials**

	<i>Friction force [N]</i>
<i>Subject no.1</i>	$4.57 \pm 1.22$
<i>Subject no.2</i>	$5.95 \pm 1.08$
<i>Subject no.3</i>	$8.44 \pm 1.25$
<i>Subject no.4</i>	$0.84 \pm 0.22$
<i>Subject no.5</i>	$1.97 \pm 1.06$
<i>Subject no.6</i>	$6.70 \pm 2.67$
<i>Subject no.7</i>	$9.75 \pm 1.48$
<i>Subject no.8</i>	$5.99 \pm 1.08$
<i>Subject no.9</i>	$2.08 \pm 1.62$
<i>Subject no.10</i>	$10.18 \pm 1.88$
<i>Subject no.11</i>	$10.98 \pm 2.30$
<i>Subject no.12</i>	$4.66 \pm 1.67$
<i>Subject no.13</i>	$2.76 \pm 1.68$
<i>Subject no.14</i>	$2.28 \pm 0.75$



**Figure 4-13 Experimental friction force**

#### **4.2.5 DEFORMABLE FOOT WITH NO FRICTION FORCES**

Here the plantar aponeurosis of the foot is modeled as a linear spring; this gives the ability of deforming in length to the foot. The free body diagram is shown in Figure 4-14 and the equations are shown in APPENDIX B/4. As it has been stated before in

previous chapters and it can be easily concluded from the figure, the linear deformations of the plantar aponeurosis is the same as the angular deformations of the medial longitudinal arch which is modeled using the angle  $\alpha_1$  in the figure.

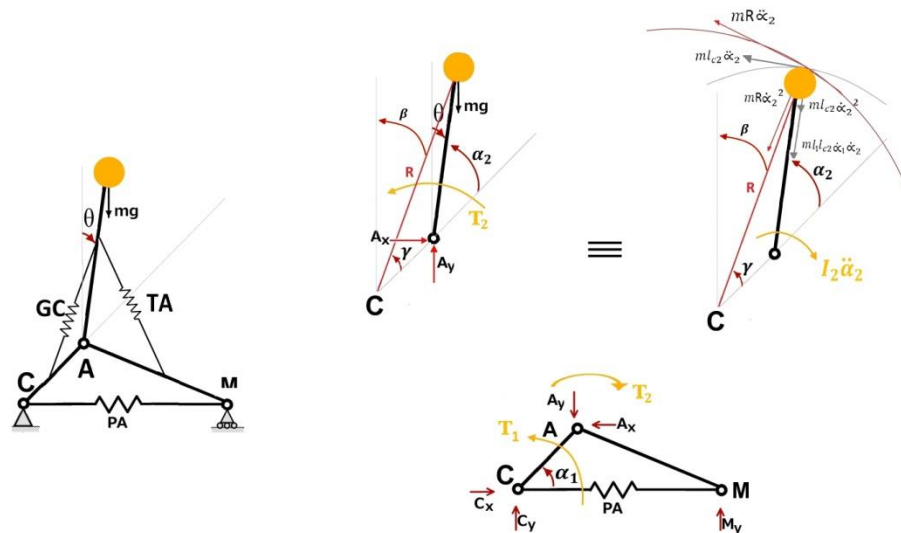


**Figure 4-14 Free body diagram for deformable foot with no friction forces with normal approach**

As stated before in swaying foot models,  $T_2$  is not an external torque; it represents the resultant internal torque exerted by muscles and is explicable by sensory fusion behavior of human brain. In this model (like the previous two models) the number of unknowns is less than the number of equations, so to solve this problem  $T_2$  has been used as a control strategy  $T_2 = k\theta$  where  $k \approx mgl_{c2}$ . The second control strategy is used for  $T_1$  as:  $T_1 = k_1\alpha_1$ ;  $k_1$  has been assigned equal to 10000 according to literature [5].

But still the unknowns' number was less than the equations; so  $C_x$  was given to system as an input. Since this signal has mean value equal to 5.14 with STD equal to 0.7, it could be imagined as a constant signal with some noise, so it is given to system as constant value equal to 5 [N].

Figure 4-15 shows the angular displacements for this model. These signals are oscillating inside the theoretical intervals for each of them, showing that the foot is standing balanced during this simulation.

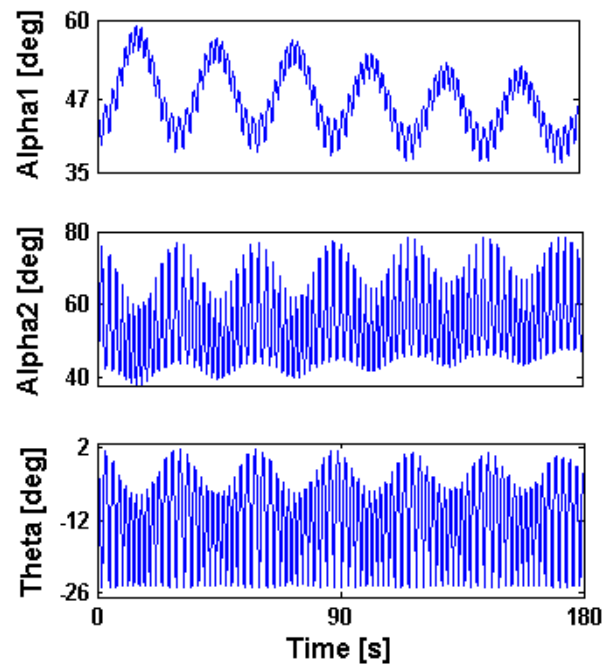


**Figure 4-15 Angular displacements for deformable foot model with no friction forces**

Figure 4-16 shows the output signals for this model including  $M_y$ ,  $C_y$  and plantar aponeurosis length. As it can be estimated from figure, mean value of  $M_y$  is equal to 212.45 and the mean value of  $C_y$  is equal to 560.13; the ratio between them ( $\overline{C_y}/\overline{M_y}$ ) is 2.63. When this ratio is calculated data point by data point between  $C_y$  and  $M_y$ , the average value of ratios is equal to 1.96 and the validation time is 63.8% of total simulation time which means that in this percentage of time the ratio is in the valid interval of “1/3 & 2/3” rule with 5% tolerance.

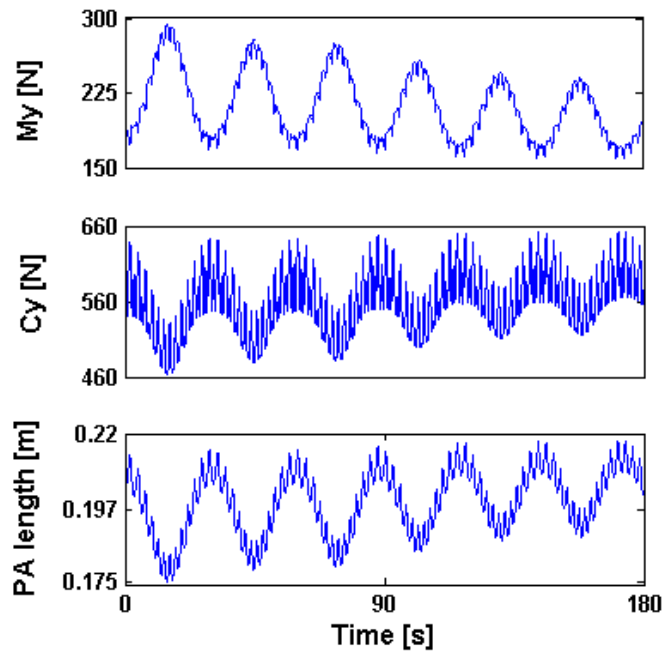


Figure 4-16 Output signals for deformable foot model with no friction forces

Like previous section, here the calculation of validation time has been done with 5% tolerance which is illustrated in Figure 4-17.

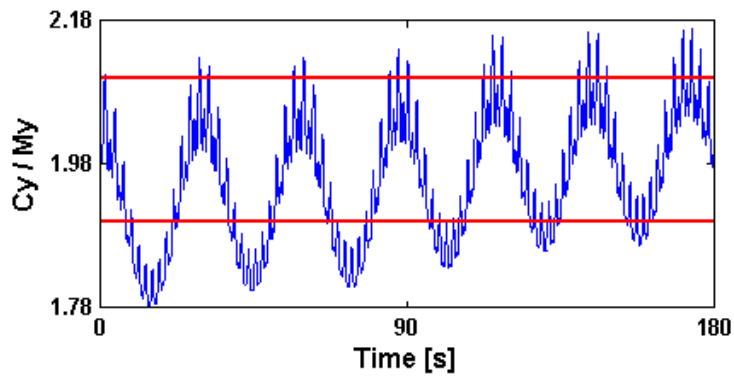


Figure 4-17  $C_y$  and  $M_y$  for deformable foot model with no friction forces; red lines show 5% tolerance

This figure shows the ratio between  $C_y$  and  $M_y$  in time; the red lines indicate the 5% tolerance. Again here GRF distribution follows the pattern that of experimental data

( $C_y/M_y$  is never less than 1 for all of data points) and again the validation time is less than the validation time in experiments.

Figure 4-16 shows also the changes in the length of plantar aponeurosis (S) in time. This parameter has its mean value equal to  $0.199 \pm 0.01$  meters, oscillating with maximum peak-to-peak value 0.043. The measured S from the subject whose parameters are being used for the models is 0.2. Calculating the absolute error between the values of S from model and 0.2 (using equation 4-2), it is observed that this set of errors has mean value equal to  $4.23\% \pm 2.68\%$ .

$$err = \frac{|S - 0.2|}{0.2} * 100 \quad 4-2$$

Since we were looking for any evidence of the role of PA deformations (and therefore medial longitudinal arch deformations) in posture, this can be assumed to be in support of the hypothesis of this study. But the problem is that these deformations are happening in greater values than expected. As it can be seen in the figure, in some places the deformations are happening in the range of  $\pm 2$  cm, which is impossible due to the physiology of human foot.

### 4.3 CONCLUSION

Five different models for human foot were studied, modeled and simulated. The main idea that has been looked for in all of these models is the accuracy of “1/3 & 2/3” rule.

The first one is a static model which is used to show that data analysis is in the right path. This model is not connected with the aims of this thesis because it is completely static.

Second model is still a static model but in this one the friction forces beneath foot is added to the model. It is discussed that this model is not reasonable and it cannot be simulated.

In third model some dynamics have been added to the top of human body but the foot is still static and without any frictions. It is shown that if calcaneus is assumed

to be a roller joint, the model will be unreasonable and impossible but by assuming calcaneus as a fixed joint this problem will be solved. But this case is not so realistic since calcaneus is not really fixed. However the validation time of this case is 30% which is far below the validation time of experimental data.

The fourth model is similar to the third one except for the friction forces that have been added here beneath the foot. The validation time in this model is around 70%. This is better than the validation time of the previous model but still less than the validation time of experimental data. In this case the friction coefficient was calculated but it was not inside the valid interval that has been explained in literature.

The fifth model is a dynamic model. It consists of postural sway on top of a deformable human foot. Again the validation time is around 70%. Cy/My ratio is never less than 2, this shows that the model is in the right path although it cannot achieve the validation time of the experimental data. Additionally the linear deformation for PA is calculated and it seems to be limited around its initial value. This deformation bears the same meaning as the angular deformation of medial longitudinal arch and shows its existence in the postural parameters. But in this model this deformation is not limited inside the expected interval. In some points the deformation got far out of its physiological limits.



## CHAPTER5

### CONCLUSION

#### 5.1 SUMMARY

This study was done with the purpose of discussing the pattern of pressure distribution on the foot sole between metatarsals and calcaneous, so obtaining the relation between them in quiet stance. This would lead to understanding the variety between strategies of different people in standing still. There was a basic hypothesis which was examining throughout this work. This hypothesis explains that the pressure distribution beneath the foot is 1/3 in metatarsals and 2/3 in calcaneous. But even though calcaneous bears most of the load and body pressure in quiet stance but it is the metatarsals that maintains the postural dynamics and hence keeps the body stable.

First phase of the thesis is experimental. For experiments, 14 healthy subjects were examined in some tests during which relating data was gathered using three devices:

- Pressure mat: MatScan<sup>®</sup> 3150 (TekScan, Inc.)
- Forceplate: FP4060-07-1000 (Bertec, Co.)
- 3D motion capture system: MVN Biomech (Xsens Inc.)

The gathered data was analyzed using a code written in MATLAB. Various parameters –which thought to be helpful for the purpose of the study- were calculated and reviewed.

In the second phase of thesis, five planar models were proposed and simulated. The last model which studied the deformations of the foot by simulating the deformations of medial longitudinal arch in saggital plane, showed more accurate results than others. In this model the whole body posture model was treated as a double inverted pendulum thus giving the opportunity to model the foot deformations as a separate DoF. This separate DoF was the angular displacement of the rigid link between calcaneous and ankle. Because the foot was modeled as a simple truss, this angular displacement and linear displacement of metatarsals are two dependent kinematic variables and the linear displacement biologically is equivalent to linear changes in the length of plantar aponeurosis in the foot sole.

## **5.2 DISCUSSIONS**

### **5.2.1 EXPERIMENTS**

First a brief pre-validation was done using experimental data. In this validation the COPx signals which were obtained from pressure mat were compared with the equivalent signals obtained from force plate. This validation showed that they are almost the same and as a result it is concluded that both of these devices were giving approximately the same information using different means.

Second ground reaction force distribution (along anterior-posterior direction) which was of a great interest throughout this study was calculated in bipedal cases to check for the “1/3 & 2/3” rule. Regarding the literature, ground reaction force in calcaneous ( $C_y$ ) needs to be twice of that in metatarsals ( $M_y$ ). To check this, two parameters were defined: validation time and instability factor. The former is the time period during which the rule is been complied and the latter is the frequency of stability disturbance, i.e. the number of times that  $\frac{C_y}{M_y}$  ratio changes between values more than two and values less than two with a tolerance of 5%.

In bipedal cases the mean of validation time percentage for all of the subjects was 92.17% and STD was equal to 8.55%. The least validation time was 73.7%. Instability factor and validation time had a reverse relation. Subjects who comply the rule in almost 100% of the time have instability factor near to zero.

Separating open-eyes and closed-eyes case types, it was observed that validation time percentage was slightly higher and instability factor was lower in the first one. Validation time percentage and average instability factor for open-eyes cases were 94.39% and 159.57 respectively and for closed-eyes cases they were 89.42% and 241.21 respectively. Hence it can be concluded that in closed-eyes trials the “1/3 & 2/3” rule was violated more often than open-eyes trials.

It was expected for right and left foot to bear different amounts of load but it did not happen. Almost in all of the cases both feet were bearing nearly the same load and functioning approximately similar. For more details on this,  $M_y$  on right foot was compared with  $M_y$  on left foot. In right footed subjects the  $\frac{M_{y-R}}{M_{y-L}}$  ratio was slightly higher than 1 ( $mean = 1.05$  and  $STD = 0.15$ ) and for left footed subjects it was slightly smaller than 1 ( $mean = 0.91$  and  $STD = 0.07$ ). The same was done for  $C_y$  too and similar results were observed. It can be concluded that  $M_y$  and  $C_y$  were both a bit larger for dominant foot than the other one.

Third, previous analysis was done for unipedal trials. In these trials again the “1/3 & 2/3” rule could be observed and as it was expected the error of  $M_y$  and  $C_y$  from 1/3 and 2/3 respectively were higher than those in bipedal cases. In unipedal-right foot case there were errors up to 25% and in unipedal-left foot case the error for half of the subjects were more than 10%. These large errors are because of unipedal stance not being stable enough. So the foot loses its stability easily and needs to use different regions of its surface to stand still, hence puts the focus of ground reaction force on those regions and tries to stabilize. This makes  $C_y$  decrease and specifically  $M_y$  increase. So by losing stability, meeting  $M_y$  is one of the strategies to gain stability back. So the subjects try to use some rapid meets on metatarsals to keep themselves standing still and stable. This is the main idea and hypothesis that was being looked for in this thesis.

Vision is one of the most important sensors in maintenance of body posture and stability. By closing eyes in trials this sensor was switched off and so the body lacked enough information for this maintenance. In unipedal cases where there were

more circumstances to lose the stability of body posture, this lack was clearer. Most of the subjects had larger validation time and smaller instability factors in open-eyes trials rather than closed-eyes ones.

The other idea was dominant foot being stronger than non-dominant one, so standing unipedal on dominant foot would be more stable than standing on non-dominant foot. Unlike bipedal, no enough evidence was found to prove this statement.

The fourth stage of the thesis was to calculate the ground reaction force distribution along lateral-medial direction. In this approach two pressure elements were considered: Lat, which is the pressure focused on the lateral part of the foot excluding calcaneus and ROI which is a specific region around sesamoid. ROI validation time - the time period during which  $\frac{ROI}{Lat} \geq 1$ - and ROI instability factor - the number of times that the subject has changed the focus of pressure between ROI and Lat - were calculated. The mean value of these time periods is 70.46% and the STD equal to 30.74% with a total factor equal to 4212.

Observations show that although Lat has a larger area than ROI, subjects prefer to use ROI more than Lat. When stability is disturbed, putting the majority of GRF on metatarsal helps more than any other strategy to regain the stability –such as meeting the lateral part of the foot. So our hypothesis seems to be true in most of the times for this population.

Additionally behavior of each subject in open-eyes is significantly similar to that in closed-eyes. Meaning that the ROI instability factor of a specific subject in open-eyes trial may be slightly different than that in closed-eyes trial but it would not be a large difference interval.

The fifth step of the procedure was calculating the correlation between  $COP_x$  and different pressure components. The correlation coefficients showed that  $M_y$  signals had the greatest effect on  $COP_x$  signals. Comparing between right and left feet,  $RM_y$  and  $LC_y$  have greater effects on  $COP_x$  than  $LM_y$  and  $RC_y$  respectively. This can be considered as another observation for our hypothesis. In unipedal experiments during

which the subjects have undergone more instabilities,  $M_y$  has the great effect on re-stabilization of the subjects and hence their  $COP_x$ . But in bipedal cases where there are less instabilities, the  $M_y$  may be less correlated with  $COP_x$  in some cases.

The sixth and last step was to find the pattern of changes in the length of plantar fascia. This was done again using the COM signals. Resulting values for this length proved the primary assumption of the presented model true, fascia is changing so smoothly during quiet stance.

### **5.2.2 MODELING**

Various scenarios and theories are simulated as foot models. The primary idea is that a rigid foot model cannot explain or predict the behavior of human foot accurately. In these simulations the GRF distribution has been used to investigate this theory. In literature it has been stated that the GRF should be distributed as 1/3 in metatarsals and 2/3 in calcaneous. And the experimental data approved this theory with some tolerance.

The first model was the simplest rigid foot with no friction forces. This static model was able to show the GRF distribution in favor of the “1/3 & 2/3” rule but it had no dynamics. It is used just to show that data analysis and segmentation of pressure beneath foot (defining the calcaneous and metatarsals sections) is in the right path.

In second model friction forces were added to the first one. But with equations it could be proved that the model was not rationally valid and cannot be simulated.

The third model had some dynamics so it could have postural sway but no friction forces. This model again was proved to be rationally impossible in case of calcaneous being a roller joint. But when calcaneous became a fixed joint, the model happened to be valid and possible but with no sufficient validation time compared to experimental data. So it was concluded that the model was not explaining the behavior of the human foot correctly.

The fourth model is similar to the third one except for the friction forces that have been added here beneath the foot. The validation time in this model is around 70%

which is better than the validation time of the previous model but still less than the validation time of experimental data.

The fifth model is a dynamic model consisting of postural sway on top of a deformable foot. Although validation time is near to the previous model which is a rigid foot with swaying body, but this model has the privilege of showing foot deformations. Linear deformation for PA, which is equal to angular deformation of medial longitudinal arch in terms of human body function in postural study, is calculated. This deformation is oscillating around the initial value of PA length. It shows that the PA is changing its length and therefore is deforming during standing still and helping the postural parameters and stability this way. But the problem of this model is that in some regions this deformation gets out of its physiological limits.

In Appendix C the same model is shown but in this case the equations are used based on Zatsiorsky's works [38]. Although this model is equivalent to the last model of previous chapter, the output signals of them do not behave similarly. Output signals of the model in Appendix C are diverging in time. Because of the limitations of this approach (number of equations less than number of unknowns) it was necessary to give the  $M_y$  signal from experiments as an input to this system and this is possible to be one reason of unexpected behavior of the output signals.

### **5.3 FUTURE WORK**

The last model needs to be completed by adding friction forces because in reality always there is friction force beneath foot and calcaneus is not a fixed joint. Changes in friction forces can cause different behaviors of human foot towards deformations in medial longitudinal arch and hence in plantar aponeurosis.

This has been partly done in Appendix D. As a try to find the best parameters and gains of the system, stability test was done but without any results. To improve this matter another model was implemented but it did not go through the stability test successfully either. This model and the stability tests details are explained in Appendix D. In the end it is concluded that having friction forces would not be

enough as a solution to this problem and more information on the system would be needed. Fixing this problem can be the most important thing to be done after this thesis.

Some conditions such as ‘eyes-closed/eyes-open’ and ‘unipedal/bipedal’ can be added to the model as switches, to fortify the model. This will increase the complexity of the model and its understanding but it also makes it able to act more similar to human body. This part remained as a future work for the model but it has been considered in the experiments and data gathering.

The experimental procedure should be repeated with more subjects, so it can be possible to categorize the subjects by their gender, dominant foot, etc. And different types of surfaces must be used beneath the subjects’ feet to examine the surface type (and therefore the friction forces role) in quiet stance. As it is explained previously, any change in this type of conditions that can cause changes in friction forces, may lead to different behaviors in human postural control system and in deformations of medial longitudinal arch and plantar aponeurosis.

Most of the assumptions that have been made here are for normal healthy people. But if the experiments get repeated for flat-feet people it may give interesting information. This kind of information can be used in shoe industry or to help them in sports or even routine life.



## REFERENCES

1. Standring, S., *Gray's Anatomy: The Anatomical Basis of Clinical Practice* 2008.
2. Winson, G., A. Lundberg, and C. Bylund, *The pattern of motion of the longitudinal arch of the foot*. *The Foot*, 1994. **4**(3): p. 151-154.
3. Yavuz, M., G. Botek, and B.L. Davis, *Plantar shear stress distributions : Comparing actual and predicted frictional forces at the foot – ground interface*. 2007. **40**: p. 3045–3049.
4. Gefen, A., *Stress analysis of the standing foot following surgical plantar fascia release*. *Journal of biomechanics*, 2002. **35**(5): p. 629–37.
5. Kim, W. and A.S. Voloshin, *Role of plantar fascia in the load bearing capacity of the human foot*. *Journal of biomechanics*, 1995. **28**(9): p. 1025-1033.
6. Rouhani, H., et al., *Ambulatory assessment of 3D ground reaction force using plantar pressure distribution*. *Gait & posture*, 2010. **32**(3): p. 311-6.
7. Ledoux, W.R., *A biomechanical model of the human foot with emphasis on the plantar soft tissue*. 1999.
8. Kärki, S., et al., *Plantar pressure distribution measurements: An approach to different methods to compute a pressure map*. *Age (years)*, 2009. **23**(3): p. 19-30.
9. Bolgla, L.A. and T.R. Malone, *Plantar fasciitis and the windlass mechanism: a biomechanical link to clinical practice*. *Journal of athletic training*, 2004. **39**(1): p. 77.
10. Wright, W.G., Y.P. Ivanenko, and V.S. Gurfinkel, *Foot anatomy specialization for postural sensation and control*. *Journal of neurophysiology*, 2012. **107**(5): p. 1513-21.
11. Kiemel, T., A.J. Elahi, and J.J. Jeka, *Identification of the plant for upright stance in humans: multiple movement patterns from a single neural strategy*. *Journal of Neurophysiology*, 2008. **100**(6): p. 3394-3406.

12. Winter, D.A., et al., *Ankle muscle stiffness in the control of balance during quiet standing*. Journal of neurophysiology, 2001. **85**(6): p. 2630-2633.
13. Winter, D.A., *ABC (anatomy, biomechanics and control) of balance during standing and walking*1995: Waterloo Biomechanics.
14. Massey Jr, F.J., *The Kolmogorov-Smirnov test for goodness of fit*. Journal of the American statistical Association, 1951. **46**(253): p. 68-78.
15. Hicks, J., *The mechanics of the foot: II. The plantar aponeurosis and the arch*. Journal of anatomy, 1954. **88**(Pt 1): p. 25.
16. Haibach, P.S., et al., *Virtual time-to-contact of postural stability boundaries as a function of support surface compliance*. Experimental brain research, 2007. **177**(4): p. 471-482.
17. Gerbino, P.G., E.D. Griffin, and D. Zurakowski, *Comparison of standing balance between female collegiate dancers and soccer players*. Gait & posture, 2007. **26**(4): p. 501-507.
18. Jerosch, J., et al., *Is prophylactic bracing of the ankle cost effective?* Orthopedics, 1996. **19**(5): p. 405-414.
19. Fong, S.-M. and G.Y. Ng, *The effects on sensorimotor performance and balance with Tai Chi training*. Archives of physical medicine and rehabilitation, 2006. **87**(1): p. 82-87.
20. Schmitt, H., B. Kuni, and D. Sabo, *Influence of professional dance training on peak torque and proprioception at the ankle*. Clinical journal of sport medicine, 2005. **15**(5): p. 331-339.
21. Pearce, J., *Romberg's Sign*. Journal of neurology, neurosurgery, and psychiatry, 1993. **56**(1): p. 51.
22. Nataraj, R., M.L. Audu, and R.J. Triolo, *Comparing joint kinematics and center of mass acceleration as feedback for control of standing balance by functional neuromuscular stimulation*. J. Neuroeng. Rehabil, 2012. **9**(25).
23. Ambrozic, L., et al. *Wearable Sensory System for Robotic Prosthesis*. in RAAD. 2013. Portoroz, Slovakia.
24. Collins, J. and C. De Luca, *Upright, correlated random walks: A statistical-biomechanics approach to the human postural control system*. Chaos: An Interdisciplinary Journal of Nonlinear Science, 1995. **5**(1): p. 57-63.
25. Collins, J.J. and C.J. De Luca, *Random walking during quiet standing*. Physical review letters, 1994. **73**(5): p. 764-767.

26. Neumann, D.A., *Kinesiology of the musculoskeletal system: foundations for rehabilitation* 2013: Elsevier Health Sciences.
27. Hicks, J., *The three weight-bearing mechanisms of the foot*. Biomechanical studies of the musculo-skeletal system, 1961: p. 161.
28. Scott, S.H. and D.A. Winter, *Biomechanical model of the human foot: kinematics and kinetics during the stance phase of walking*. Journal of biomechanics, 1993. **26**(9): p. 1091-1104.
29. Simkin, A. and I. Leichter, *Role of the calcaneal inclination in the energy storage capacity of the human foot—a biomechanical model*. Medical and Biological Engineering and Computing, 1990. **28**(2): p. 149-152.
30. Kitaoka, H.B., et al., *Material properties of the plantar aponeurosis*. Foot & Ankle International, 1994. **15**(10): p. 557-560.
31. Winter, D.A., et al., *Stiffness control of balance in quiet standing*. Journal of neurophysiology, 1998. **80**(3): p. 1211-1221.
32. Winter, D.A., *Biomechanics and motor control of human movement* 2009: John Wiley & Sons.
33. Garcia, M., et al., *The simplest walking model: stability, complexity, and scaling*. Journal of biomechanical engineering, 1998. **120**(2): p. 281-288.
34. Kuo, A.D., *A simple model of bipedal walking predicts the preferred speed–step length relationship*. Journal of biomechanical engineering, 2001. **123**(3): p. 264-269.
35. Mergner, T., *A neurological view on reactive human stance control*. Annual Reviews in Control, 2010. **34**(2): p. 177-198.
36. Mergner, T., C. Maurer, and R. Peterka, *A multisensory posture control model of human upright stance*. Progress in brain research, 2003. **142**: p. 189-201.
37. Derler, S. and L.-C. Gerhardt, *Tribology of skin: review and analysis of experimental results for the friction coefficient of human skin*. Tribology Letters, 2012. **45**(1): p. 1-27.
38. Zatsiorsky, V.M., *Kinetics of Human Motion* 2002: Human Kinetics.



## APPENDIX A

### T-TABLE

Table A-1 T-table for t-test

<i>Degrees of Freedom</i>	<i>Probability, p</i>			
	<b>0.1</b>	<b>0.05</b>	<b>0.01</b>	<b>0.001</b>
<b>1</b>	6.31	12.71	63.66	636.62
<b>2</b>	2.92	4.30	9.93	31.60
<b>3</b>	2.35	3.18	5.84	12.92
<b>4</b>	2.13	2.78	4.60	8.61
<b>5</b>	2.02	2.57	4.03	6.87
<b>6</b>	1.94	2.45	3.71	5.96
<b>7</b>	1.89	2.37	3.50	5.41
<b>8</b>	1.86	2.31	3.36	5.04
<b>9</b>	1.83	2.26	3.25	4.78
<b>10</b>	1.81	2.23	3.17	4.59
<b>11</b>	1.80	2.20	3.11	4.44
<b>12</b>	1.78	2.18	3.06	4.32
<b>13</b>	1.77	2.16	3.01	4.22
<b>14</b>	1.76	2.14	2.98	4.14
<b>15</b>	1.75	2.13	2.95	4.07
<b>16</b>	1.75	2.12	2.92	4.02
<b>17</b>	1.74	2.11	2.90	3.97

**Table A-1 (continued)**

<b>18</b>	1.73	2.10	2.88	3.92
<b>19</b>	1.73	2.09	2.86	3.88
<b>20</b>	1.72	2.09	2.85	3.85
<b>21</b>	1.72	2.08	2.83	3.82
<b>22</b>	1.72	2.07	2.82	3.79
<b>23</b>	1.71	2.07	2.82	3.77
<b>24</b>	1.71	2.06	2.80	3.75
<b>25</b>	1.71	2.06	2.79	3.73
<b>26</b>	1.71	2.06	2.78	3.71
<b>27</b>	1.70	2.05	2.77	3.69
<b>28</b>	1.70	2.05	2.76	3.67
<b>29</b>	1.70	2.05	2.76	3.66
<b>30</b>	1.70	2.04	2.75	3.65
<b>40</b>	1.68	2.02	2.70	3.55
<b>60</b>	1.67	2.00	2.66	3.46
<b>120</b>	1.66	1.98	2.62	3.37
$\infty$	1.65	1.96	2.58	3.29

## APPENDIX B

### MODEL EQUATIONS

1. Simple rigid foot model with no friction forces

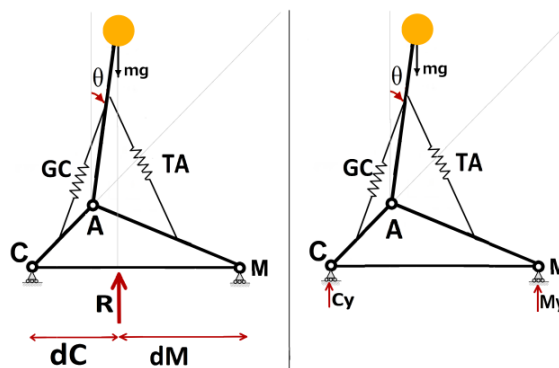


Figure B-1 Rigid foot with no friction forces

In the point of application of R:

$$1.1. M_y d_M - C_y d_C = 0 \Rightarrow \frac{C_y}{M_y} = \frac{d_M}{d_C}$$

2. Swaying foot model with no friction forces

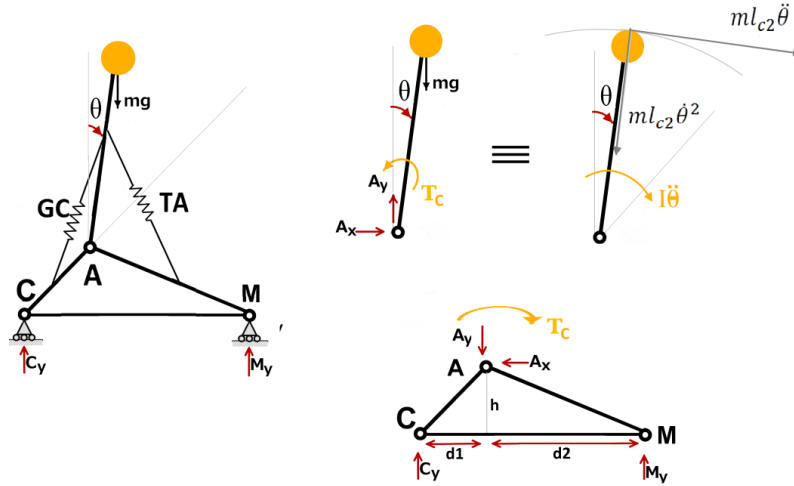


Figure B-2 Swaying foot with no friction forces and calcaneus a fixed joint

In triangle:

$$\begin{aligned}
 2.1. \sum f_x = 0 &\Rightarrow A_x = 0 \\
 2.2. \sum f_y = 0 &\Rightarrow A_y = C_y + M_y \\
 2.3. \sum M_A = 0 &\Rightarrow -C_y d_1 - T_c + M_y d_2 = 0 \\
 &\xrightarrow{s=d_1+d_2} T_c = M_y S - A_y d_1
 \end{aligned}$$

In upper link:

$$\begin{aligned}
 2.4. \sum f_x = 0 &\Rightarrow A_x = -ml_{c2} \dot{\theta}^2 \sin \theta + ml_{c2} \ddot{\theta} \cos \theta \\
 2.5. \sum f_y = 0 &\Rightarrow A_y - mg = -ml_{c2} \dot{\theta}^2 \cos \theta - ml_{c2} \ddot{\theta} \sin \theta \\
 2.6. \sum M_A = 0 &\Rightarrow T - mgl_{c2} \sin \theta = -ml_{c2}^2 \ddot{\theta} - I\ddot{\theta}
 \end{aligned}$$

So:

$$2.7. 1,4 \Rightarrow \dot{\theta}^2 \sin \theta = \ddot{\theta} \cos \theta$$

After making C a fixed joint:

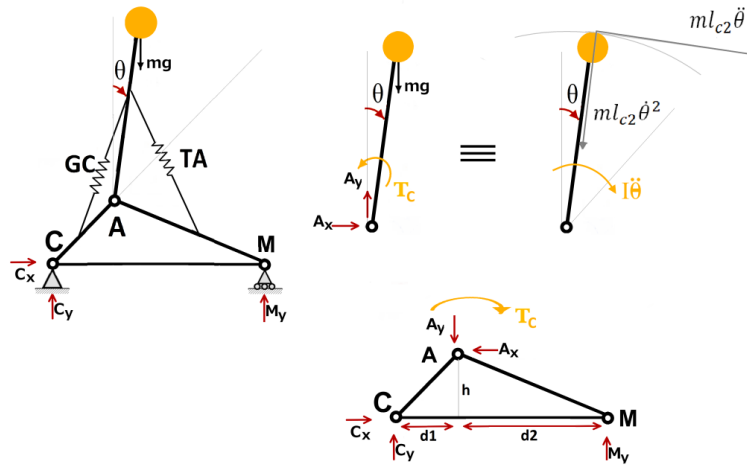


Figure B-3 Swaying foot with no friction forces and calcaneus a roller joint

In triangle:

$$\begin{aligned}
 2.8. \quad \sum f_x = 0 &\Rightarrow A_x - C_x = 0 \\
 2.9. \quad \sum f_y = 0 &\Rightarrow A_y = C_y + M_y \\
 2.10. \quad \sum M_A = 0 &\Rightarrow -C_y d_1 - T_c + M_y d_2 + C_x h = 0 \\
 &\xrightarrow{S=d_1+d_2} T_c = M_y S - A_y d_1 + C_x h
 \end{aligned}$$

In upper link:

$$\begin{aligned}
 2.11. \quad \sum f_x = 0 &\Rightarrow A_x = -ml_{c2}\dot{\theta}^2 \sin \theta + ml_{c2}\ddot{\theta} \cos \theta \\
 2.12. \quad \sum f_y = 0 &\Rightarrow A_y - mg = -ml_{c2}\dot{\theta}^2 \cos \theta - ml_{c2}\ddot{\theta} \sin \theta \\
 2.13. \quad \sum M_A = 0 &\Rightarrow T_c - mgl_{c2} \sin \theta = -ml_{c2}^2 \ddot{\theta} - I\ddot{\theta}
 \end{aligned}$$

So:

$$\begin{aligned}
 2.14. \quad 8,11 &\Rightarrow A_x = C_x = ml_{c2}(-\dot{\theta}^2 \sin \theta + \ddot{\theta} \cos \theta) \\
 2.15. \quad 9,12 &\Rightarrow C_y + M_y = mg - ml_{c2}(\ddot{\theta} \sin \theta + \dot{\theta}^2 \cos \theta) \\
 2.16. \quad 10,13 &\Rightarrow T_c = M_y S - A_y d_1 + C_x h = mgl_{c2} \sin \theta - (I + ml_{c2}^2)\ddot{\theta}
 \end{aligned}$$

And the control torque is assumed equal to:  $T_c = k_t \theta$

### 3. Swaying foot model with friction forces

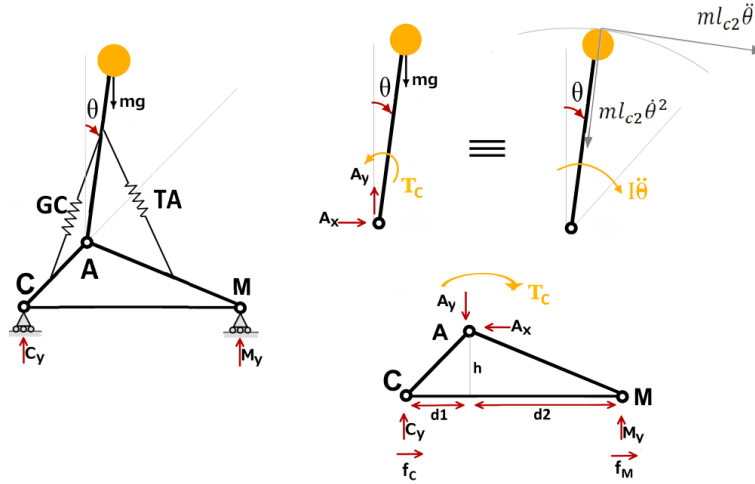


Figure B-4 Swaying foot with friction forces

In triangle:

$$\begin{aligned}
 3.1. \sum f_x = 0 &\Rightarrow -A_x + f_c + f_M = 0 \\
 3.2. \sum f_y = 0 &\Rightarrow A_y = C_y + M_y \\
 3.3. \sum M_A = 0 &\Rightarrow -C_y d_1 + f_c h - T_c + M_y d_2 + f_M h = 0 \\
 &\xrightarrow{S=d_1+d_2} T_c = M_y S - A_y d_1 + (f_c + f_M) h
 \end{aligned}$$

In upper link:

$$\begin{aligned}
 3.4. \sum f_x = 0 &\Rightarrow A_x = -ml_{c2}\dot{\theta}^2 \sin \theta + ml_{c2}\ddot{\theta} \cos \theta \\
 3.5. \sum f_y = 0 &\Rightarrow A_y - mg = -ml_{c2}\dot{\theta}^2 \cos \theta - ml_{c2}\ddot{\theta} \sin \theta \\
 3.6. \sum M_A = 0 &\Rightarrow T_c - mgl_{c2} \sin \theta = -ml_{c2}^2 \ddot{\theta} - I\ddot{\theta}
 \end{aligned}$$

So:

$$\begin{aligned}
 3.7. 1,4 &\Rightarrow f_c + f_M = \mu_C C_y + \mu_M M_y = ml_{c2}(-\dot{\theta}^2 \sin \theta + \ddot{\theta} \cos \theta) \\
 &\text{if } \mu_C = \mu_M = \mu \Rightarrow \mu = \frac{A_x}{C_y + M_y} = \frac{ml_{c2}(-\dot{\theta}^2 \sin \theta + \ddot{\theta} \cos \theta)}{C_y + M_y} \\
 3.8. 2,5 &\Rightarrow C_y + M_y = mg - ml_{c2}(\ddot{\theta} \sin \theta + \dot{\theta}^2 \cos \theta) \\
 3.9. 3,6 &\Rightarrow T_c = M_y S - A_y d_1 + (f_c + f_M) h = mgl_{c2} \sin \theta - (I + ml_{c2}^2)\ddot{\theta}
 \end{aligned}$$

And the control torque is assumed equal to:  $T_c = k_t \theta$

4. Deformable foot with no friction forces

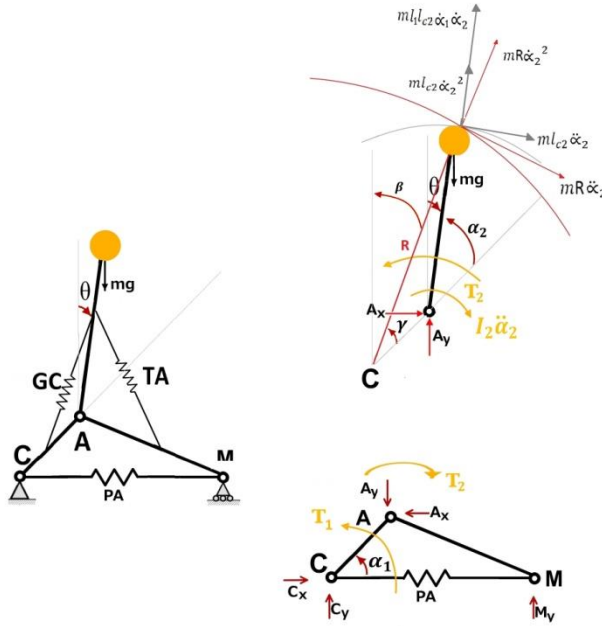


Figure B-5 Deformable foot with no friction forces

- 4.1.  $A_x = C_x$
- 4.2.  $A_y = C_y + M_y$
- 4.3.  $-T_2 + T_1 - C_y l_1 \cos \alpha_1 + M_y (S - l_1 \cos \alpha_1) + C_x l_1 \sin \alpha_1 - (I_2 + ml_{c2}^2) \ddot{\alpha}_2 - (I_2 + mR^2) \ddot{\alpha}_1 = 0$
- 4.4.  $A_x + ml_{c2} (\dot{\alpha}_2^2 \cos(\alpha_1 + \alpha_2) + \ddot{\alpha}_2 \sin(\alpha_1 + \alpha_2)) + mR (\dot{\alpha}_1^2 \sin \beta + \ddot{\alpha}_1 \cos \beta) + 2ml_{c2} \dot{\alpha}_1 \dot{\alpha}_2 \cos(\alpha_1 + \alpha_2) = 0$
- 4.5.  $A_y - mg + ml_{c2} (\dot{\alpha}_2^2 \sin(\alpha_1 + \alpha_2) - \ddot{\alpha}_2 \cos(\alpha_1 + \alpha_2)) + mR (\dot{\alpha}_1^2 \cos \beta - \ddot{\alpha}_1 \sin \beta) + 2ml_{c2} \dot{\alpha}_1 \dot{\alpha}_2 \sin(\alpha_1 + \alpha_2) = 0$
- 4.6.  $-T_2 + [I_2 + m(l_{c2}^2 + l_1 l_{c2} \cos \alpha_2)] \ddot{\alpha}_1 + (I_2 + ml_{c2}^2) \ddot{\alpha}_2 + ml_1 l_{c2} \sin \alpha_2 \dot{\alpha}_1^2 + mgl_{c2} \cos(\alpha_1 + \alpha_2) = 0$

Control strategies:

- 4.7.  $T_1 = k_1 \alpha_1$
- 4.8.  $T_2 = k_2 \theta = k_2 \left( \frac{\pi}{2} - (\alpha_1 + \alpha_2) \right)$

Since the number of unknowns is more than the number of equations here,  $C_x$  (measured in experiments) has been given to system as an input.

$$\beta = \frac{\pi}{2} - (\alpha_1 + \gamma) \text{ while: } \frac{\sin \gamma}{l_{c2}} = \frac{\sin(\pi - \alpha_2)}{R}$$

So:

$$4.9. \quad \ddot{\alpha}_1 = \left\{ (I_2 + ml_{c2}^2) (A_x + ml_{c2} \cos(\alpha_1 + \alpha_2) (\dot{\alpha}_2^2 + 2\dot{\alpha}_1\dot{\alpha}_2)) + ml_{c2} \sin(\alpha_1 + \alpha_2) (T_2 - mgl_{c2} \cos(\alpha_1 + \alpha_2) - ml_1 l_{c2} \dot{\alpha}_1^2 \sin \alpha_2) + mR(I_2 + ml_{c2}^2) \dot{\alpha}_1^2 \sin \beta \right\} / m \left\{ (I_2 + ml_{c2}^2) (l_{c2} \sin(\alpha_1 + \alpha_2) - R \cos \beta) + ml_1 l_{c2}^2 \sin(\alpha_1 + \alpha_2) \cos \alpha_2 \right\}$$

$$4.10. \quad \ddot{\alpha}_2 = - \left\{ (I_2 + ml_{c2}^2 + ml_1 l_{c2} \cos \alpha_2) (A_x + ml_{c2} \cos(\alpha_1 + \alpha_2) (\dot{\alpha}_2^2 + 2\dot{\alpha}_1\dot{\alpha}_2)) + mR \cos \beta (T_2 - mgl_{c2} \cos(\alpha_1 + \alpha_2)) + 2mR(I_2 + ml_{c2}^2) (\dot{\alpha}_1^2 + \dot{\alpha}_1\dot{\alpha}_2) \sin \beta + m^2 R l_1 l_{c2} \dot{\alpha}_1^2 \sin(\beta - \alpha_2) \right\} / m \left\{ (I_2 + ml_{c2}^2) (l_{c2} \sin(\alpha_1 + \alpha_2) - R \cos \beta) + ml_1 l_{c2}^2 \sin(\alpha_1 + \alpha_2) \cos \alpha_2 \right\}$$

$$4.11. \quad M_y = - \left[ (I_2 + mR^2) \ddot{\alpha}_1 + (I_2 + ml_{c2}^2) \ddot{\alpha}_2 + T_2 - T_1 - A_y (S - l_1 \cos \alpha_1) - C_x l_1 \sin \alpha_1 \right] / S$$

$$4.12. \quad C_y = A_y - M_y$$

## APPENDIX C

### DOUBLE INVERTED PENDULUM

In this model like the deformable foot model presented in chapter 4, the plantar aponeurosis of the foot is modeled as a linear spring and it has been assumed to have postural sway on top of the human body. The free body diagram for this model is shown below.

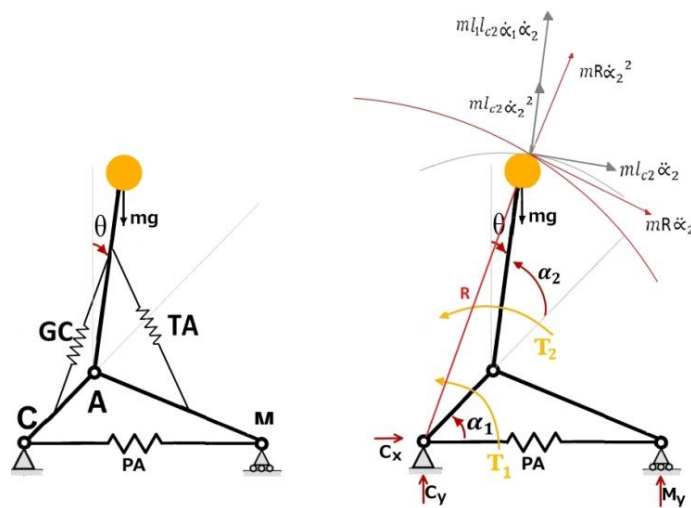


Figure C-1 Deformable foot model with no friction forces, double inverted pendulum approach

Here the problem has been changed into a double inverted pendulum which has been analyzed previously in Zatsiorsky's works. The equations are used from Zatsiorsky's book [38] (with some changes) and are shown below.

$$T_1 = [I_2 + m(l_1^2 + l_{c2}^2 + 2l_1l_{c2} \cos \alpha_2)] \ddot{\alpha}_1 + [I_2 + m(l_{c2}^2 + l_1l_{c2} \cos \alpha_2)] \ddot{\alpha}_2 \\ - ml_1l_{c2} \sin \alpha_2 \dot{\alpha}_2^2 - 2ml_1l_{c2} \sin \alpha_2 \dot{\alpha}_1 \dot{\alpha}_2 \\ + mg(l_1 \cos \alpha_1 + l_{c2} \cos(\alpha_1 + \alpha_2)) - M_y S$$

$$T_2 = [I_2 + m(l_{c2}^2 + l_1l_{c2} \cos \alpha_2)] \ddot{\alpha}_1 + (I_2 + ml_{c2}^2) \ddot{\alpha}_2 + ml_1l_{c2} \sin \alpha_2 \dot{\alpha}_1^2 \\ + mgl_{c2} \cos(\alpha_1 + \alpha_2)$$

Equations are solved to obtain  $\ddot{\alpha}_1, \ddot{\alpha}_2$ :

$$\ddot{\alpha}_1 = \{(I_2 + ml_{c2}^2)[T_1 - T_2 + M_y S + (\dot{\alpha}_1 + \dot{\alpha}_2)^2 ml_1l_{c2} \sin \alpha_2 - mgl_1 \cos \alpha_1] \\ + ml_1l_{c2}[-\cos \alpha_2 T_2 + mgl_{c2} \cos \alpha_2 \cos(\alpha_1 + \alpha_2) \\ + ml_1l_{c2} \dot{\alpha}_1^2 \sin \alpha_2 \cos \alpha_2]\} / \{m^2 l_{c2}^2 l_1^2 (\sin \alpha_2)^2 + I_2 ml_1^2\}$$

$$\ddot{\alpha}_2 = -\ddot{\alpha}_1 - \{ml_1l_{c2}(T_1 - T_2 + M_y S) \cos \alpha_2 - ml_1^2 T_2 \\ + m^2 l_{c2} l_1^2 [l_{c2}(\dot{\alpha}_1 + \dot{\alpha}_2)^2 \sin \alpha_2 \cos \alpha_2 + l_1 \dot{\alpha}_1^2 \sin \alpha_2 \\ + g \cos(\alpha_1 + \alpha_2) - g \cos \alpha_1 \cos \alpha_2]\} \\ / \{m^2 l_{c2}^2 l_1^2 (\sin \alpha_2)^2 + I_2 ml_1^2\}$$

Since in this model the number of unknowns is less than the number of equations, so to solve this problem  $T_2$  has been used as a control strategy  $T_2 = k_2 \theta = k_2 \left(\frac{\pi}{2} - (\alpha_1 + \alpha_2)\right)$  where  $k_2 \approx mgl_{c2}$ .  $T_1$  has no physiological equivalent as a torque, it resembles the bone bending resistance; therefore after solving the equations and implementing them in Simulink it has been made equal to zero.

After these two control strategies using  $T_1$  and  $T_2$ , still the unknowns' number was less than the equations. So  $M_y$  measured in experiments has been used as an input to this model. Since in experiments data has been gathered by 100Hz, it needed to get synchronized by the frequency of other input and output signals in MATLAB. It was

observed that running this model, all of the output signals had 70-80 data points in a second, so  $M_y$  signal was down sampled to 80Hz and then inserted to the model.

This model has been simulated using MATLAB, Simulink. For a primary test in this simulation the angle  $\alpha_1$  has been fixed to  $45^\circ$ , making the foot rigid.

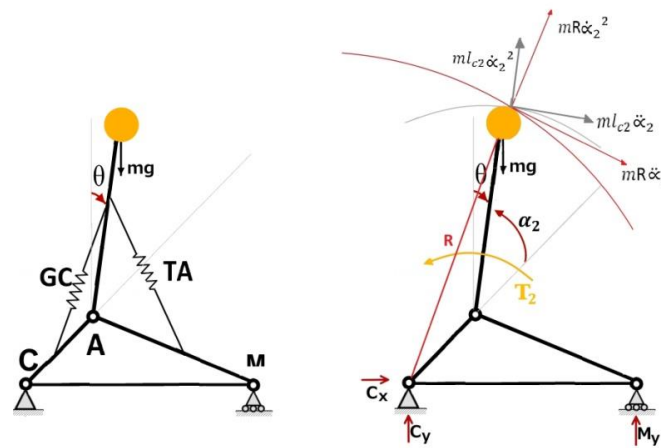


Figure C-2 Single inverted pendulum foot model

This gives the output signals as below, showing that the human foot has been standing stable during the simulation. Although  $M_y$  is used from the experimental data and hence is not a perfectly oscillating signal,  $C_y$  is oscillating inside its limits.

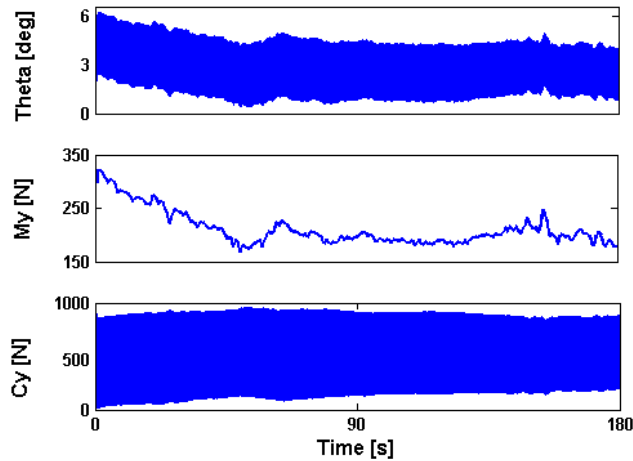


Figure C-3 Output signals for single inverted foot model

Then  $C_y/M_y$  ratio was calculated in time; this signal is shown in the figure below. The average value of this ratio is  $2.09 \pm 0.16$  and as it can deduced from the figure, the time percentage during which this ratio is oscillating around 2 with 5% tolerance is 39.21%.

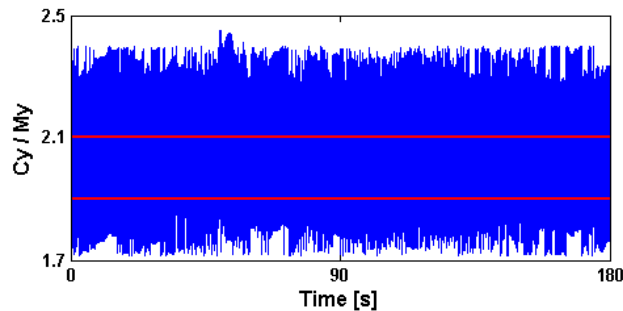


Figure C-4  $C_y/M_y$  ratio with 5% tolerance

But when this model was simulated with  $\alpha_1$  not being fixed, hence letting the plantar aponeurosis length to change, the results are not satisfying at all. The output signals as shown below are diverging in time and the foot cannot stand up still in long duration of times.

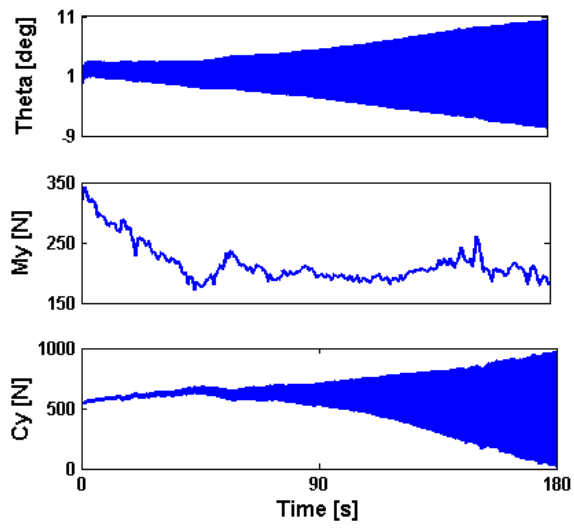


Figure C-5 Output signals for double inverted pendulum



## APPENDIX D

### STABILITY OF THE SYSTEM

In stability theory it is stated that the behavior of a dynamic system under perturbations can be analyzed using the linearized form of the system; at the equilibrium of such a linearized system (with an  $n$ -dimensional state space) there is a certain  $n \times n$  matrix. The eigenvalues of this matrix can explain the behavior of the system in nearby points.

If all eigenvalues are negative real numbers or complex numbers with negative real parts then the equilibrium point is a stable fixed point and the nearby points converge to it at an exponential rate.

As it can be seen in the figures presented in Chapter 4, the models have been simulated for the same duration of the experiments (180 seconds). But in the last model which is a deformable foot without friction forces, when the simulation time gets longer the output signals diverge in time; for example PA length shown in figure below.

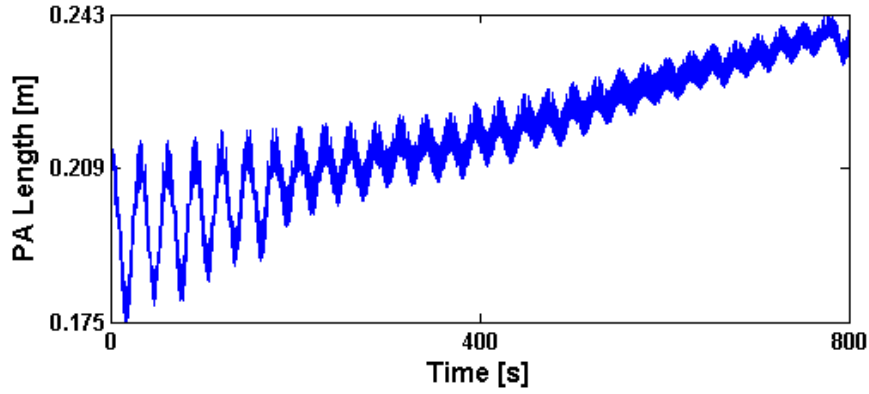


**Figure D-1 PA length for deformable foot model with no friction forces (for longer time than experimental duration)**

So the last deformable model has been studied for its stability. Aiming this, the system equations needed to get linearized in the first step, so some assumptions were done such as:

1.  $\dot{\alpha}_1^2 = \dot{\alpha}_2^2 = 0$
2.  $\alpha_1 \approx 45^\circ \Rightarrow \sin \alpha_1 = \cos \alpha_1 = \frac{\sqrt{2}}{2}$
3.  $\alpha_2 \approx 45^\circ \Rightarrow \sin \alpha_2 = \cos \alpha_2 = \frac{\sqrt{2}}{2}$   
 $\Rightarrow \begin{cases} \sin(\alpha_1 + \alpha_2) = 1 \\ \cos(\alpha_1 + \alpha_2) = 0 \end{cases}$
4.  $0 < \beta < 10^\circ \Rightarrow \begin{cases} \sin \beta = \beta \\ \cos \beta = 1 \end{cases}$

So the linearized form of the equations for this model will be as:

$$\ddot{\alpha}_1 = \left\{ A_x(I_2 + ml_{c2}^2) + ml_{c2} \left( k_2 \left( \frac{\pi}{2} - (\alpha_1 + \alpha_2) \right) - mgl_{c2} \right) \right\} \\ /m \left\{ (I_2 + ml_{c2}^2) \left( l_{c2} - \sqrt{l_1^2 + l_{c2}^2 + \sqrt{2}l_1l_{c2}} \right) + \frac{\sqrt{2}}{2}ml_1l_{c2}^2 \right\}$$

$$\begin{aligned}\ddot{\alpha}_2 = & - \left\{ A_x \left( I_2 + ml_{c2}^2 + \frac{\sqrt{2}}{2} ml_1 l_{c2} \right) \right. \\ & \left. + mk_2 \left( \frac{\pi}{2} - (\alpha_1 + \alpha_2) \right) \left( l_{c2} - \sqrt{l_1^2 + l_{c2}^2 + \sqrt{2} l_1 l_{c2}} \right) \right\} \\ & / m \left\{ (I_2 + ml_{c2}^2) \left( l_{c2} - \sqrt{l_1^2 + l_{c2}^2 + \sqrt{2} l_1 l_{c2}} \right) + \frac{\sqrt{2}}{2} ml_1 l_{c2}^2 \right\}\end{aligned}$$

Then the space state representation of the system should be written, considering the

system states defined as:  $\begin{cases} x_1 = \alpha_1 \\ x_2 = \dot{\alpha}_1 \\ x_3 = \alpha_2 \\ x_4 = \dot{\alpha}_2 \end{cases}$ , so the system equations rewritten in state space

form would be following:

$$\begin{aligned}\dot{x}_2 = & \left\{ A_x (I_2 + ml_{c2}^2) + ml_{c2} \left( k_2 \left( \frac{\pi}{2} - (x_1 + x_3) \right) - mgl_{c2} \right) \right\} \\ & / m \left\{ (I_2 + ml_{c2}^2) \left( l_{c2} - \sqrt{l_1^2 + l_{c2}^2 + \sqrt{2} l_1 l_{c2}} \right) + \frac{\sqrt{2}}{2} ml_1 l_{c2}^2 \right\}\end{aligned}$$

$$\begin{aligned}\dot{x}_4 = & - \left\{ A_x \left( I_2 + ml_{c2}^2 + \frac{\sqrt{2}}{2} ml_1 l_{c2} \right) \right. \\ & \left. + mk_2 \left( \frac{\pi}{2} - (x_1 + x_3) \right) \left( l_{c2} - \sqrt{l_1^2 + l_{c2}^2 + \sqrt{2} l_1 l_{c2}} \right) \right\} \\ & / m \left\{ (I_2 + ml_{c2}^2) \left( l_{c2} - \sqrt{l_1^2 + l_{c2}^2 + \sqrt{2} l_1 l_{c2}} \right) + \frac{\sqrt{2}}{2} ml_1 l_{c2}^2 \right\}\end{aligned}$$

Considering the linearized form of  $A_x$  is  $A_x = -m \left( l_{c2} \dot{x}_4 + \right.$

$$\left. \dot{x}_2 \sqrt{l_1^2 + l_{c2}^2 + \sqrt{2} l_1 l_{c2}} \right).$$

These equations should be written in matrix form so we would have:  $\dot{\vec{x}} = \underline{A}\vec{x} + \underline{B}u$ ,

where  $\vec{x} = \begin{bmatrix} x_1 \\ x_2 \\ x_3 \\ x_4 \end{bmatrix}$ . But as it is obvious from the equations, A and B matrices will only

contain terms of  $k_2$  and none of  $k_1$ . This is due to the fact that the equations 4.4 and

4.6 of APPENDIX B are being used to solve for  $\ddot{\alpha}_1$  and  $\ddot{\alpha}_2$ . In order to have  $k_1$  in the equations for these two, we need to use 4.3 and 4.6 but the problem is 4.3 has to be used for finding  $M_y$  and  $C_y$  as well and this makes all of these variables to be dependent to each other, which is not a desirable aspect at all.

To solve this problem we went on with a new model: “Deformable foot with friction forces”.

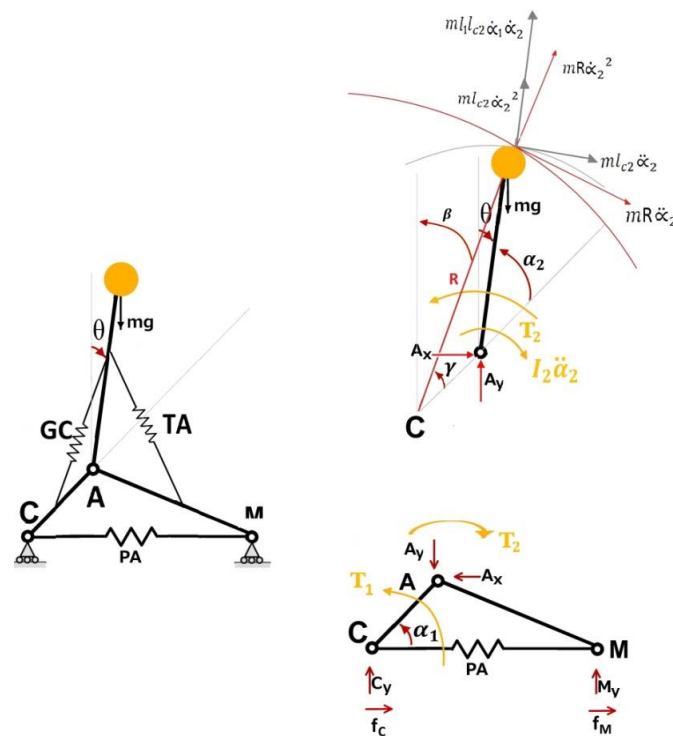


Figure D-2 Deformable foot model with friction forces

In triangle:

1.  $A_x = f_c + f_M = \mu C_y + \mu M_y$
2.  $A_y = C_y + M_y$
3.  $-T_2 + T_1 - C_y l_1 \cos \alpha_1 + M_y (S - l_1 \cos \alpha_1) + f_M l_1 \sin \alpha_1 + f_C l_1 \sin \alpha_1 - (I_2 + ml_{c2}^2) \ddot{\alpha}_2 - (I_2 + mR^2) \ddot{\alpha}_1 = 0$

$$\Rightarrow -T_2 + T_1 - A_y l_1 \cos \alpha_1 + M_y S + A_x l_1 \sin \alpha_1 - (I_2 + m l_{c2}^2) \ddot{\alpha}_2 - (I_2 + m R^2) \ddot{\alpha}_1 = 0$$

In upper link:

4.  $A_x + m l_{c2} (\dot{\alpha}_2^2 \cos(\alpha_1 + \alpha_2) + \ddot{\alpha}_2 \sin(\alpha_1 + \alpha_2)) + m R (\dot{\alpha}_1^2 \sin \beta + \ddot{\alpha}_1 \cos \beta) + 2 m l_{c2} \dot{\alpha}_1 \dot{\alpha}_2 \cos(\alpha_1 + \alpha_2) = 0$
5.  $A_y - m g + m l_{c2} (\dot{\alpha}_2^2 \sin(\alpha_1 + \alpha_2) - \ddot{\alpha}_2 \cos(\alpha_1 + \alpha_2)) + m R (\dot{\alpha}_1^2 \cos \beta - \ddot{\alpha}_1 \sin \beta) + 2 m l_{c2} \dot{\alpha}_1 \dot{\alpha}_2 \sin(\alpha_1 + \alpha_2) = 0$
6.  $-T_2 + [I_2 + m(l_{c2}^2 + l_1 l_{c2} \cos \alpha_2)] \ddot{\alpha}_1 + (I_2 + m l_{c2}^2) \ddot{\alpha}_2 + m l_1 l_{c2} \sin \alpha_2 \dot{\alpha}_1^2 + m g l_{c2} \cos(\alpha_1 + \alpha_2) = 0$

In this case it would be possible to find  $\ddot{\alpha}_1$  and  $\ddot{\alpha}_2$  from equations 3 and 6, so they both have  $k_1$  and  $k_2$  terms. Equations 1 and 2 similarly can be used to find  $M_y$  and  $C_y$ .

As it was reviewed in “swaying foot model with friction forces”, in literature it has been shown that the friction coefficient underneath the foot, when the foot skin is dry, is greater than 0.2 and typically around 0.5 [37]. Since the skin beneath a human foot has almost the same physical properties in all of its points, it is rational to assume the friction coefficients in calcaneous and metatarsals to be equal ( $\mu_C = \mu_M$ ). Therefore:  $A_x = f_C + f_M = \mu C_y + \mu M_y$ , and system of equations consisting of equations 1 and 2 will be as:  $\begin{cases} A_x = \mu C_y + \mu M_y \\ A_y = C_y + M_y \end{cases}$  but it can be shown that this system cannot generate any solutions for  $C_y$  and  $M_y$ :

$$C_y = \frac{\begin{vmatrix} A_x & \mu \\ A_y & 1 \end{vmatrix}}{\begin{vmatrix} \mu & \mu \\ 1 & 1 \end{vmatrix}} = \frac{A_x - \mu A_y}{0}$$

$$M_y = \frac{\begin{vmatrix} \mu & A_x \\ 1 & A_y \end{vmatrix}}{\begin{vmatrix} \mu & \mu \\ 1 & 1 \end{vmatrix}} = \frac{\mu A_y - A_x}{0}$$

Therefore there is a need for more information to solve the equations of this model. Maybe this information can be provided from experimental data or by adding other configurations to the model but anyway adding only friction forces to the system would not be sufficient.